University of Massachusetts Amherst
ScholarWorks@UMass Amherst

Masters Theses 1911 - February 2014

2013

Holocene Paleo-environmental Variability Reconstructed from a Lake Sediment Record from Southeast Greenland

Gregory A. De Wet
University of Massachusetts Amherst

Follow this and additional works at: https://scholarworks.umass.edu/theses

 Part of the Biogeochemistry Commons, Climate Commons, Geochemistry Commons, Geology Commons, and the Sedimentology Commons

De Wet, Gregory A., "Holocene Paleo-environmental Variability Reconstructed from a Lake Sediment Record from Southeast Greenland" (2013). *Masters Theses 1911 - February 2014*. 1032.
Retrieved from https://scholarworks.umass.edu/theses/1032

This thesis is brought to you for free and open access by ScholarWorks@UMass Amherst. It has been accepted for inclusion in Masters Theses 1911 - February 2014 by an authorized administrator of ScholarWorks@UMass Amherst. For more information, please contact scholarworks@library.umass.edu.

Holocene paleo-environmental variability reconstructed from a lake sediment record from Southeast Greenland

A Thesis Presented

By

GREGORY ANDREW DE WET

Submitted to the Graduate School of the
University of Massachusetts Amherst in partial fulfillment
of the requirements for the degree of

MASTER OF SCIENCE

May 2013

Department of Geosciences

Holocene paleo-environmental variability reconstructed from a lake sediment record from Southeast Greenland

A Thesis Presented

By

GREGORY ANDREW DE WET

Approved as to style and content by:

_____
Raymond S. Bradley, Chair

_____
Nicholas L. Balascio, Member

_____
Julie Brigham-Grette, Member

_____
R. Mark Leckie, Department Head

Department of Geosciences

DEDICATION

To my grandfather, for teaching me about how important education and hard work is in life, and for allowing me to pursue what I love. To my brother and sister, for putting up with all my science heavy talk around the dinner table. To Caroline, for much more than I care to put here. And most of all to my parents, Carol and Andy, who have fostered and supported me throughout this entire academic endeavor. Thank you all so much.

ACKNOWLEDMENTS

This project was only possible with the help of a multitude of people from both within UMass Amherst and beyond. First I would like to thank my advisor, Dr. Raymond Bradley. I cannot put into words how much I have learned over the past two years here at UMass and I could not have asked for a better role model and advisor. Ray's knowledge in the field of paleoclimatology is nearly unparalleled and I hope to continue to learn and grow under his supervision. Thank you Ray, for allowing me to pursue a multitude of different avenues and methods regarding paleoclimate research, with your help and support I feel I have learned a great many new techniques that I will apply going forward with my PhD. I know it was dangerous to let a new Masters student loose on a sediment core, but I couldn't have asked for better introduction to paleoclimatology and paleolimnology and am looking forward to our next project.

I would also like to thank Dr. Nicholas Balascio for his unwavering support and knowledge. Nick, you were my surrogate advisor for much of this project when Ray was off saving the world. I really appreciate all the time spent in the lab showing me how to do things and discussing the meaning of all kinds of data. I certainly would not have gotten very far with this project without your guidance and input. You will make a great professor and I hope in our future collaborations I can repay the generosity and patience you showed with me.

Special thanks also to Dr. Isla Castañeda, for taking time out of her incredibly schedule to give me a whirlwind introduction to biogeochemistry. It was really amazing to learn about this exciting new field of paleoclimate research and I can't wait to get back into the biogeochem lab.

I would also like to thank everyone in the Climate System Research Center, especially Anthony Coletti and Jeremy Wei, for a great deal of support and mutual appreciation for what we do as scientists. The faculty and students here at UMass are phenomenal and make a huge difference when pursuing a degree.

Finally I would like to extend a heartfelt thank you to Sam Davin, my colleague in arms in SE Greenland. Sam, it was a fantastic experience to work through this project with you. From our amazing time in SE Greenland to our horrible meal at the Rt. 9 diner at 3am I couldn't have done it without you. I wish you all the best going forward and look forward to working with you in the future.

ABSTRACT

HOLOCENE PALEO-ENVIRONMENTAL VARIABILITY RECONSTRUCTED FROM A LAKE SEDIMENT RECORD FROM SOUTHEAST GREENLAND

MAY 2013

GREGORY A. DE WET, B.S., BATES COLLEGE

M.S., UNIVERSITY OF MASSACHUSETTS, AMHERST

Directed by: Distinguished Professor Raymond S. Bradley

Arctic climate variability over the Holocene has been both extensive and, at times, abrupt. Current understanding of these changes is still quite limited with few high-resolution paleoclimate records available for this period. In order to place observed and predicted 21st century climate change in perspective, reliable and highly resolved paleo-reconstructions of Arctic climate are essential. Using an 8.5 m sediment core from Nanerersarpik Lake, this project will characterize climate changes during the Holocene, including the deglacial transition, the rapid changes that are known to have occurred around 8,200 years ago, the transition from Holocene thermal maximum (HTM) to the colder Neoglacial period, and intervals of abrupt climate change during the late Holocene such as the Medieval Warm Period and Little Ice Age.

The 8.5 m sediment core from Nanerersarpik contains a dense gray clay in the lower 0.5m. The upper 8.0m of sediment is light brown and organic-rich with centimeter to half-centimeter laminations, interrupted by mass-movement events. Paleoenvironmental conditions have been interpreted using magnetic susceptibility, grain size, biogenic silica, TOC, C/N, organic lipid biomarkers, and $\delta^{13}C_{org}$, as well as with high-resolution spectral reflectance and scanning XRF profiles. These parameters allow us to interpret changes in

autochthonous productivity and clastic input throughout the Holocene. A chronology for the record has been established using 7 radiocarbon dates. The age-model indicates Nanerersarpik Lake contains an ~8,500-yr sediment record with a linear age/depth relationship and a sedimentation rate of 0.1cm/yr, allowing for potentially decadal scale resolution of environmental changes.

An abrupt transition from dense glacial clay to laminated organic rich sediment occurs near the base of the core. This is interpreted as marking the retreat of glacial ice from the catchment around 8,250 cal yr BP. High frequency variations dominate the spectral, scanning XRF, and magnetic susceptibility data and indicate some correlation with Holocene climate intervals. Biogenic silica and TOC analysis indicate broad scale changes in primary productivity generally consistent with known Holocene climatic intervals: the deglacial period, the Holocene Thermal Maximum, and the Neoglacial, with high variability during the late Holocene. High resolution biogenic silica data over the past 1500 cal yr BP show some correspondence to Greenland Ice Core paleotemperature reconstructions, suggesting biogenic silica may be responding to temperature on short timescales and should be used as a paleo-environmental proxy in future studies. Alkenones and glycerol dialkyl glycerol tetraethers were present in Nanerersarpik sediments, suggesting this location or others in SE Greenland might be suitable for future high-resolution paleotemperature studies using biomarkers.

TABLE OF CONTENTS

Page

LIST OF TABLES

LIST OF FIGURES

CHAPTER I

INTRODUCTION

1.1) Introduction and objectives:

Modern climate, especially at high latitudes, is changing rapidly in response to anthropogenic greenhouse gas emissions. Observed and predicted 21st century climate change must be put in perspective through analysis of reliable and highly resolved paleo-reconstructions of past climate (Kaplan and Wolfe, 2006). The Arctic in particular is predicted to respond substantially to projected warming (Callaghan et al., 2010) through the amplification of climate feedbacks specific to the region (Overland et al., 2008; Serreze et al., 2009). The Holocene epoch (11,500 cal yr B.P. to the present) presents a unique opportunity to understand Arctic climate as atmospheric and ocean circulation patterns were similar to their current configuration and natural insolation forcing caused significant environmental changes (Johnsen et al., 2001; Mayeweski et al., 2004; Kaufman et al., 2004) without the overprint of significant anthropogenic influence. High-resolution paleoclimate reconstructions of Arctic climate during this period therefore allow projected changes to be contextualized and increase our understanding of how high-latitude climate will respond in the future. However, our current understanding of Holocene climate change is still quite limited with few high-resolution terrestrial paleoclimate records available for this period. The goal of this project is to produce a highly-resolved paleoclimate record from climatically sensitive Southeast Greenland to address this issue.

Within the Arctic, much of the existing evidence for how climate has varied in the past has been reconstructed from marine sediments or ice cores. While marine sediment cores have documented climate change during the Holocene (Andersen et al., 2004;

Justwan et al., 2008; Jennings et al., 2011), and are useful in that they generally record a more regional signal and can be very highly resolved, they do not necessarily record how these changes have been manifested on land. Greenland ice core records, while extremely highly resolved (Johnsen et al., 2001; Thomas et al., 2007; Kobashi et al., 2011), record local conditions on the ice sheet and are therefore not always indicative of regional climate. Lake sediments can provide an important bridge between these two archives and shed light on terrestrial environmental variability in the Arctic. The margins of the Greenland Ice Sheet (GIS) are an excellent area to analyze lakes as they are not only ubiquitous features of the landscape, but also may record multiple climate signals related to changes related to the GIS, atmospheric pattern variability, and ocean current changes. Furthermore, the coasts are expected to experience large temperature changes in the future (Kattsov et al., 2007; Bitz et al., 2010).

Lake records are useful as archives of past climate; however, the links between environmental changes and lacustrine proxies can be complex. Climate changes are filtered through both the lake catchment and in-situ lacustrine processes before being recorded in the sediment (Anderson et al., 2012). In spite of this potential disconnect, many lake systems have proven to be robust recorders of climate change in the Arctic if these processes can be accounted for and understood (e.g. Kaufman et al., 2004; Kaplan and Wolfe, 2006; Massa et al., 2012). Lake sediments are powerful in that a multitude of relevant paleoclimate proxies can be applied to them that respond to numerous different facets of climate change and they can also act as independent internal checks on the accuracy of the reconstructions (Meyers, 1983; Meyers and Ishiwatari, 1993; Smol and Cumming, 2000). Well dated, multiproxy paleoclimate reconstructions from lakes in the

Arctic can greatly increase our understanding of paleoenvironmental variability in the region.

The objective of this investigation is to produce a continuous, high-resolution paleoclimate reconstruction from southeastern Greenland based on analysis of a lake sediment core from Nanerersarpik Lake (Figure 1.1) A multiproxy analysis was carried out using physical, chemical, and biological proxies. Rates of primary production were estimated from total organic carbon (TOC), total nitrogen (TN), lipid biomarker, and biogenic silica (BSi) concentrations, and carbon and nitrogen isotope values. Clastic/minerogenic input was analyzed using magnetic susceptibility (MS), sediment elemental composition, and sediment density. Paleotemperatures were estimated using established transfer functions based on concentrations of long-chain alkenones and branched glycerol dialkyl glycerol tetraethers. Based on these proxies, periods of known climate change during the Holocene have been identified; the local transition from glacial to deglacial conditions, the transition from Holocene thermal maximum (HTM) to the colder Neoglacial period, as well as shorter-lived intervals throughout the Holocene such as the Medieval Climate Anomaly and the Little Ice Age.

The Nanerersarpik Lake record is part of a regional reconstruction of SE Greenland Holocene paleoclimate, in conjunction with records from three other lakes within 50km of the study site (Flower Valley Lake, Kulusuk Lake, and Lower Sermilik Lake) (Figure 1.1). Colleagues at the University of Massachusetts, Amherst (Dr. Nicholas Balascio and Masters student Sam Davin), are investigating the other SE Greenland lakes. Nanerersarpik paleo-environmental data are also compared to previously

published records from throughout the Arctic to determine the local timing and magnitude of Holocene climate change at this site.

1.2) Modern local climate

Temperature and precipitation data have been collected at a meteorological station in the settlement of Tasiilaq on Angmassalik Island (Figure 1.1) for the past 118 years (Cappelen et al., 2010) Generally, the majority of precipitation occurs during the winter and fall (Figure 1.2 and Table 1.1). February has been the coldest month on average during this time span (-7.9°C) and July the warmest (6.9°C). May, June, July, and August have average temperatures above freezing.

Table 1.1: Tasiilaq Met. Station Data (1895-2010)

Month	Average Temp. (°C)	Average Precipitation(mm)
January	-7.3	91.0
February	-7.9	79.0
March	-6.9	83.6
April	-3.4	62.8
May	1.3	57.4
June	4.9	44.4
July	6.9	43.8
August	6.3	58.4
September	3.6	85.7
October	-0.6	95.4
November	-4.1	86.3
December	-6.1	82.8

1.3) Regional Climate Context

1.3.1) Marine climate forcings

Understanding climate variability of the SE Greenland region is valuable due to its location at the crux of influence of multiple climate systems, climate signals associated with the GIS, ocean circulation variability, as well as important modes of atmospheric circulation. Located less than 50km from the coast and only 100m from a large fjord, Nanerersarpik is proximal to multiple important marine systems that influence both regional and global climate, such as the regions of formation of North Atlantic Deep Water (NADW) (Broecker and Denton, 1989). NADW variability and subsequent changes to the Atlantic Meridional Overturn Circulation (AMOC) have caused abrupt climate change during the Holocene, such as the so called "8.2 event" (Alley et al., 1997, Clark et al., 2002). It also is just onshore from the boundary between the polar waters of the East Greenland Current and the warmer Atlantic waters of the Irminger Current (Justwan et al., 2008; Jennings et al., 2011). Depending on the strength and intensity of the Irminger, warm Atlantic waters can be transported as far north as Baffin Bay (Zweng and Munchow, 2006) and have been attributed to 1°C warmer summer temperatures in SW Greenland (Hanna et al., 2009). Both of these currents have responded/contributed to Holocene climate change and shifts in their intensity can dramatically affect regional climate (Masson-Delmotte et al., 2012).

1.3.2 The Greenland Ice Sheet

The GIS exerts significant influence over both regional and global climate due its high reflectivity and potential contribution of freshwater to the North Atlantic (Masson-Delmotte et al., 2012), as well as controls on regional atmospheric circulation (Steffen and Box, 2001). Changes to both the thickness of the interior Greenland Ice Sheet,

(Vinther et al., 2009) and its margins, have occurred during the Holocene (eg. Briner et al., 2010) and are likely to continue with rising Arctic temperatures (Gregory et al., 2004; Masson-Delmotte et al., 2012). More locally, Nanerersarpik is proximal to the margin of the GIS and paleo-environmental data from the lake may shed light on the Holocene history of the ice sheet in SE Greenland. Furthermore, high resolution studies such as this help to answer the question of whether abrupt and sometimes short lived climate change events recorded in ice cores are present and can be identified in lacustrine archives.

1.3.3 The North Atlantic Oscillation and other atmospheric patterns

Changes related to large-scale atmospheric modes such as the North Atlantic Oscillation (NAO) and the Atlantic Multidedal Oscillation (AMO) also play a major in Greenland climate (eg. Hurrell and Deser, 2009; Von Gunten et al., 2012). For instance, large changes in N. Atlantic surface air temperature, wind patterns, and precipitation can occur from shifts in the phase of the NAO. NAO variability can also indirectly change climate by affecting sea ice cover and high latitude deep water formation in the Arctic (Hurrell and Deser, 2009). Generally, the modern NAO describes the balance of air masses between the Azores high pressure center and Icelandic low. The NAO is considered to be in a positive phase when the pressure gradient between the Icelandic Low and the Azores high is large. This positive phase broadly translates to stronger heat and moisture transport across the mid-Atlantic resulting in warmer temperatures and higher precipitation in Northern Europe and colder, drier air over Northeastern Canada and Greenland. While the NAO has can vary on short times scales (daily) it has been

shown that one phase can remain dominant for extended periods of time and affect climate in the North Atlantic (eg. Trouet et al., 2009).

1.4) Regional Holocene Climate History

Broadly, climate trends in the Arctic during the Holocene are well-established, although the timing and intensity of the intervals discussed below are not spatially uniform and only beginning to be understood (Mayewski et al., 2004; Kaufman et al., 2004; Wanner et al., 2008).

1.4.1) Last Glacial Maximum (LGM) and deglaciation history

While the extent of glaciation in SE Greenland during the Last Glacial Maximum (22-17 ka BP) is generally understood, the thickness of ice in the region is still unclear, with some authors (Dowdeswell et al., 1994; Landvik, 1994; Funder et al., 1998) calling for a limited ice sheet with numerous nunataks and the ice margin estimated to reach only part way out along the continental shelf. Others suggest the ice sheet was more extensive and nearly reached the continental shelf break (Stein et al., 1996; Kuijpers et al., 2003; Hakansson et al., 2007; Roberts et al., 2008). On nearby Amassalik Island (30km to the SW) Humlum and Christiansen (2008) found evidence for a well-defined trimline of glacial erosion up to altitudes of 600-900m, suggesting that peaks above this elevation were exposed during the LGM. Trimline features were also observed proximal to Nanerersarpik, where rounded, striated topography gives way to jagged, alpine features above ~800m.

The GIS is interpreted to have reached its present margins in the region by 7-8ka BP (Funder and Hansen, 1996; Christiansen et al., 1999) and Humlum and Christiansen (2008) suggest that Angmassalik Island was largely deglaciated by this time. Local deglaciation was more complex, with no estimates available for the Nanerersarpik region specifically. The preponderance of glaciers in the area today, though restricted to high mountain cirques, suggests that valley and mountain glaciers likely persisted beyond the retreat of the ice sheet itself, though whether they survived the Early Holocene is uncertain.

1.4.2) Holocene Thermal Maximum

The HTM is a warm interval during the Early Holocene that was driven largely by increased summer insolation (7.5% higher in summer 9000 years ago than today at 70°N (Kutzbach, 1981). This external forcing was manifested differently across the Arctic due to effects of the residual Laurentide Ice Sheet and local and regional feedbacks. In general, peak warmth in Greenland occurred between 9 and 5ka (Wagner et al., 2000; Kaufman et al., 2004; Klug et al., 2008; Perren et al., 2012). In parts of Southern and Western Greenland for example, the HTM marked the most productive (and inferred warmest) interval of the entire Holocene (Kaplan et al., 2004; Axford et al., 2013). The Holocene Thermal Maximum was extremely dry in Greenland, with arid conditions lasting up to ~5-6 cal kyr BP (Wagner et al., 2000; McGowan et al., 2003; Anderson and Leng, 2004; Anderson and Stedmon, 2007).

1.4.3) Neoglaciation

Summer insolation values decreased steadily throughout the Holocene leading to a transition from the HTM to a colder interval known as the Neoglacial period. This is generally recorded by lake sediment proxies as a decrease in primary production and increased aridity and windiness (eg. Massa et al., 2012; Axford et al., 2013). Paleoclimate reconstructions from multiple sites around Greenland found the culmination of this Neoglacial period took place during the late Holocene as part of the Little Ice Age (Wagner et al., 2002; Kaplan et al., 2004; Perren et al., 2012).

In some areas of the North Atlantic and the Arctic, Neoglacial cooling was interrupted by a millennial scale warming event known as the Medieval Climate Anomaly (Mayewski et al., 2004; Mann et al., 2009; Kobashi et al., 2012). This short-lived warming was followed by a return to colder conditions known as the Little Ice Age, forced by lower summer insolation in the Northern Hemisphere, highly variable solar activity, and numerous large volcanic eruptions (Overpeck et al., 1997; Wanner et al., 2008; Mann et al., 2009; Kaufman et al., 2009; Marcott et al., 2013).

CHAPTER II

STUDY AREA

2.1) Regional Setting

Nanerersarpik Lake is located on the shore of Angmassalik Fjord in Southeast Greenland (66°54’47.58’’N, 37°08’44.98’’W) near the Innuit settlement of Kummiut approximately 45 kilometers from the coast (Figure 1.1). The regional underlying bedrock is part of the Nagssugtoqidian mobile belt complex of 2700 m.y. old gneisses and at the study site consists mainly of quartzo-feldspathic gneiss and some supracrustal metasediments (Bridgwater, 1976).

The lake sits 100m above Angmassalik fjord on a shoulder of bedrock (Figure 2.1). The surrounding catchment is small and steep-sided, totaling 5.7km^2. The lake basin is bordered on the northern and eastern sides by low bedrock ridges of approx. 150m height (Figure 2.2). Glacial erratics are present along the summits of these features. The ridges slope steeply down to the basin floor, grading into vegetated fan/delta deposits that extend ~20m from the base of the ridges into the lake (Figure 2.3). Immediately to the west is a much higher ridge (average height of 900m). The slope of exposed bedrock is partially covered in places with talus material, and at least 4 large talus fans extend directly into Nanerersarpik (Figure 2.4).

A small U-shaped notch is present in the bedrock ridge making up the northwestern boundary of the lake catchment (Figure 2.5). From this notch the only relatively significant source of flowing water enters the lake, a small (0.5m wide) stream (note: observation was made in mid-summer, many more inputs likely present in spring during the nival melt). Along the small valley incised by the stream below the notch is

the greatest concentration of glacial erratics present in the catchment. To the south, the basin is more open and the ground rises to only a few meters above the lake level (Figures 2.1 and 2.6).

The lake itself is quite clear and has a surface area of 0.62 km^2 (Figures 2.1 & 2.7). Lake bottom bathymetry reveals a single main basin (Figure 2.8). Cores were collected from the deepest part of the basin (54m water depth) in the southern half of the lake (star in Figure 2.9). Hydrolab data collected in the spring of 2010 show the lake as being only slightly oxygen limited in the deepest part of the lake (Figure 2.10). The current outflow of Nanerersarpik is located along the southeastern shore between a break in a low bedrock ridge. The outflow is a ~10 m wide shallow braided channel system that pools in a small pond before entering Ammassalik Fjord (Figure 2.11).

Figure 1.1: Location of study area in SE Greenland (left). 4 lakes were cored in the Spring of 2010 to contribute to a regional understanding of SE Greenland paleoclimate. This invesigation focused on the sediment record of Nanerersarpik lake (northernmost in image below). Lower Sermilik, Flower Valley, and Kulusuk Lakes are being investigated by colleagues from the University of Massachusetts, Amherst.

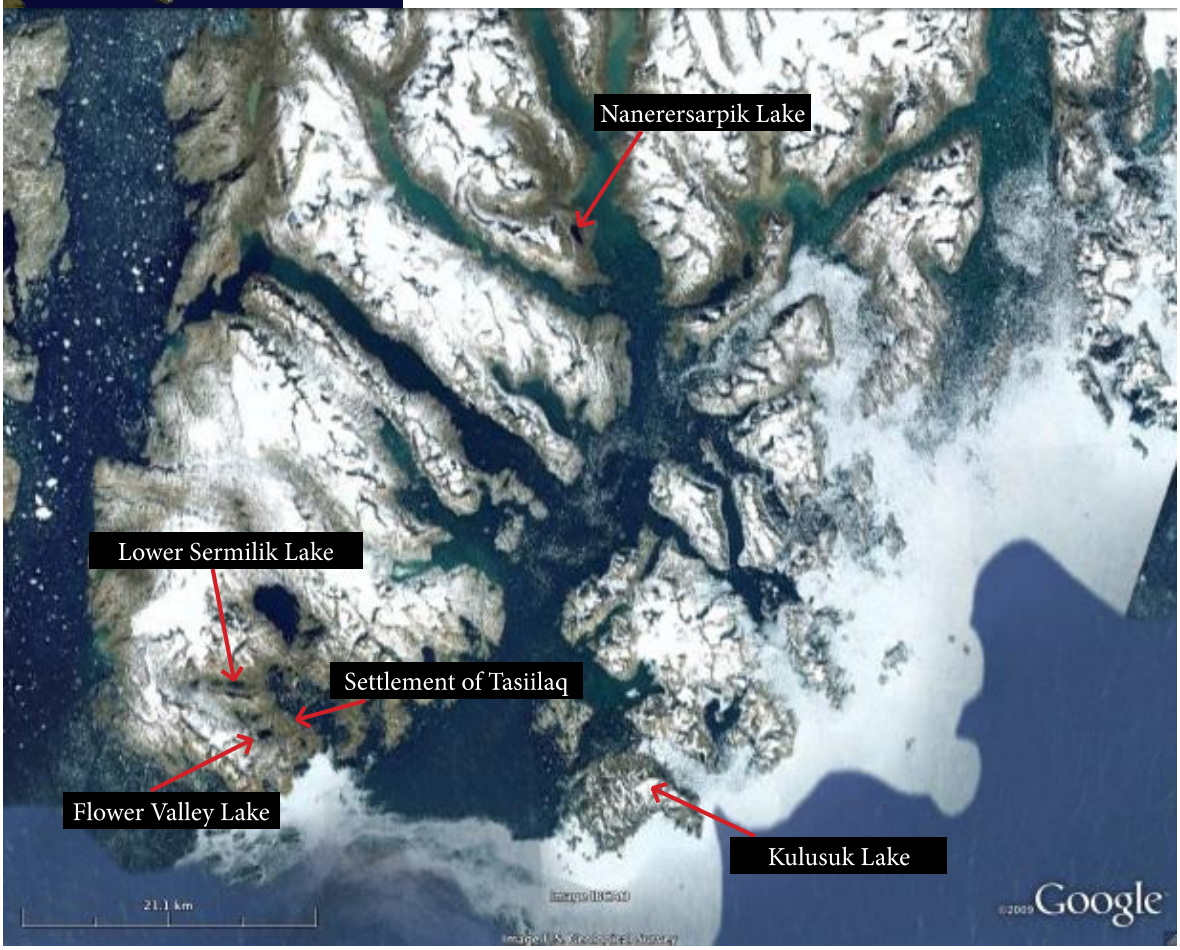

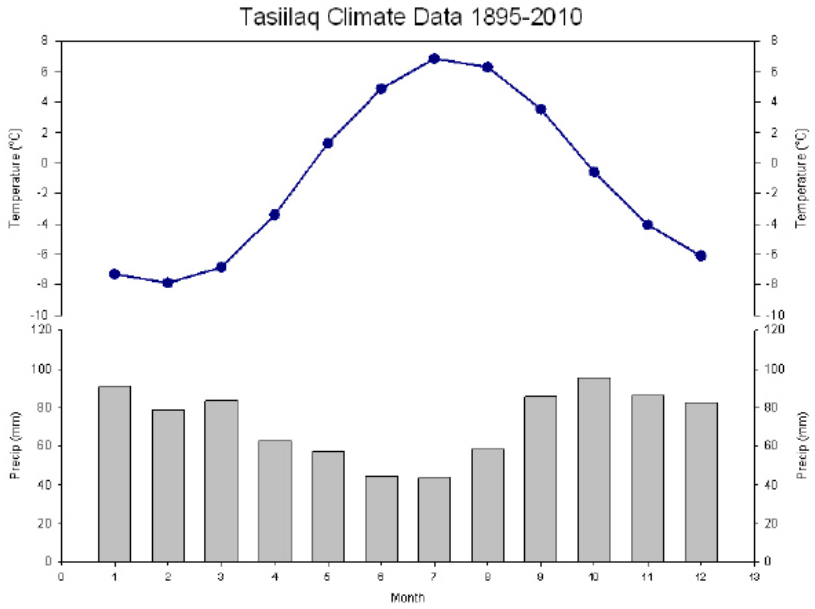

Figure 1.2: Monthly averages of precipitation (mm) and temperature (ºC) from meteorological station in Tasiilaq on Angmassalik Island from 1895-2010.

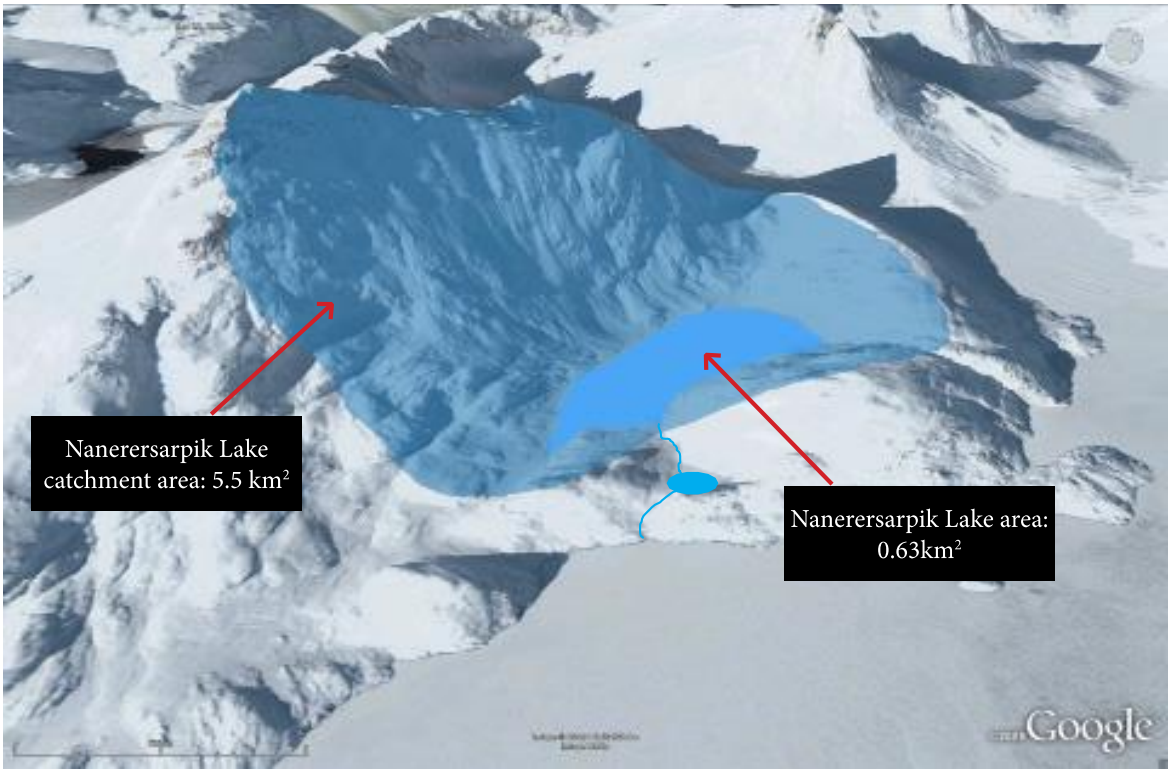

Figure 2.1: Catchment and lake area of Nanerersarpik in SE Greenland. Snow and ice-covered Angmassalik Fjord visible directly to east of lake as areas of no topographical relief. The ridges to the north and east of the lake rise to aprox. 150m. Ridge to the west rises to aprox. 900m. Current outflow out of SE side of lake is shown in blue.

Figure 2.2: Image looking northeast of founded ridges to the north and east of Nanerersarpik Lake.

Figure 2.3: Vegetated fan extending from base of bedrock ridge out to edge of Nanerersarpik as seen from top of eastern ridge.

Figure 2.4: Ridge forming western boundary of Nanerersarpik catchment. Note talus fans extending directly into lake.

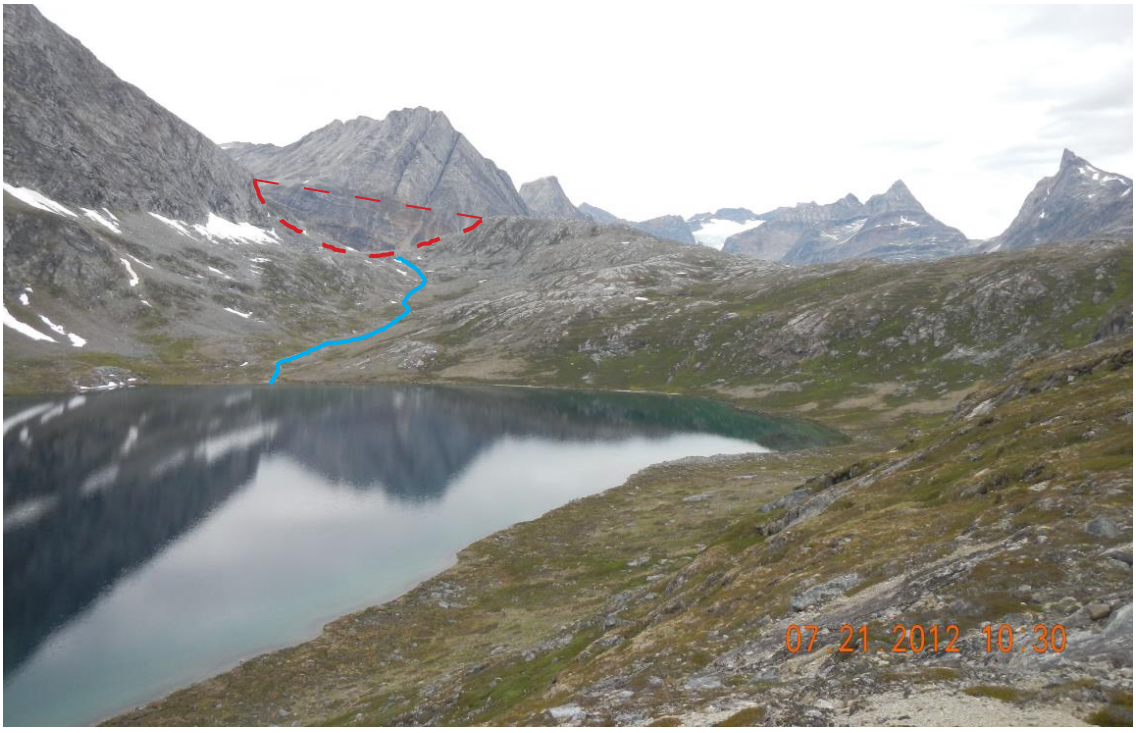

Figure 2.5: View to the northwest from the eastern edge of Nanerersarpik Lake catchment. Notch in bedrock ridge is denoted in red. The only source of water entering the lake at time of observation in late July was a small stream below notch (denoted in blue). The highest density of glacial erratics observed in the catchment were below notch on either side of the stream.

Figure 2.6: Image looking south from northern shore of lake. There is no evidence of outflow from extreme southern section of the lake, but the U-shaped valley suggests it may have been the path of a glacier down to the fjord.

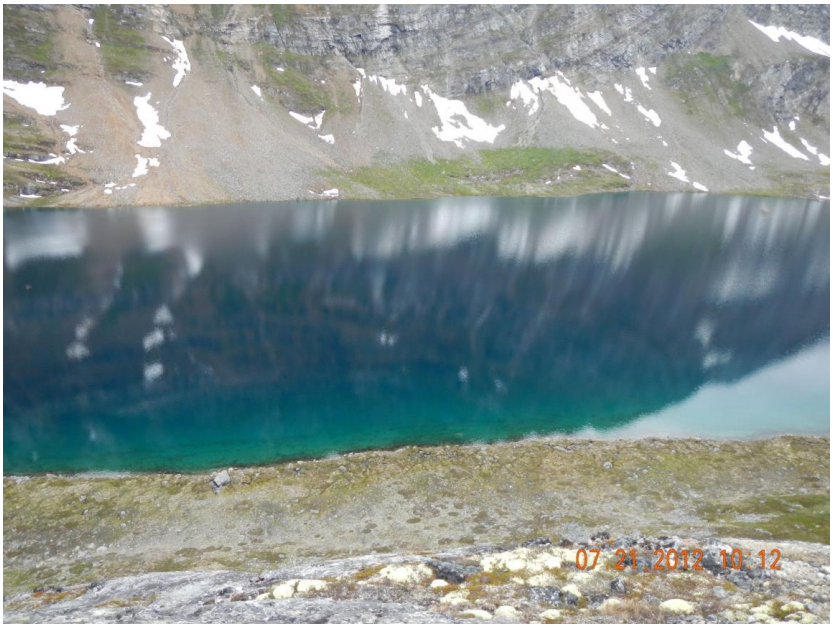

Figure 2.7: Image of Nanerersarpik Lake from eastern bedrock ridge, note clear water and steep sides of lake basin.

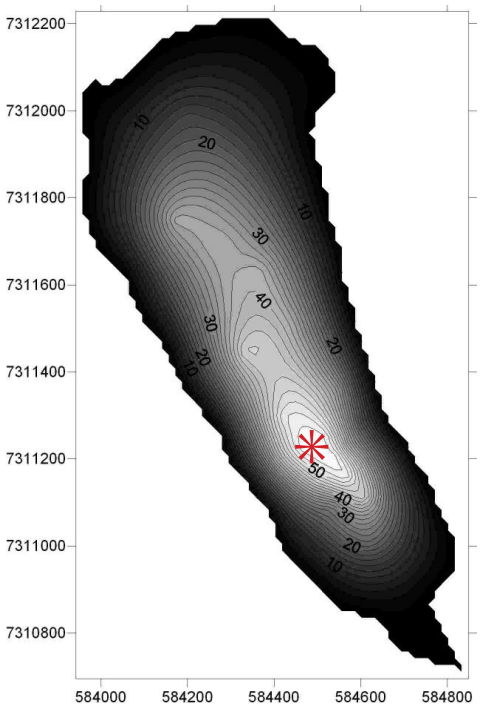

Figure 2.8: Bathymetric profile of Nanerersarpik Lake basin. Our sediment core was collected from the deepest part of the basin (aprox. 54m). Coordinates are in UTM.

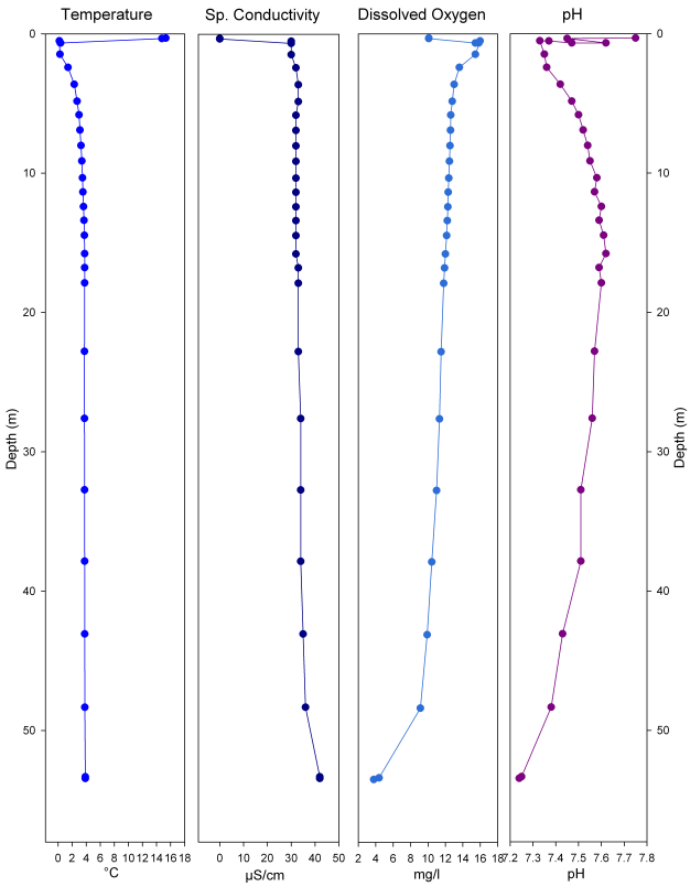

Figure 2.9: Hydrolab data from Nanerersarpik Lake collected in the Spring of 2010.

Figure 2.10: Outflow of Nanerersarpik Lake. The outflow stream exits the lake between a break in the bedrock ridge that makes up the southeastern boundary of the catchment. The stream is wide (10m) and only 0.5m deep. Upper image was taken from eastern ridge looking to the south. Lower image was taken from the middle of the outflow looking east towards Angmassalik Fjord.

CHAPTER III

METHODS

3.1) Core Collection

Coring was conducted at Nanerersarpik Lake in the Spring of 2010 by Dr. Raymond Bradley and other colleagues from UMass, Amherst when the lake was ice-covered. The majority of the cores were collected using a Uwitec tripod-mounted percussion coring system. Coring took place at adjacent "A" and "B" sites, with 4 core sections recovered from each site. The B core drives were taken at depths known to overlap missing sections of A to ensure a complete sediment record (Figure 3.1). A ~1m long surface core was also taken using a Nansen Percussion corer. To ensure complete recovery of surface sediments a ~1m surface core was also taken using a Uwitec gravity corer.

After collection, the cores were transported to University of Massachusetts, Amherst and stored in a refrigerated core storage room.

3.2) Composite core record and removal of turbidites/instantaneous slump events

A composite record was created from the A and B cores from Nanerersarpik Lake (Figure 3.1). Overlapping core intervals were identified through correlation of similar stratigraphic layers identified by the magnetic susceptibility profiles of each core section (Figure 3.2). Layers with characteristic high magnetic susceptibility values (generally turbidites) made the identification of multiple congruent layers possible.

Once this preliminary composite core was assembled, turbidites/mass movement events were identified and removed using 3 primary criteria: high magnetic susceptibility

values (above the baseline of ~20-30 SI x 10^{-5}) (Figure 3.2), a visually identifiable fining upward sequence (Figure 3.3), and high Ti counts (from the Itrax core scanner) (Figure 3.4). In this way a total of 42 turbidites/mass movement events were identified and removed from the composite Nanerersarpik sediment record that was then interpreted for paleoenvironmental analysis (Figure 3.5) (Table 3.1). It should be noted that 3 of these events did not display the fining upward sequence typically displayed by turbidites but were identified as anomalous events that were not part of normal pelagic sedimentation and were subsequently removed from the final composite paleoclimate record. The largest turbidite removed was 77cm long and the smallest was 0.5cm. It is possible that not all sub-cm scale instantaneous sedimentation events were removed from the composite record. Overall, 303cm of sediment were positively attributed to turbidites and removed, shortening the length of the composite core from 841cm to 538cm (Figure 3.6).

Table 3.1) Turbidite depths and ages

Turbidite #	Core Section	Section Depth (cm)	Composite Depth (cm)	Age (cal yr BP)
1	DB1-A1A	(51-56)(2.5-17)	51-71	774
2	A1A	28-29	82-83	906
3	A1A	39-44.5	93-98.5	1045
4	A1A	53-58.5	107-112.5	1162
5	A1A	63-70	117-124	1192
6	A1A	71-74.5	125.5-128.5	1206
7	A1A	83-84.5	137-138.5	1324
8	A1A	86.5-89.5	140.5-143.5	1346
9	A1A	94-96	148-150	1405
10	A1B	18-20.5	202-204.5	2364
11	A1B	25-26.5	209-210.5	2444
12	A1B-B1B1	(30-33)(56.5-57)	214-218	2454
13	B1B1	58-62	219-223	2459
14	B1B1	77.5-81	238.5-242	2513

15	B1B2	5.5-7.5	266-268	2627
16	B1B2	11.5-13.5	272-274	2691
17	B1B2-A2A	17.5-19.5 & 49	278-280.5	2767
18	A2A	52-54.5	283.5-286	2820
19	A2A	61-62.5	292.5-294	2950
20	A2A	77.5-78	309-309.5	3251
21	A2A	83-111	314.5-342.5	3348
22	A2B-B2A	(10.5-19)(56-57)	382-392	4376
23	B2A	59.5-62	394.5-397	4436
24	B2A	67-70	402-405	4570
25	B2A	73.5-84	408.5-419	4659
26	B2A	93.5-94	428.5-429	4927
27	B2A	101.5-102.5	436.5-437.5	5135
28	B2A	108-109	443-444	5284
29	B2B	3.5-5.5	444.5-446.5	5298
30	B2B-A3A	(6-10.5)(12-84)	447-524	5298
31	A3A	88.5-96.5	528.5-536.5	5403
32	A3A	104-106	544-546	5611
33	A3A	124.5-129.5	564.5-569.5	6113
34	A3B-B3A1	(5-9.5)(90.5)	585-592	6434
35	B3A1	103-104.5	604.5-606	6692
36	B3A1	118.5-129	620-630.5	6891
37	B3A2	5.5-7	637.5-639	7120
38	B3A2-A4A	(22.5-24.5)(28-40)	654.5-669	7442
39	A4A	57-60.5	686-689.5	7795
40	A4A	62-65	691-694	7817
41	A4A	70-78.5	699-707.5	7913
42	A4A	86.5-87.5	715.5-716.5	8074

3.3) Sampling for radiocarbon analysis

Age estimates for the Nanerersarpik sediment record are based on 7 AMS radiocarbon samples of organic material taken from the core. Six of the samples of organic material were visually identified while the deepest sample was a mixture of organic material picked from a 1cm slice of hydrated sediment identified under a

microscope. The samples were analyzed at the Keck Carbon Cycle AMS Facility, Earth System Science Department, UC Irvine.

3.4) Non-destructive analysis:

3.4.1) Geotek core scanner

All split core sections were scanned on a Geotek Multi-Sensor Core Logger (MSCL) both at the University of Minnesota and at the University of Massachusetts, Amherst. Due to the coherency of the results only data from the core scanning at the University of Minnesota are reported here. Cores images were taken using a Nikon AF Nikkor 50mm f/1.8 D lens equipped with a Tiffen circular polarizer.

The core sections were also scanned for magnetic susceptibility using a Bartington MS2E surface scanning magnetic susceptibility sensor. Spectral reflectance was collected using a Konica Minolta CM-2600d Spectrophotometer with a MAV 8mm aperture. Scans were conducted at 0.5cm intervals.

3.4.2) Itrax XRF core scanner

All split core sections were also scanned on an Itrax XRF core-scanner (Cox Analytical Systems: http://coxsys.se/?cat=7) located at University of Massachusetts, Amherst. The Itrax provides elemental information as well as X-radiograph images. Cores were scanned at a resolution of 200 microns. X-radiograph and XRF settings for all runs are shown below in Table 3.2.

Table 3.2: Itrax XRF core scanner run settings

Voltage	Current	Exposure time	Step size	XRF exposure time	XRF voltage	XRF current	Tube
60kV	50 mA	1000ms	200microns	10 s	30 kV	55 mA	Mo

3.5) Discrete sample analysis:

3.5.1) Elemental Analyzer/Isotopic Ratio Mass Spectrometer (EA/IRMS) analysis

Discrete sediment samples were taken from the composite sediment record at 5cm intervals for biogeochemical analysis. Sediment was placed in glass vials, covered with Kim Wipes, and freeze-dried for 48 hours in a Virtis Freezmobile 12, 25, 35 Research Scale Freeze dryer. The samples were then homogenized using glass stirring rods cleaned in between each use with a three-step organic solvent rinse of increasing polarity (hexane, dichloromethane, methanol) to minimize contamination. Homogenized samples were then transferred to 50ml Falcon centrifuge tubes and acidified using 1M HCl to remove any carbonate. Samples were then diluted with de-ionized water and dried overnight in a 60°C oven. This process was repeated until a pH of 5 was reached.

Between 5 and 10 mg of freeze-dried and acidified sediment were weighed using an analytical mass balance and transferred to combusted silver capsules for bulk geochemical analyses. Modern vegetation samples collected in July of 2012 from SE Greenland were powdered using a mortar and pestle and also weighed and transferred to silver capsules for geochemical analysis. Total organic carbon content (TOC), total nitrogen content (TN), $\delta^{15}N$, and $\delta^{13}C$ were analyzed using a Costech ECS 4010 Elemental Analyzer interfaced with a Thermo Delta V Advantage isotopic ratio mass spectrometer. All isotopic ratio values are reported relative to VPDB for $\delta^{13}C$ and AIR for $\delta^{15}N$.

3.5.2) Biogenic Silica

3.5.2.1) *Sub-sampling scheme*

Biogenic silica (opal) concentrations were determined using a combination of traditional wet chemistry extractions (eg. Mortlock and Froelich, 1989) and less time-consuming Fourier Transform Infrared Spectroscopy (FTIRS) spectral analysis (Vogel et al., 2008; Rosén et al., 2010). 12 samples were analyzed traditionally to create a calibration model applied to samples measured using FTIRS. The 12 samples were selected as groups of 4 from 3 distinct sections of the core known to have varying amounts of total organic carbon to attempt to minimize model bias. Preliminary FTIRS biogenic silica analysis was carried out on the same samples taken for bulk geochemical analysis (5cm sampling interval). Two further rounds of biogenic silica analysis have also been completed on the upper 2m of the composite record to increase sampling density for the past ~3kyr BP to every centimeter.

3.5.2.2) *Traditional leaching method*

For biogenic silica analysis using the traditional extraction method the procedures utilized by the University of Minnesota were followed (http://lrc.geo.umn.edu/laccore/assets/pdf/sops/bsi.pdf).

Briefly, samples were combined with NaOH and placed in a hot water bath at 85° and aliquots removed at exact intervals of 5, 15, 30, 60, 90, 120, and 200 minutes. The digested samples were then combined with a Molybdate solution and reducing solution. Absorbance was then measured on a spectrophotometer at a wavelength of 812nm. Absorbance values were then converted to % biogenic silica according to the University of Minnesota procedure.

3.5.2.3) *Biogenic silica analysis using the FTIRS*

FTIRS can be used to calculated biogenic silica concentrations in sediments due to the fact that the vibrations in molecules containing polar bonds are excited by infrared (IR) radiation (Vogel et al., 2008). Different molecules are excited by IR radiation and absorb different wavelengths depending on the structure and atomic composition of that polar bond. Observed spectral absorbance at certain wavelengths is measured by a spectrophotometer and can be attributed to specific molecules.

For each sample 0.01g of sediment was freeze dried and homogenized. The sediment was then mixed with 0.5g of potassium bromide (KBr) using a mortar and pestle. KBr is spectrally neutral in the IR region and minimizes optical effects, such as distortion, that might influence the observed absorbance (Griffiths and De Haseth, 1986). FTIRS analysis was carried out using a Bruker Vertex 70 FTIR spectrometer with a diffuse reflectance attachment (Harrick Inc., USA). Data was collected for wavelengths between 2,666 and 25,000 nm (3,750- 400 cm^{-1}). A background scan of pure KBr was conducted during analysis every 12 samples on average to minimize instrument drift.

Measured FTIR spectra were then normalized using a baseline correction to correct for internal variations of the FTIRS that can cause baseline shifts or tilting of the measured spectra. By setting two points (3,750 and 2,210 cm^{-1}) equal to zero for each sample, a constant baseline is maintained. For Nanerersarpik Lake samples, peak areas from 1000 to 1150 cm^{-1} were integrated, which can be attributed to SiO (Farmer, 1974). This portion of the spectra was chosen because it is influenced by only a small number of other molecules, contains the maxima of SiO absorbance at 1,100cm^{-1}(Moenke, 1974; Vogel et al., 2008; Rosén et al., 2010), and provided the best agreement with the traditional method (see below).

3.5.2.4) *Biogenic silica calibration*

12 samples were analyzed using the traditional wet chemistry extraction method (after Morlock and Froelich, 1989). Due to contamination during the extraction process, only 10 samples were included in the calibration model. The 10 samples where BSi concentrations were measured were then plotted against measured FTIRS peak areas from the same samples to provide a linear regression equation relating measured % BSi from the traditional method and measured peak areas from the FTIRS (Figure 3.7). The linear regression provided a significant correlation with an r^2 of 0.91 and was applied to all BSi samples measured on the FTIRS.

3.5.3) Lipid geochemical analysis

15 samples were chosen from throughout the entire composite Nanerersarpik record for lipid biomarker analysis in the University of Massachusetts biogeochemistry laboratory. Samples were placed in Whirl-Pack sample bags, covered with Kim-wipes, frozen in a conventional freezer overnight and then freeze-dried for at least 48 hours. Samples were then homogenized in the sample bag to prevent outside contamination.

3.5.3.1) *Lipid extraction*

13 sediment samples, measuring between 3 and 10 grams, and taken from upper, organic-rich section of the composite Nanerersarpik core, were loaded into ASE cells for lipid extraction. Larger amounts of sediment (between 19 and 30 grams) were measured for 2 samples taken from the lower, more clastic section of the core due to the low organic content these sediments. A small amount of diatomaceous earth (~10% of total sediment sample) was added when loading ASE cells. Samples were then extracted using

a Dionex automated solvent extractor (ASE) with 60mL Ichem vials at a temperature of 100°C with a dichloromethane/methanol (9:1, v/v) mixture. The resulting Total Lipid Extract (TLE) was dried under a constant stream of N_2 gas using a TurboVAP. A small amount of 2:1 DCM:MeOH was then added to each sample and the TLE was transferred to 4mL vials. The TLE was then dried again using a TurboVAP and weighed to determine the mass of lipids extracted. 8 samples with large amounts of TLE (generally greater than 0.02g) were split in half so they could be accommodated by alumina oxide column chromatography.

3.5.3.2) *Alumina oxide column chromatography*

After extraction, the TLE was separated into polar (1:1 DCM:MeOH, v/v), ketone (1:1 DCM:Hexane v/v), and apolar (9:1 Hexane:DCM v/v) fractions using alumina oxide column chromatography. Alumina oxide columns consist of 5 ¾ inch glass Pasteur pipettes filled at the bottom with a small amount of packed quartz wool. The pipettes were then filled aprox. ¾ of the way with activated alumina oxide (heated at 150°C for two hours and allowed to cool for 1.5 hours) and rinsed with ~4ml of 9:1 Hexane/DCM (v/v). Three different solvent mixes (9:1 Hexane/DCM (v/v) for apolar fraction, 1:1 Hexane/DCM (v/v) for ketone fraction, and 1:1 DCM/MeOH(v/v) for polar fraction) were run through the column to separate the TLE. For each fraction, 1ml of the specific solvent mix was added to the TLE and then run through the column. This process was repeated 3 times for each fraction, resulting in 4 rinses total per fraction. A new 4mL vial was placed under the column for each fraction. Polar fractions were then filtered for analysis on a high-performance liquid chromatograph (HPLC) using a 0.45µm PTFE syringe filter with 99:1 hexane:propanol (v/v) and derivatized using 50µl of acetonitrile

and 50µl of bistrimethylsiyltrifluoroacetamide (BSTFA) at 60-70°C for one hour before analysis. 100µl of a squalene internal standard (concentration of 9.402µg/µl) was added to the ketone and polar fractions and 0.01µl of a C_{46} internal standard was added to all polar fractions.

3.5.3.4) *Compound identification and quantification*

Biomarker compounds were identified from the polar, apolar, and ketone fractions using a Hewlett Packard 6890 series gas chromatograph – mass spectrometer (GC-MS) equipped with a 5% phenyl methyl siloxane column (HP-5, 60m x 320µm x 0.25µm). The GC-MS used a temperature ramp which began at 70°C, and increased at a rate of 20°C min^{-1} to 130°C, and then increased at a rate of 4°C min^{-1} to 320°C. The final 320°C temperature was held constant for 20 minutes. Mass scans were made over the interval from 50 to 600 *m/z*. Compounds were identified based on their characteristic mass spectra fragmentation patterns, relative retention times taken from the gas chromatograph, and by comparison with literature.

Compounds were quantified using a Hewlett Packard 6890 series GC-flame ionization detector (GC-FID) equipped with the same capillary column as the GC-MS. The temperature program used for the GC-FID began at 70°C and then increased at a rate of 10°C min^{-1} to 130°C and then ramped at a rate of 4°C min^{-1} to 320°C for 10 minutes. Concentrations of individual compounds were calculated by comparing integrated peak areas with the peak area of the added squalene internal standard.

Polar fractions were also analyzed on an Agilent 1260 HPLC coupled to an Agilent 6120 MSD. Glycerol dialkyl glycerol tetraethers were identified and quantified using the methods of Hopmans et al. (2000) with some modifications (Schouten et al.,

2007). The HPLC utilized a Prevail Cyano column (150mm x 2.1mm, 3μm) using 99:1 hexane:propanol (v/v) eluent for separation. The eluent was increased linearly after 7 minutes up to 1.8% isopropanol for the next 45 minutes with a flow rate of 0.2mL min^{-1}. Scanning was carried out in selected ion monitoring (SIM) mode.

Nanersarpik Lake
-NAN-

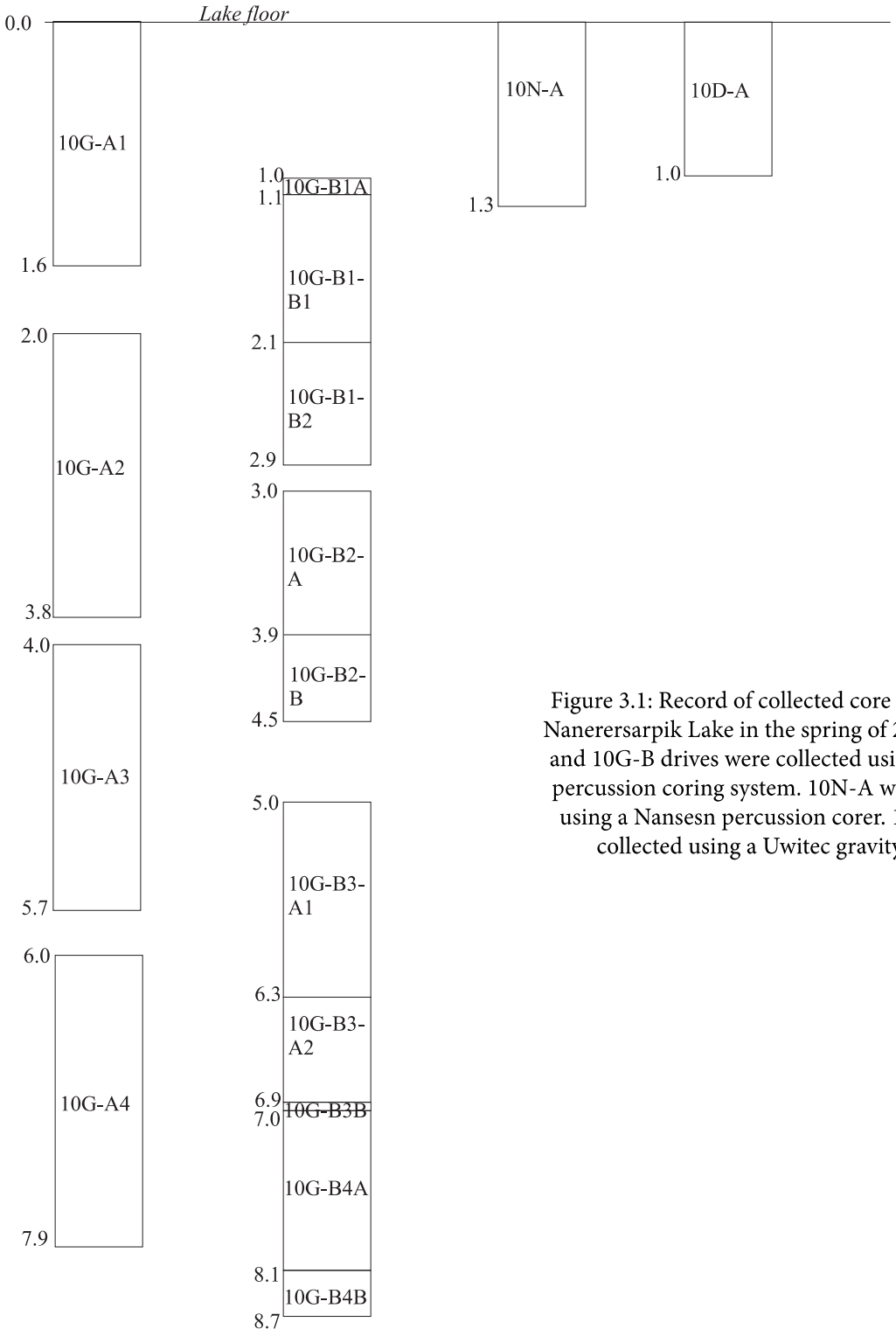

Figure 3.1: Record of collected core drives from Nanerersarpik Lake in the spring of 2010. 10G-A and 10G-B drives were collected using a Uwitec percussion coring system. 10N-A was collected using a Nansesn percussion corer. 10D-A was collected using a Uwitec gravity corer.

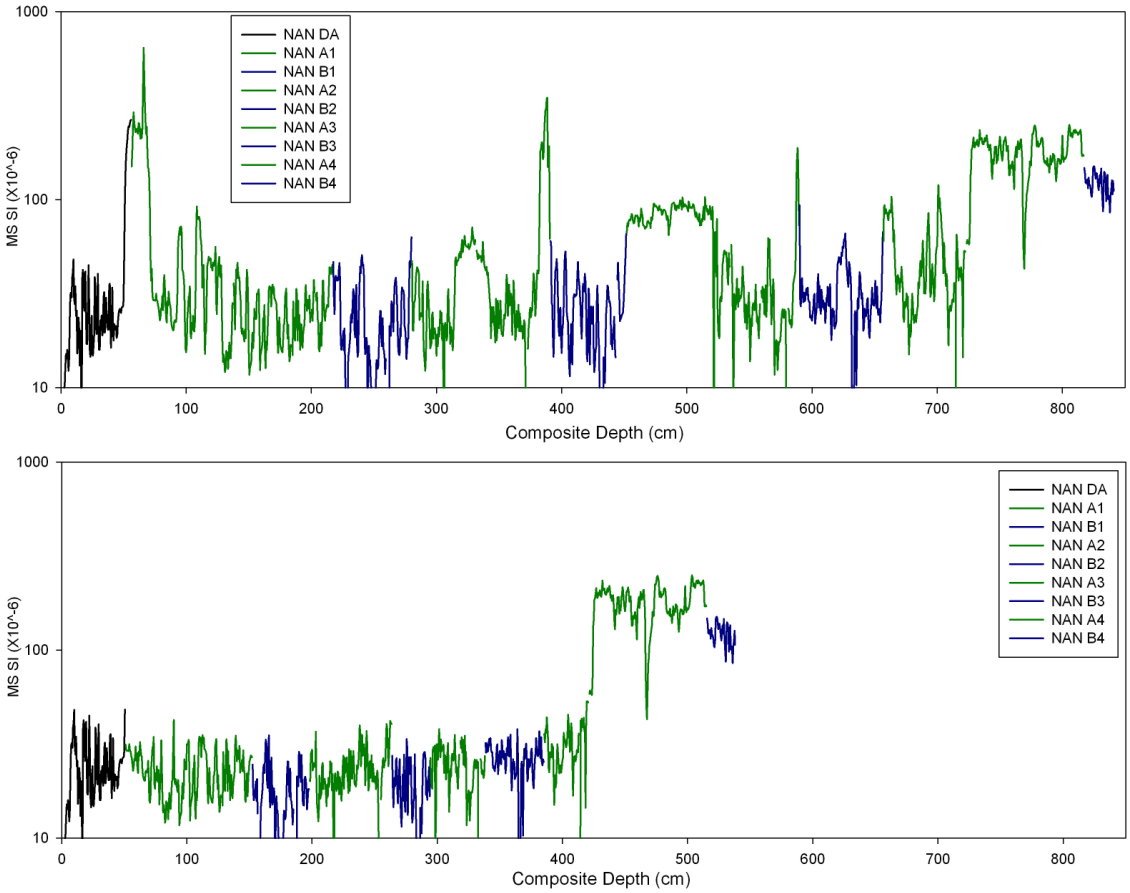

Figure 3.2: Magnetic susceptibility profiles for Daisy core section (black), A core sections (green) and B core section (blue) collected on a Geotek MSCL core scanner. Upper profile shows composite record with turbidites/ slump events (high MS). Lower profile shows composite record with these events removed, shortening the record by just over 3m. Note log scale on X axis.

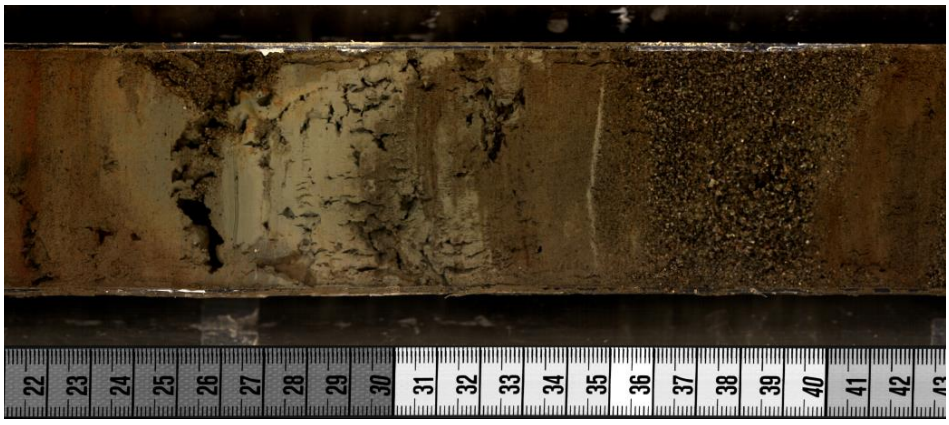

Figure 3.3: Typical fining upward sequence noted in turbidites/slump events found in Nanerersarpik Lake sediment record.

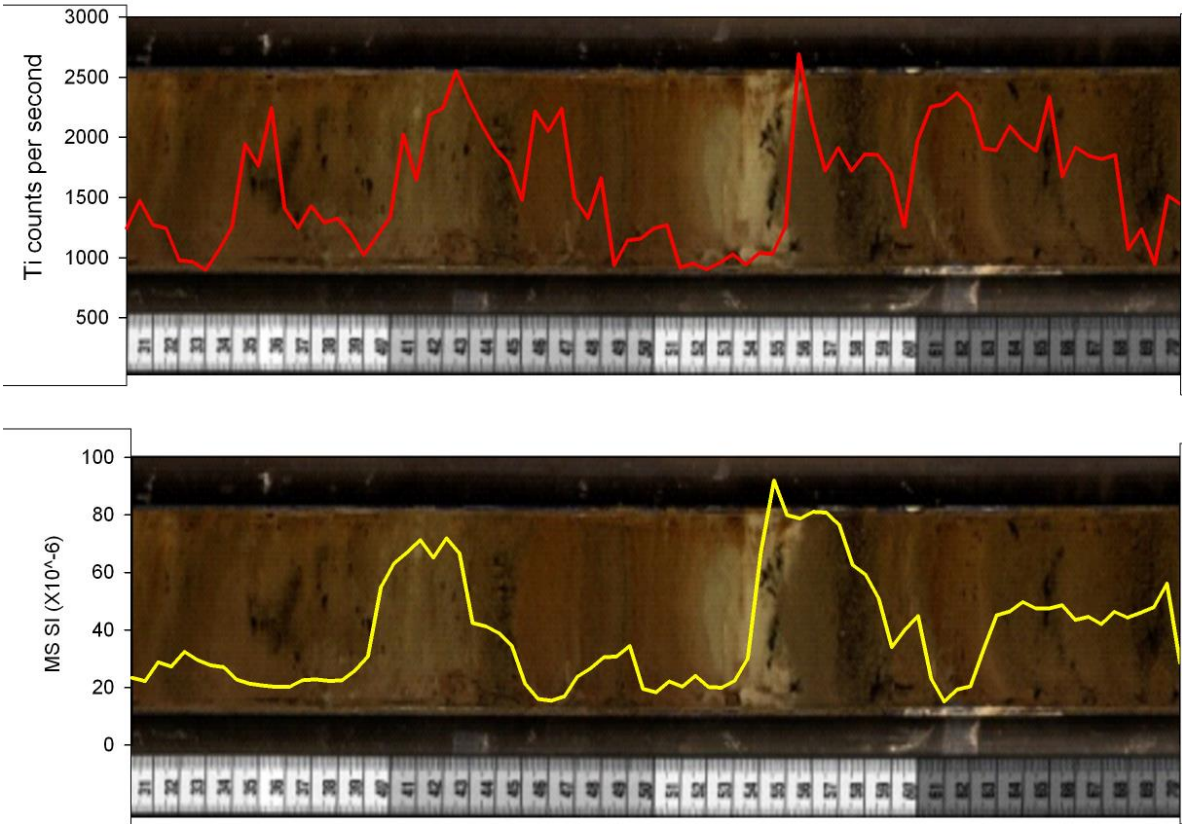

Figure 3.4: Characteristic Ti counts per second (upper panel, red line) and magnetic susceptibility (lower panel, yellow line) profiles for turbidites in the Nanerersarpik Lake sediment cores.

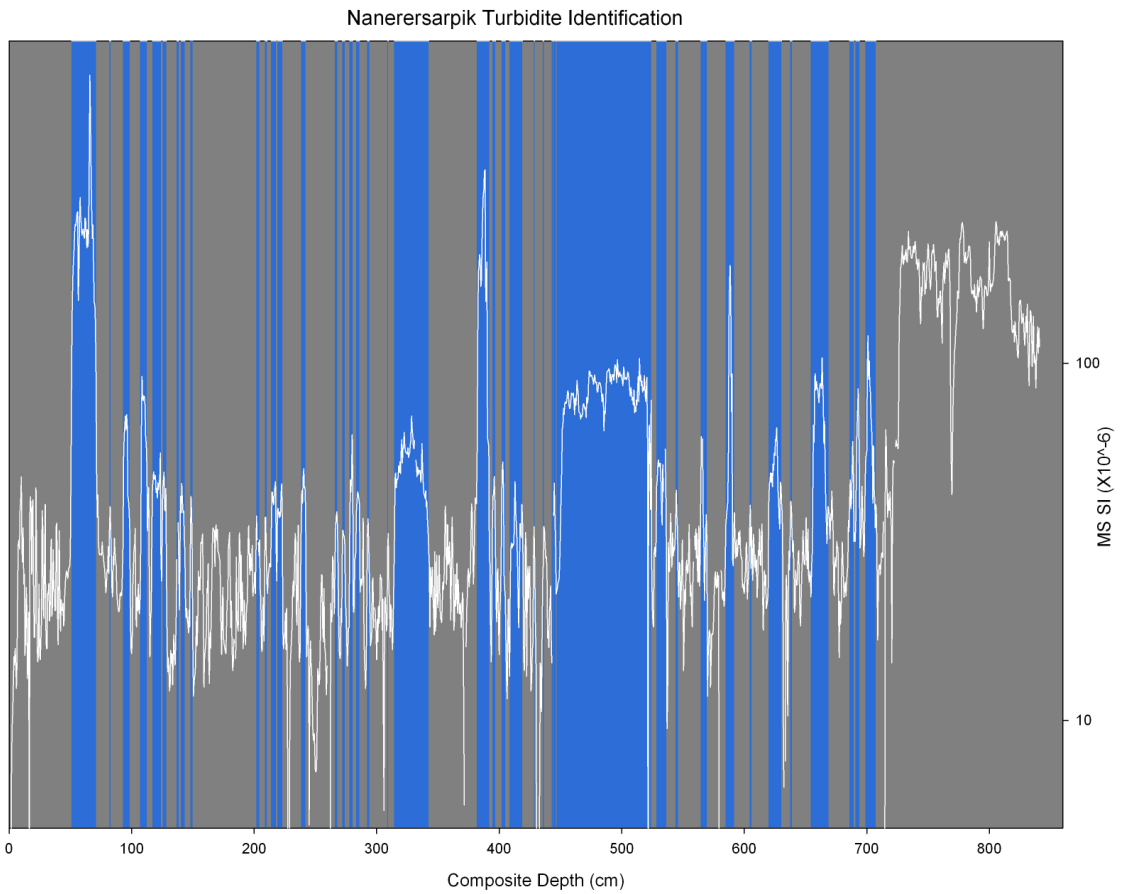

Figure 3.5: Composite Nanerersarpik Lake magnetic susceptibility profile with removed turbidites highlighted in blue (n=42). Note log scale on X axis.

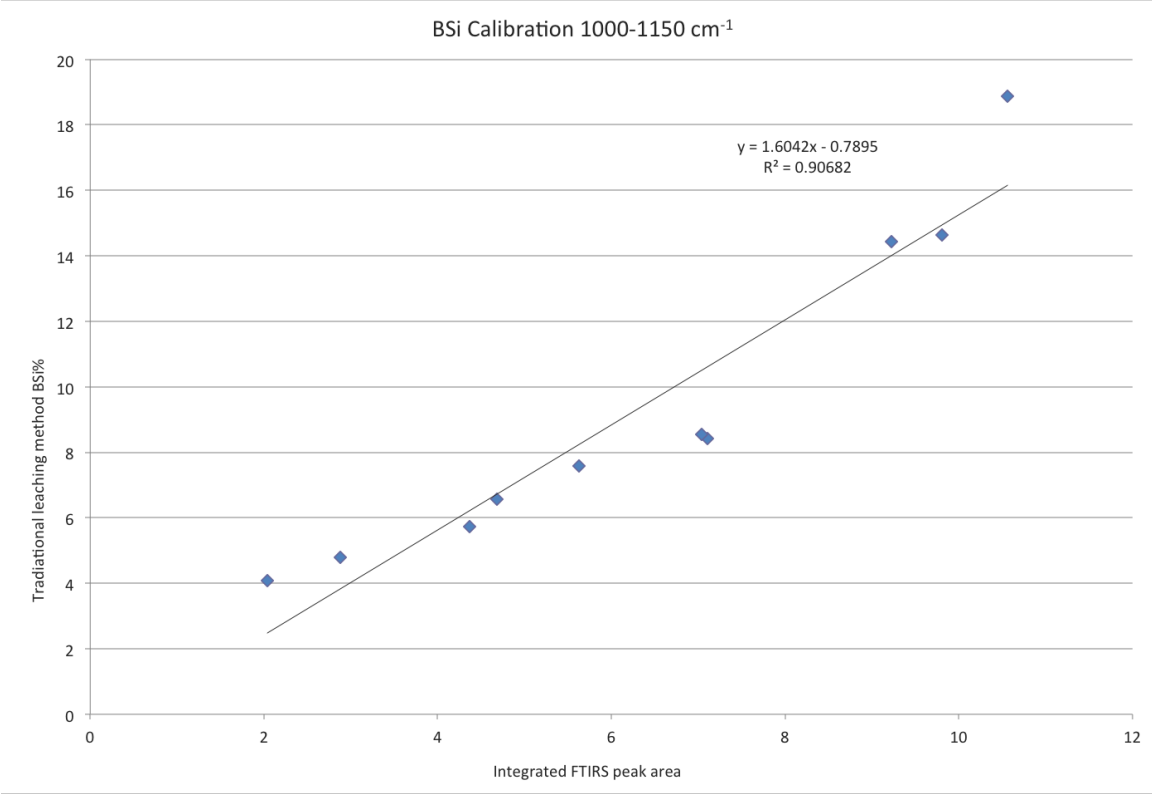

Figure 3.6: Linear regression model relating calculated BSi%s using the traditional leaching method (Mortlock and Froelick, 1989) and measured FTIRS peak areas. The resulting equation was applied to all measured FTIRS peak areas to determine BSi% downcore.

CHAPTER IV

RESULTS

4.1) Chronology

Seven AMS radiocarbon dated samples were used to create the age/depth model for the Nanerersarpik Lake sediment record (Table 4.1) (Figure 4.1). Two further radiocarbon ages on macrofossils were excluded from this analysis as they were taken from turbidites and returned older ages, stratigraphically above younger ages, and are interpreted as reworked material from the catchment. The model was created using CLAM modeling code (v.2.1, Blauw, 2010) for the open source software "R" (R Development Core Team, 2010). CLAM calculates a "best fit" curve based on the weighted average of 1000 iterations of age probability distributions. The 95% confidence intervals are based on 2σ range of the average of the iterations. Radiocarbon ages were calibrated using the northern hemisphere IntCal09.^{14}C calibration curve (Reimer et al., 2009). All ages are presented as calendar years before present (cal yr BP) or calendar thousand years before present (cal kyr BP).

As noted above, the Nanerersarpik lake sediment record contains numerous (~42) mass movement events such as slumps or turbidites. To account for the instantaneous nature of their deposition these mass movement events were removed prior to creating the age/depth model. Nanerersarpik's sedimentation rate is generally linear with a slight change in slope between samples at depths 149cm and 189.5cm. The oldest calibrated sample returned an age between ~7.6 and 8.2 cal kyr BP (95% confidence interval). This sample was taken from aprox. 20cm below a major lithologic boundary interpreted as the

transition from a glacio-fluvial system to normal lacustrine sedimentation (see below). This basal age suggests the transition occurred sometime just prior to 8.2 cal kyr BP.

Table 4.1: Radiocarbon dating sample results

Sample ID	Composite core depth (cm)	^{14}C age	^{14}C age error	Minimum Age (cal yr BP)	Maximum Age (cal yr BP)	Probability (%)
NAN10DA	39	610	20	579	652	75.2
NAN10GA1	106.5	1690	20	1537	1628	82.8
NAN10GA1	149	2420	40	2348	2543	70.7
NANB1B2	189.5	2480	20	2466	2622	64.3
NAN10GA2	240.5	3435	20	3636	3725	84.3
NAN10GA3	319	5255	20	5935	6024	64.1
NAN10GA4	408.5	7120	130	7686	8182	95

Analyses of calculated accumulation rates (yr/cm) are hampered by the presence of only 7 dating points, which produces unrealistic, angular changes in accumulation rate (Figure 4.2). Broadly, however, accumulation rates during the earliest part of the Holocene were high (~0.05 cm yr^{-1}). A decrease in accumulation rate is recorded beginning at ~6 cal kyr BP to the lowest values of the entire record (~0.034 cm yr^{-1}). It then rose to Early Holocene levels around 3.7 cal kyr BP, and continued to increase to the highest rates of the entire record (apart from one short-lived maxima at ~2.5 cal kyr BP) by 1.5 cal kyr BP. A small decrease in accumulation rate is recorded over the last ~600 years.

4.2) Sediment Composition and Geotek Core Scanner Data

The sediment record from Nanerersarpik Lake over the Holocene consists broadly of two major sedimentary units: a dense, minerogenic, gray clayey silt (bottom ~1m) (Figure 4.3) defined here as Unit A, and laminated organic-rich gyttja (upper 4.5m) (Figure 4.4) defined as Unit B. These two facies represent dramatically different sedimentary environments at Nanerersarpik Lake and are indicative of the largest scale change in paleo-environment in the catchment.

Unit A) 10.7? - 8.25cal kyr BP

Unit A consists of a gray clayey silt facies with highly variable grain sizes ranging up to gravel and pebbles. Magnetic susceptibility is multiple orders of magnitude higher in Unit A relative to Unit B (~300 vs. ~25 SI $x10^{-6}$). It is also more dense and compact than the organic rich facies above it (Figure 4.5). It should be noted that although an AMS radiocarbon date just above the stratigraphic transition from Unit A to Unit B constrains the upper age of this sedimentary unit, no dated samples were recovered from this section and therefore the calculated sedimentation rates and extrapolated age for the base of Unit A must be treated with caution.

Unit B) 8.25 cal kyr BP- Present

Unit B encompasses the entirety of normal pelagic sedimentation at Nanerersarpik Lake. The beginning of this interval is marked by an abrupt facies change from the clastic material of Unit A to laminated brown organic-rich sediment that continues without a major facies change through the top of the core. Throughout this section both MS and

bulk density display high frequency but low amplitude variations. In general MS remains relatively much lower than Unit A, but does not reach a value of zero suggesting some background level of magnetic material input to the lake (Figure 4.5).

4.3) Scanning XRF data)

The Itrax XRF scanner located at University of Massachusetts, Amherst, identifies elements based on their response to excitation by X-rays. Different elements emit characteristic wavelengths of fluorescence which are detected by the Itrax (e.g. Spofforth et al., 2008). Elemental intensities are then reported as counts per second. The Itrax is outfitted with a 3 kW Molybdenum target tube to generate X-rays, which allows for identification of a wide range of elements ranging from Al to Pb. Interpretation of elemental counts can vary on a lake to lake basis. Generally however, certain elements can be attributed to characteristic sources, e.g. Ti to a clastic, terrigenous source. Ti, K, Mn, and Si have been shown to be terrestrially sourced in some lakes and linked to erosional parameters (eg. Olsen et al., 2012). Broadly, most terrestrial elements correspond well with each other, although they do display different relationships in the very bottom of the core (blue circles in Figure 4.6)

4.3.1) Unit A

Due to the highly clastic nature of Unit A, titanium, potassium, calcium, and manganese all have maximum counts per second during this interval (Figure 4.7). Fe counts are consistently much lower in Unit A than the rest of the record, while S counts are generally also low with some variability. Si counts are highest in Unit A but display a

decreasing trend through time (Figure 4.8). These results suggest a highly erosive environment during this time, with little organic matter accumulation.

4.3.2) Unit B

Ti and Mn counts display a slowly increasing trend until about 7 cal kyr BP and then decline through the rest of the Early Holocene. Increases are recorded beginning around 6 cal kyr BP, culminating in maxima around 3.6 cal kyr BP. During the Late Holocene minima occur at ~3 and 1.7 cal kyr BP, with maxima at 2.6, 1.2 and 0.7 cal kyr BP. Ca and K concentrations follow a generally similar signal, with a notable Ca exception centered on 1.8 cal kyr BP and two positive K excursions at 7.5 and 0.7 cal kyr BP (Figure 4.7). Si decreases slowly from maxima in Unit A and remains low with little variability throughout most of the rest of the Holocene with a notable increase at 1.7 cal kyr BP. Both Fe and S concentrations increase from Unit A to Unit B, with more variation recorded in the S record (Figure 4.8). It should be noted however, that sulfur counts are extremely low in the composite core which could lead to decreased measurement accuracy.

4.4) Biogeochemical Data

The accumulation of organic matter in lakes provides an important link to past productivity both in the lake and the surrounding catchment. Generally, the vast majority of organic material preserved in lake sediments comes from plants, either non-vascular organisms like phytoplankton, or vascular plants such as grasses and trees (Meyers and Lallier-Vergés, 1999). Proxies such as the weight percent of organic carbon (TOC) and weight percent of nitrogen (TN) can shed light on the amount of primary

productivity occurring in the lake and catchment (albeit potentially also affected by other factors, such as transport and preservation). TOC is commonly used in high latitude paleo-limnology studies where small changes in temperature and/or precipitation can dramatically affect vegetation both in the catchment and in-situ (e.g. Kaplan et al., 2002; Perren et al., 2012; Axford et al., 2013). Carbon and nitrogen isotopic values, as well as the ratio of TOC/TN (C/N) can help determine the source of organic matter preserved in lake sediments (Meyers and Ishiwatari, 2003). All C/N values presented here have been multiplied by 1.167 to account for the ratio of atomic weights of nitrogen and carbon and are therefore atomic C/N ratios (Meyers and Teranes, 2001). Phytoplankton generally have low C/N ratios (4-10), while vascular plants have C/N ratios of 20 or greater (Meyers and Lallier-Vergés, 1999). Generally, lacustrine algae and C_3 land plants have similar $\delta^{13}C$ values ranging from -30‰ to -25‰ (Meyers and Ishiwatari, 1993).

4.4.1) Unit A

Unit A is characterized by low to non-existent values of total organic carbon and total nitrogen (Figures 4.9 & Figure 4.10). $\delta^{13}C$ values are relatively less negative in Unit A versus Unit B, varying between -23‰ and -26‰. $\delta^{15}N$ values record limited variations, with maxima just above 0‰ and minima of ~-3.6‰ Due to the lack of organic material in this section of the core the isotopic values presented here must be treated with caution and are generally not used in climate interpretations.

4.4.2) Unit B

Unit B is characterized by higher concentrations of all primary productivity biogeochemical proxies than in Unit A. Total organic carbon weight percent (TOC) during this interval is highly variable, with the greatest concentrations reaching just over

5% and low values of approx. 1.7%. Initially TOC increases above the transition from Unit A from near zero values at 8.25 cal kyr BP to an Early Holocene maximum of ~4.6% by 7.1 cal kyr BP. Organic carbon concentrations then decrease throughout the mid-Early Holocene, reaching values just under 2.5% by 5.5 cal kyr BP. TOC then slowly increases over the next 2 thousand years to just over 5%. A steep decline is then noted, with the lowest value of Unit B (1.7%) recorded at ~1.75 cal kyr BP. High variability dominates the TOC signal of the Late Holocene, with values ranging from 2-5.2%. The $\delta^{13}C$ record is also highly variable through Unit B, ranging from -28.7‰ to -23‰ with one excursion to ~-18.7‰. Generally isotopically light values are accompanied by high TOC percentages, with a notable exception at ~1.75 cal kyr BP (Figure 4.9)

Nitrogen weight percent (TN) is also highly variable within this unit, ranging from 0.04% up to 0.59% (Figure 4.10). Nitrogen concentrations increase sharply at the base of Unit B just above the facies transition. They then decrease slightly and remain relatively lower during much of the next 4,000 years until about 3.2 cal kyr BP when they increase to ~0.38‰ and remain variable throughout the rest of the record. A distinct increasing trend in TN is seen over the last 230 years. $\delta^{15}N$ values from the beginning of Unit B (~8.25 cal kyr BP) until ~4 cal kyr BP record high variability, with some values at or just above 0‰, while others reach heavily depleted values of -8.5‰ with one data point of -21‰. After 4 cal kyr BP $\delta^{15}N$ stabilizes somewhat, with most values falling at or just above 0‰ with only three samples depleted to ~-5‰.

4.5) Biogenic silica

Biogenic silica (BSi) is an amorphous form of silicon, formed through biogenic precipitation by siliceous organisms such as diatoms, radiolarians, and sponges and has been shown to be an accurate measure of the past abundance of siliceous microfossil abundances in lakes (Conley, 1988). BSi has proved to be a useful lacustrine primary productivity proxy on long time scales (Williams et al., 1997; Colman et al., 1999; Rosén et al., 2010). It has been shown to vary on short time scales with temperature and hasbeen calibrated as a proxy for summer temperature (Blass et al., 2007; McKay et al., 2008).

4.5.1) Nanerersarpik biogenic silica record

Calculated biogenic silica concentrations for the Nanerersarpik Lake record are presented in Figure 4.11. BSi values increased rapidly from zero in Unit A to nearly 13% by 7.7cal kyr BP. Opal concentrations were highly variable during the Early Holocene, with maxima at 6.2 cal kyr BP (15.5%) and at 3.4 cal kyr BP (18.4%). The lowest value of this period was recorded at 5 cal kyr BP (just over 2%). It should be noted that during this Early Holocene interval the sampling resolution for BSi is every 5cm, and likely does not capture the full range of variability from this period.

During the Late Holocene BSi values were also highly variable, with the highest and lowest concentrations of BSi separated by ~200 years. From high values approx. 3.4 cal kyr BP, BSi decreased with high frequency fluctuations until ~1.5 cal kyr BP. Opal concentrations then increased rapidly to theesecond highest concentration seen in the entire record (~21%) by 1.3cal kyr BP. From this peak, they declined until about 250 cal yr BP, reaching the lowest concentration in Unit B at this time (1%). A sharply increasing trend over the more modern period culminates in the highest values of the entire record (>25%) at 60 cal yr BP.

4.6) Organic biomarker results

15 sediment samples from the Nanerersarpik Lake record were analyzed for lipid biomarkers. To date, aliphatic hydrocarbons (*n*-alkanes), long chain 1,15 *n*-alkyl diols, long-chain alkenones, and glycerol dialkyl glycerol tetraethers have been identified and quantified from the processed total lipid extracts.

4.6.1) Polar fraction analysis

½ of the polar fraction of the TLE for 15 samples from Nanerersarpik Lake was analyzed on the HPLC in the University of Massachusetts biogeochemistry laboratory to determine concentrations of both isoprenoid glycerol dialkyl glycerol tetraethers (GDGTs) and branched glycerol dialkyl glycerol tetraethers (brGDGTs) (Figure 4.12). Isoprenoid GDGTs are membrane lipids synthesized by a wide range of Archea. BrGDGTs are thought to be produced mainly by anaerobic soil bacteria, although it is possible they are produced in lakes as well.

While absolute concentrations of these compounds can be meaningful, generally ratios or indices of different concentrations of GDGTs are more relevant. The Branched and Isoprenoid Tetraether (BIT) index compares the relative abundance of soil derived (branched) GDGTs against GDGT IV (Crenarcheol) and can be used as a proxy of terrestrial vs. aquatic input (Castañeda and Schouten, 2011). BIT index values range from 0-1, 1 indicating a purely terrestrial source, 0 being purely aquatic. Nanerersarpik BIT Index values are shown in Figure 4.13, suggesting a dominantly terrestrial biomarker source.

BrGDGTs can also be analyzed based on the Cyclisation of Branched Tetraethers (CBT) and the Methylation of Branched Tetraethers (MBT). CBT is interpreted as a proxy for soil pH based on empirical observations. MBT is influenced primarily by soil temperature, and somewhat by soil pH. Temperature reconstructions using brGDGTs therefore take into about both MBT and CBT and are based on calibration sets of globally distributed soils (Table 4.2, modified from Castañeda and Schouten, 2011). MBT/CBT temperature estimates based on published calibrations are shown in Figure 4.14. Generally, MBT/CBT shows little variance in temperature over the Holocene at Nanerersarpik, with all three calibrations producing similar trends.

Table 4.2: GDGT calibration data sets and transfer functions

Calibration Equation	*n*	r^2	Geographical location	Reference
CBT = 3.33-0.38 x pH	134	0.7	Global soils	Weijers et al. (2007b)
MBT = 0.122 + 0.187 x CBT + 0.020 x MAAT	134	0.7	Global soils	Weijers et al. (2007b)
MAAT = 50.47 -74.18 x (*f*GDGTIII) – 31.60 x (*f*GDGTII) – 34.69 x (*f*GDGTI)*	38	0.94	East Africa	Tierney et al. (2010b)
T = 6.803 – 7.062 x CBT + 37.09 MBT	139	0.62	Global lakes	Sun et al. (2011)
T = 47.4 – (20.9x GDGT I) – (37.1 x GDGT II) – (53.5 x GDGT III)	90	0.88	Scandinavian lakes	Pearson et al. (2011)

* "*f*" denotes the fractional abundances of the brGDGTs relative to the *total* brGDGTs.

Other polar compounds beyond GDGTs are also of interest when analyzing lake sediments. Sterols, and their saturated counterparts, stanols, can have varying numbers and locations of double bonds, alternate positions of methyl groups, and different carbon numbers, all of which can be indicative of certain groups of organisms (Castañeda and Schouten, 2011). Dinostanol is found in many dinoflagellate species and has been used as to characterize concentrations of dinoflagellates in lake sediments (Volkman, 2003).

Loliolide (and its counterpart isololiolide) are anoxic degradation products of a pigment present in diatoms and have been used as biomarkers of diatom abundance. Similarly long-chain alkenones are known to be produced by haptophyte algae and can also be used a biomarker. Results for the abundances of these compounds, as well as the relative abundance of each organism, are presented in Figures 4.15 and 4.16.

4.6.2) A-polar fraction analysis

Within the apolar fraction of the TLE, aliphatic hydrocarbons (*n*-alkanes) are simple straight chain hydrocarbons that vary in length based on source organism. Longer chain *n*-alkanes (C_{27} – C_{35}) are found in the leaf waxes of higher plants. Mid chain length *n*-alkanes (C_{23} –C_{25}) are found in emergent aquatic plants, while their short chain (C_{17} – C_{21}) homologues are characteristic of aquatic algae. The concentrations of these compounds, and associated ratios and indices, are indicative of the source of organic material in sediments (Castaneda and Schouten, 2011). *N*-alkane data from Nanerersarpik Lake are shown in Figure 4.16. Long-chain n-alkanes are dominant throughout the record and also suggest terrestrially-sourced organic matter.

4.6.3) Ketone fraction analysis

Within the ketone fraction of the TLE, long-chain alkenones (LCAs) were identified in Nanerersarpik Lake sediments. LCAs are composed of C_{37}-C_{39} di, tri, and tetra-unsaturated methyl and ethyl ketones (Figure 4.18) and are produced by haptophyte algae. The ratio of the abundance of these alkenones varies depending on temperature (increasing tri-unsaturated ketone with increasing temperature) and can be analyzed as a paleo-temperature proxy. Similar to the MBT/CBT proxy described above, temperature reconstructions are based on calibrated data sets utilizing globally distributed data. This

relationship of alkenone concentration and temperature is described by the U^{k}_{37} Index first described by Brassell et al. (1986). Subsequent variations have been introduced, and different transfer functions calculated based on new calibration data. Presented in Figure 4.19 are alkenone based temperature reconstructions using two marine calibrations (Muller, 1998; Conte, 2006) and 3 lake-based calibrations (Zink et al., 2001; Chu et al., 2005; D'Andrea et al., 2011). The lake based calibrations use the U^{k}_{37} index while the marine calibrations use the $U^{k'}_{37}$ index which does not include the $C_{37:4}$ ketone (equations shown in Table 4.3, modified from Castañeda and Schouten, 2011). Alkenones from Nanerersarpik sediments generally contain all 3 ketones, likely making the U^{k}_{37} the most applicable (Figure 4.20).

$U^{k}_{37} = (C_{37:2} - C_{37:4}) / (C_{37:2} + C_{37:3} + C_{37:4})$

$U^{k'}_{37} = (C_{37:2}) / (C_{37:2} + C_{37:3})$

Table 4.3: Alkenone temperature transfer functions

Calibration equation	*n*	r^2	Calibrated to	Geographical location	Reference
$U^{k}_{37} = 0.0211T-0.725$	9	0.68	Summer lake temp	Germany	Zink et al. (2001)
$U^{k'}_{37}= 0.0328T + 0.126$	38	0.83	Mean annual air temp	China	Chu et al. (2005)
$T = 39.9U^{k}_{37} + 36.418$	21	0.75	*in-situ* water temp	Lake George, North Dakota	Toney et al. (2010)
$T = 40.8\ U^{k}_{37} + 31.8$	34	0.96	*in-situ* water temp	Braya Sø (Greenland)	D'Andrea et al. (2011)
$U^{k'}_{37}= 0.033T + 0.044$	370	0.98	Annual mean SST	Global marine	Müller et al. (1998)
$(T = -0.957 + 54.293(U^{K'}_{37}) - 52.894(U^{K'}_{37})^2 + 28.321(U^{K'}_{37})^3$	576	0.97	Annual mean SST	Global marine	Conte et al. (2006)

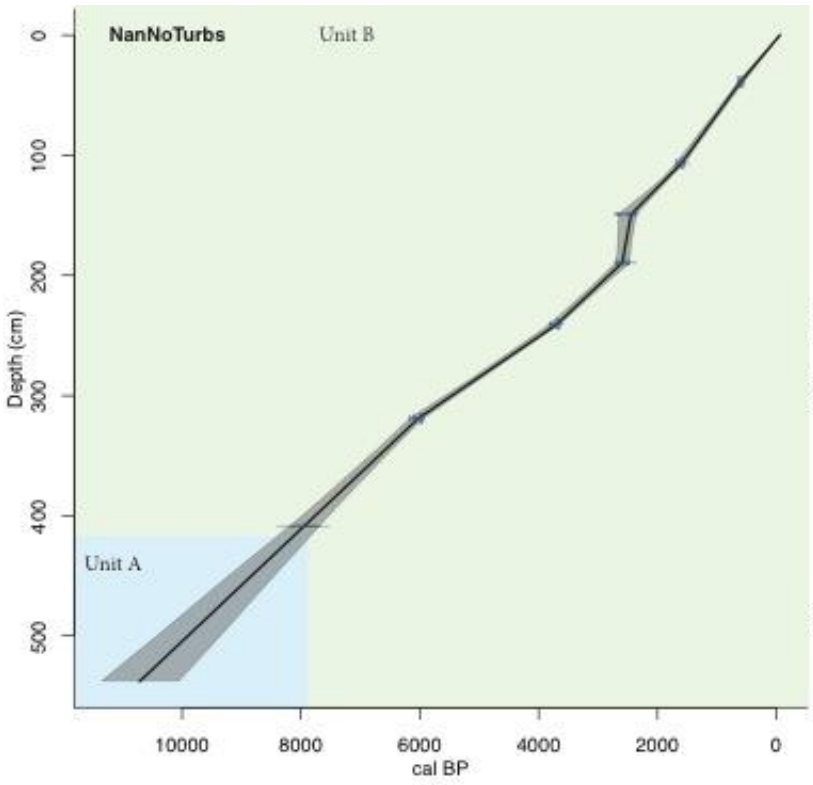

Figure 4.1: Nanerersarpik Lake age model

Age model is based on 7 AMS radiocarbon dates taken from macrofossils within the core. The model was created using CLAM modeling software (v.2.1, Blauw, 2010) and radiocarbon ages were calibrated using the northern hemisphere IntCal09.14C calibration curve (Reimer et al., 2009). Nanerersarpik's sedimentation rate is generally linear with a slight change in slope between samples at depths 149cm and 189.5cm.

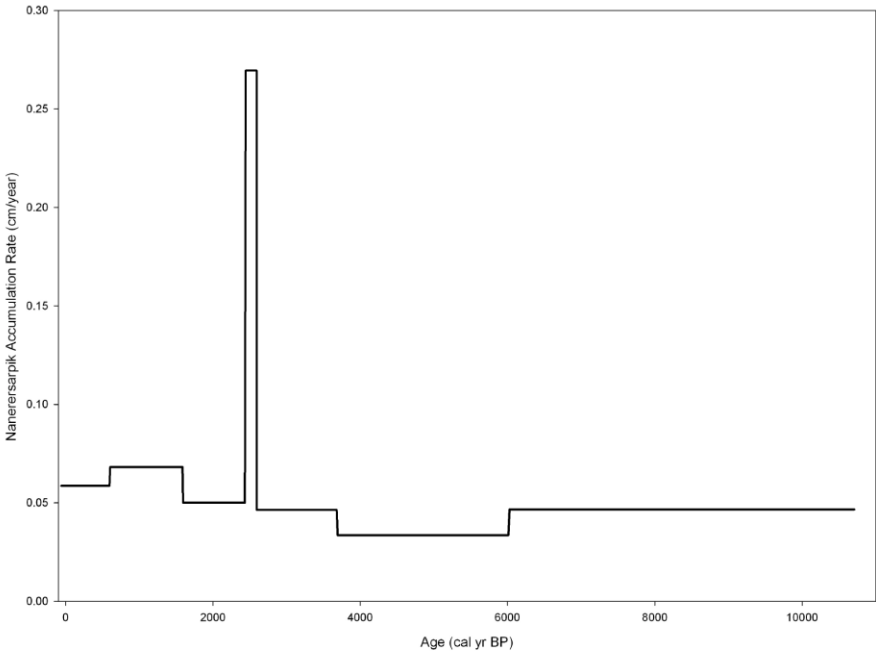

Figure 4.2: Nanerersarpik sediment accumulation rate

The presence of only 7 dating points creates unrealistic, angular changes in accumulation rate. Generally, however, accumulation rates at Nanerersarpik have been similar over the course of the Holocene with a notable exception at 2.5 cal kyr BP.

Figure 4.3: Characteristic core image of sediment Unit A from Nanerersarpik Lake.
Unit A consists of dense, minerogenic clayey silt with high magnetic susceptibility.

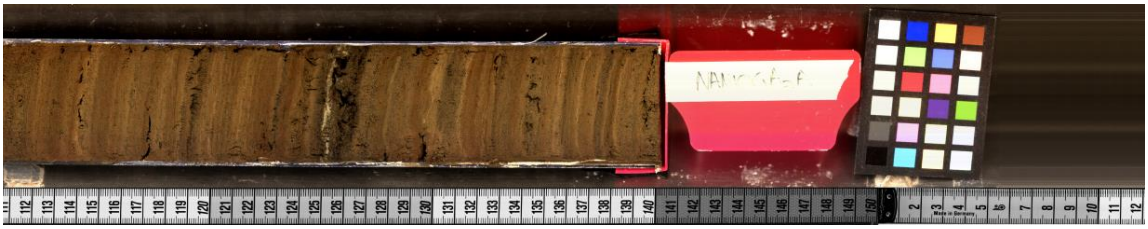

Figure 4.4: Characteristic core image of sediment Unit B from Nanerersarpik Lake.
Unit B is a laminated organic rich gyttja with low magnetic susceptibility.

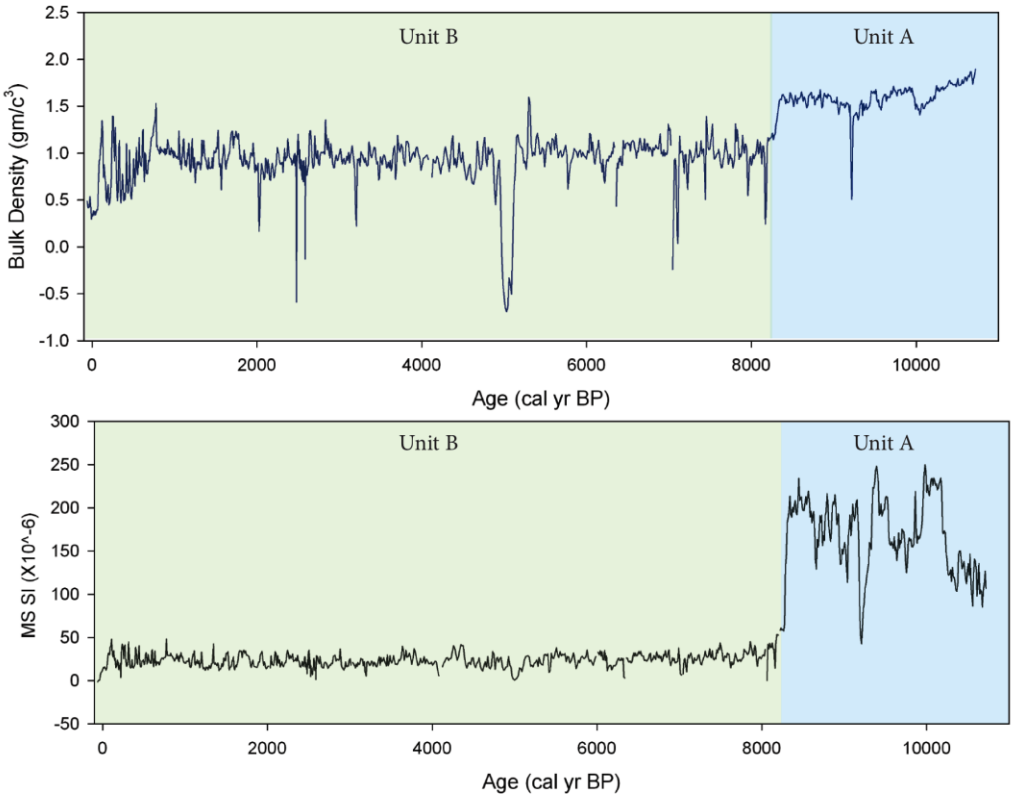

Figure 4.5: Bulk density and magnetic susceptibility values from the composite Nanerersarpik Lake record.
Note much higher values for both bulk density and MS in Unit A relative to Unit B.

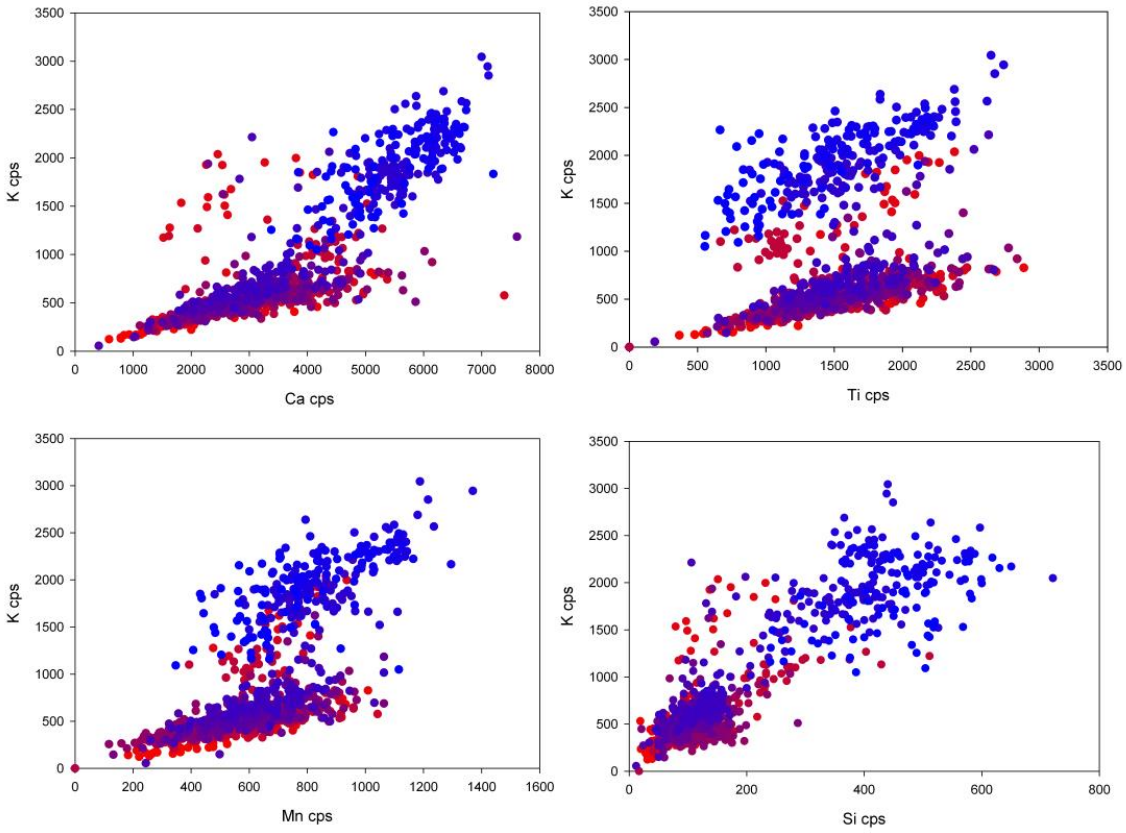

Figure 4.6: Correlations of terrestrial elements from Nanerersarpik Lake as recorded by the Itrax core scanner. Circles grade in color by depth from the top of the core (red) to the bottom of the core (blue).

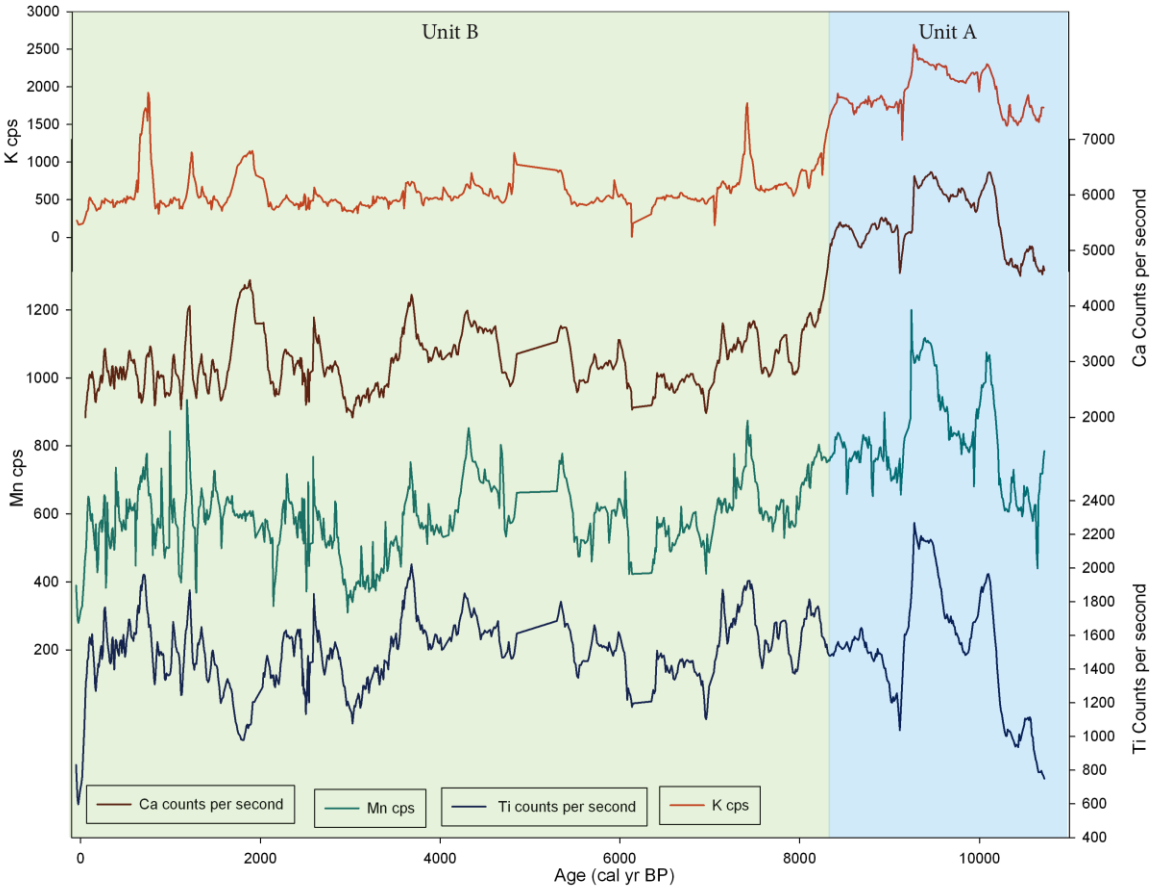

Figure 4.7: Scanning XRF profiles of clastic minerals from Nanerersarpik sediment core
Note high values in Unit A, high variability in Unit B.

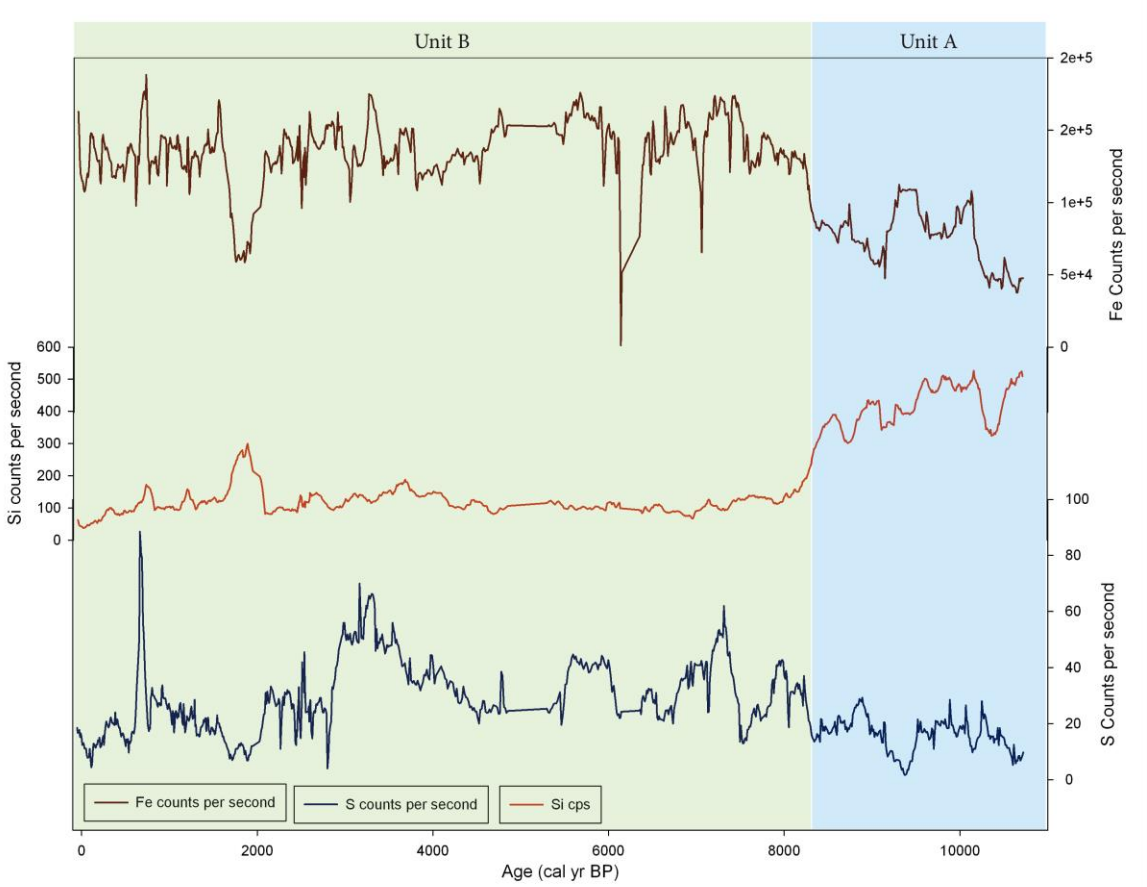

Figure 4.8: Scanning XRF profiles of iron, sulfur, and silicon from Nanerersarpik sediment core.

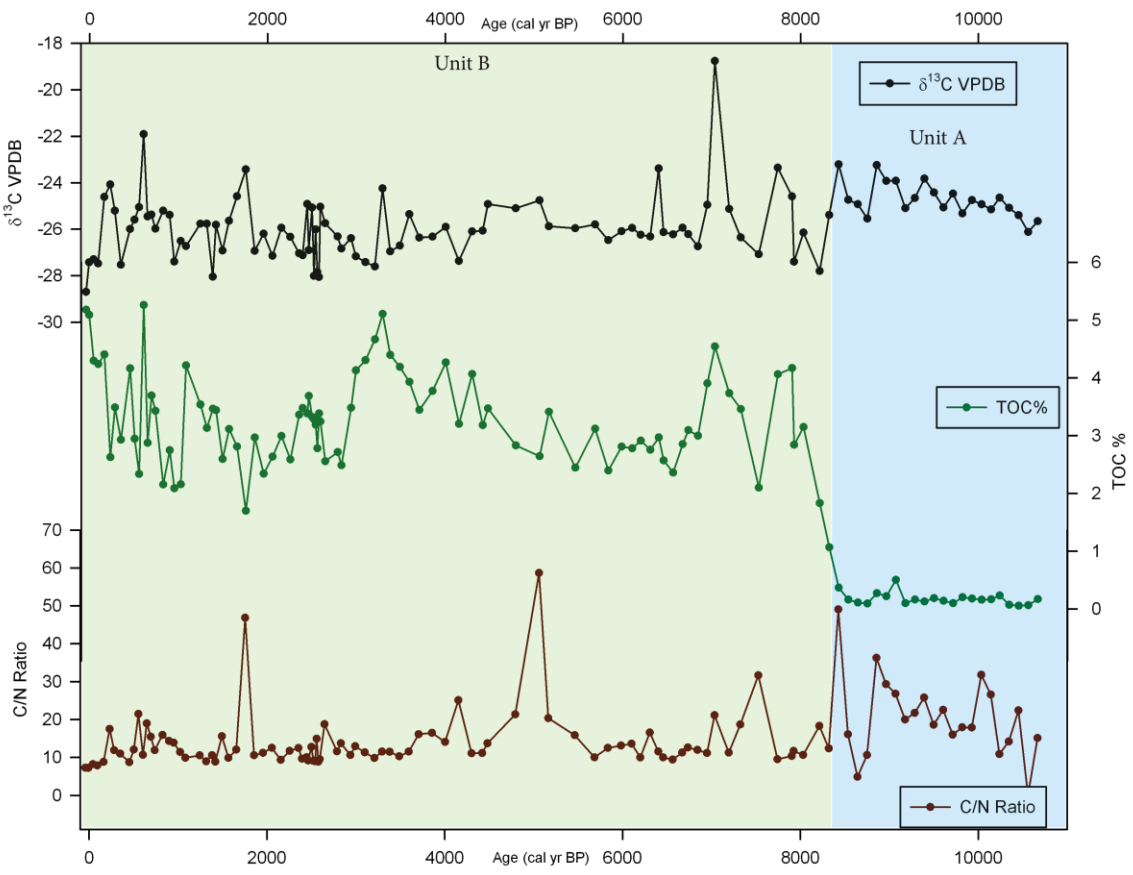

Figure 4.9: Bulk carbon geochemical data
TOC% is just above 0 in Unit A and is highly variable in Unit B, ranging from ~1.7%-5%. The $\delta^{13}C$ record is also highly variable through Unit B, ranging from -28.7‰ to -23‰ with one excursion to ~-18.7‰. Generally isotopically light values are accompanied by high TOC percentages, with a notable exception at ~1.75 cal kyr BP.

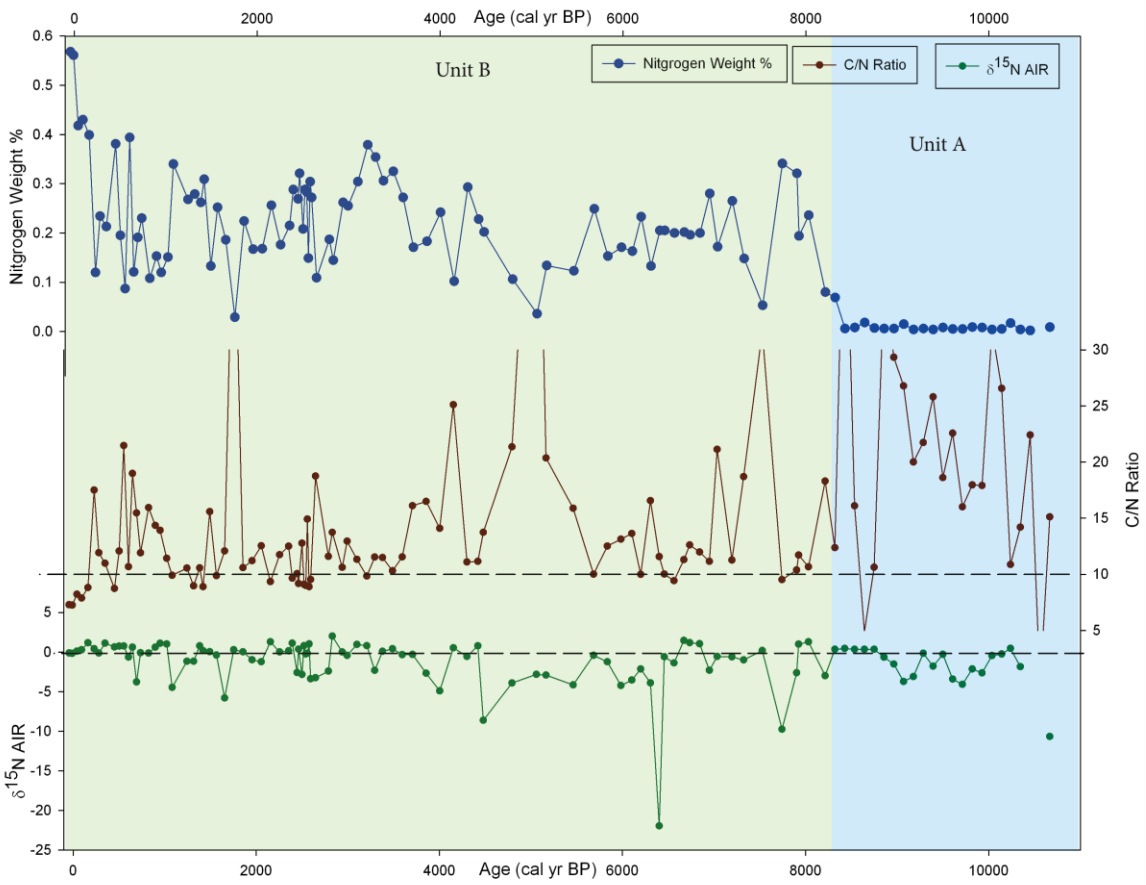

Figure 4.10: Bulk nitrogen geochemical data
Dashed line at 10 in C/N ratio denotes boundary of mainly algal versus vascular plants.
Dashed line at 0‰ in $\delta^{15}N$ plot denotes atmospheric nitrogen value.

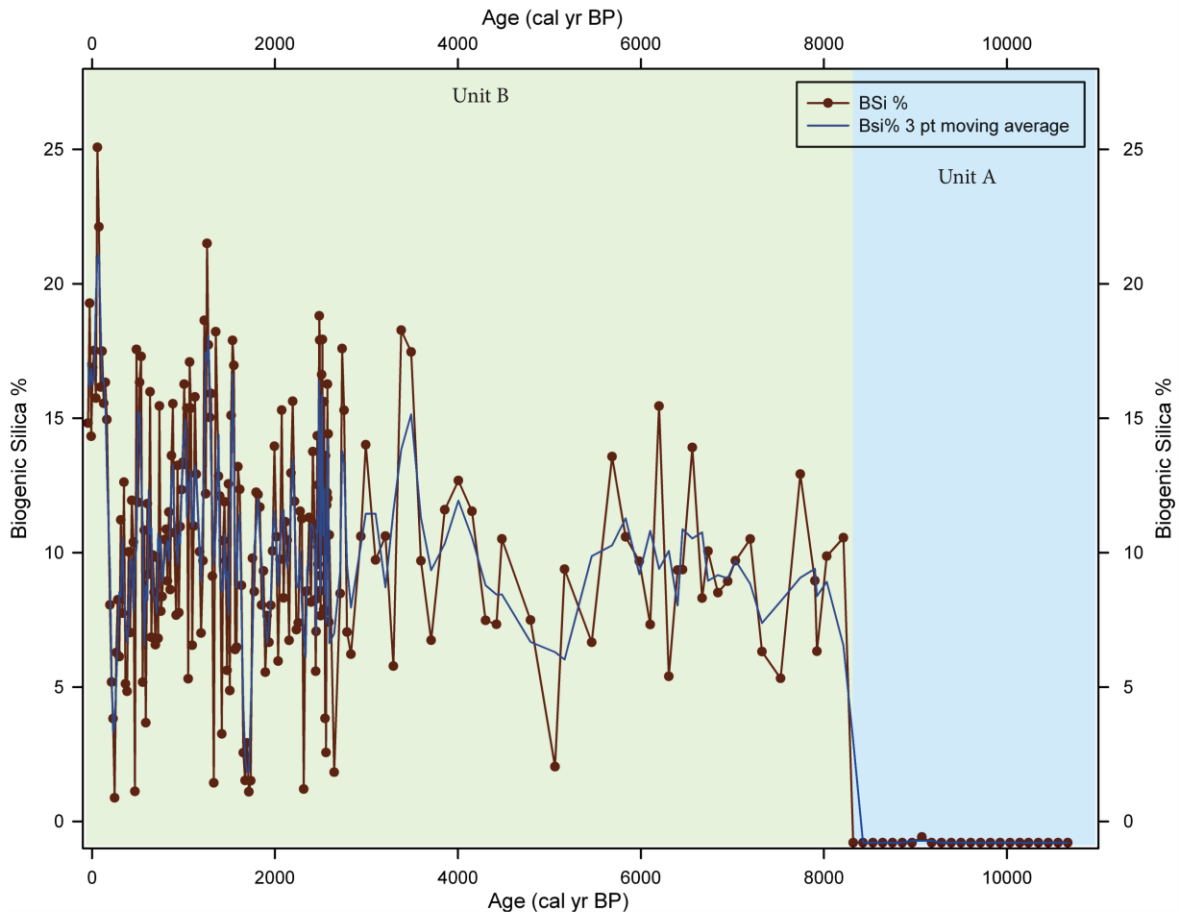

Figure 4.11: FTIRS derived biogenic silica record from Nanerersarpik Lake
Sampling interval for majority of the sediment was every 5cm, increased to every centimeter for the most recent ~3,000 years. BSi has been shown to reflect abundances of siliceous microfossils (Conley, 1988). The high frequency and high amplitude variability of the BSi record is not shared by any other proxies from Nanerersarpik.

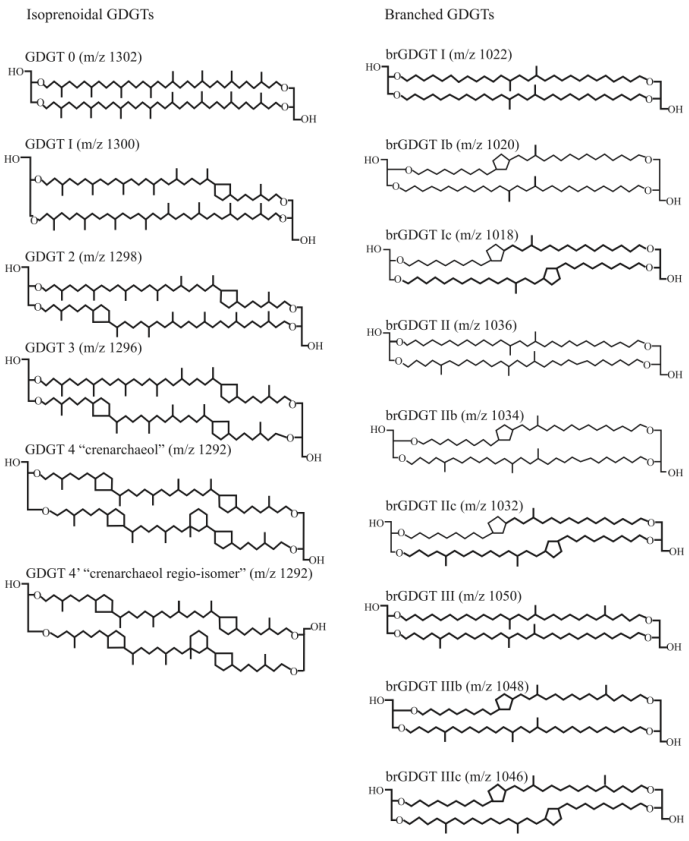

Figure 4.12: Molecular structure of isoprenoid and branched glycerol dialkyl glycerol tetraethers (GDGTs). These biomarkers were analyzed in the Nanerersarpik Lake record to calculate the BIT Index as well as MBT/CBT based paleo-temperatures. See text for details. (Modified from Castañeda and Schouten, 2011).

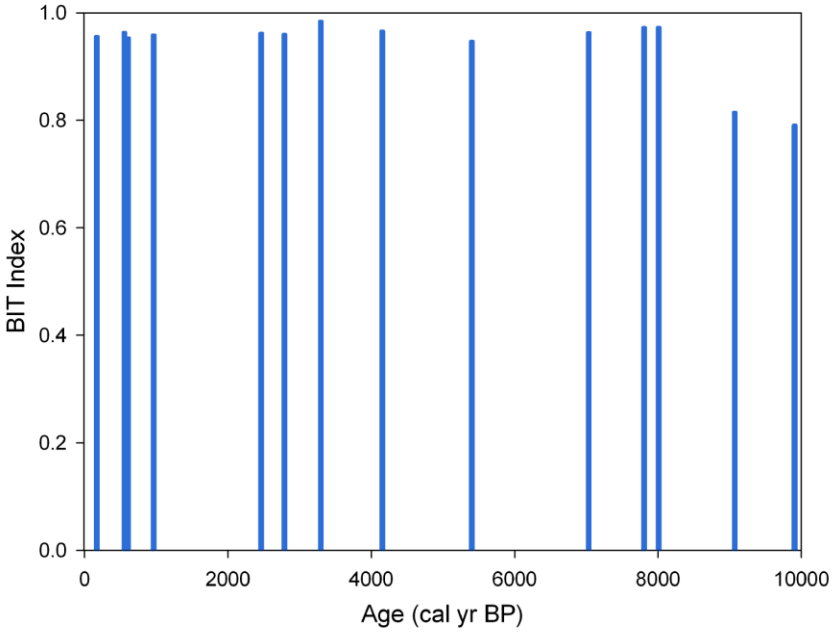

Figure 4.13: BIT Index values from Nanerersarpik Lake. The Branched and Isoprenoid Tetraether Index compares the relative abundance of soil derived (branched) GDGTs with GDGT IV produced Archea living in the lake. The index ranges between 0 and 1, with 1 being a purely terrestrial source and 0 indicating a purely aquatic source. Nanerersarpik values suggest a dominantly terrestrial source for organic matter.

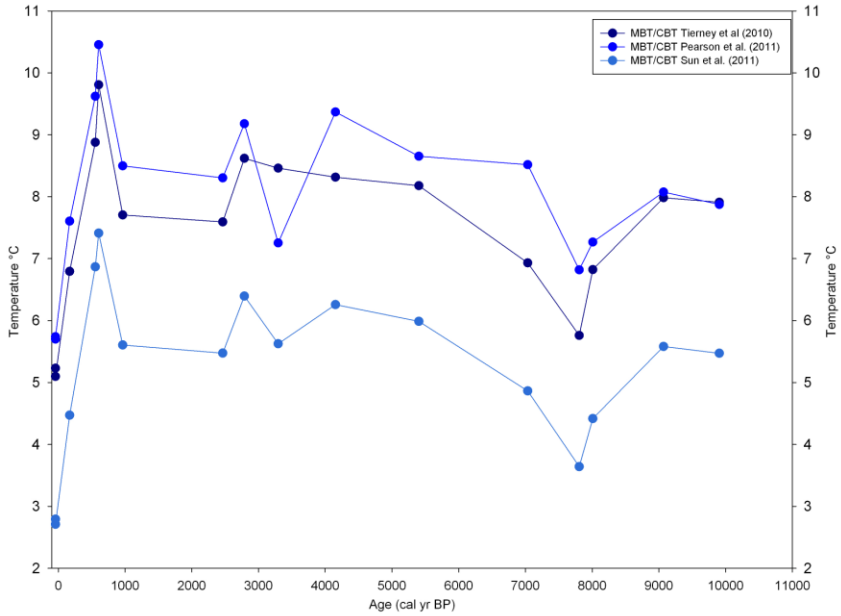

Figure 4.14: Paleo-temperature reconstructions based on GDGTs from Nanerersarpik Lake sediments. Due to low sampling density (n=15) and high uncertainty associated with this method reconstructed temperatures should be regarded with caution. See text for details.

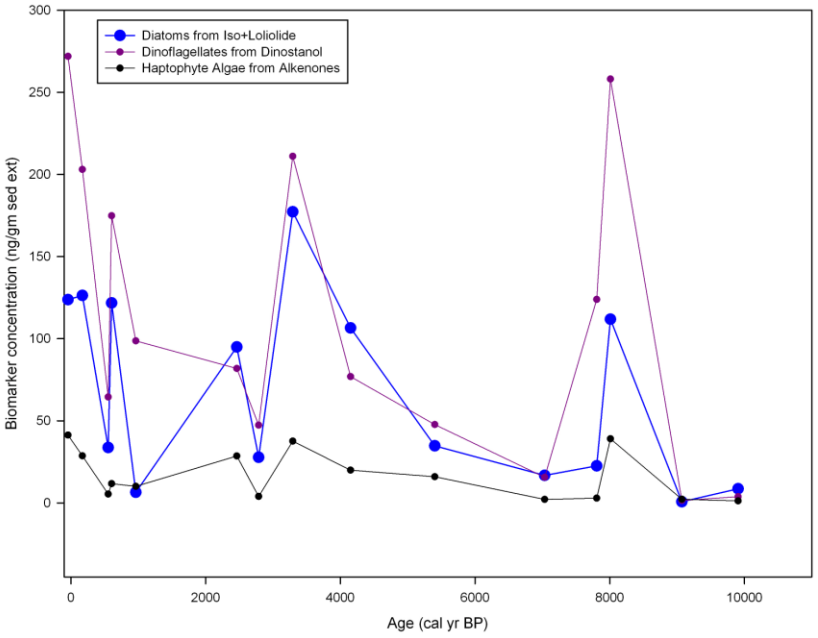

Figure 4.15: Abundances of algal biomarkers from Nanerersarpik lake sediments.

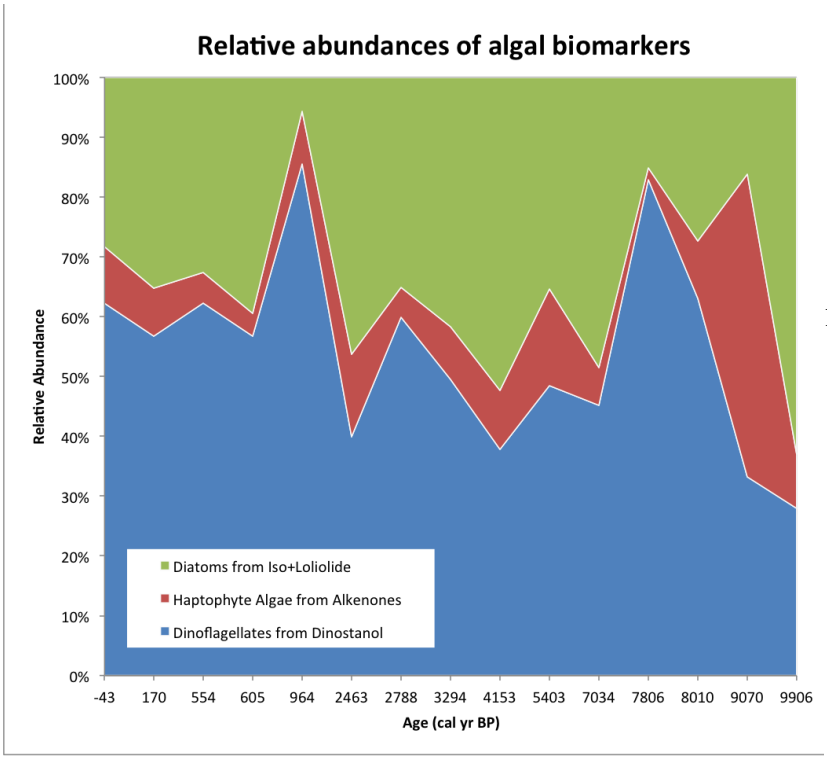

Figure 4.16: Relative abundances of lacustrine primary producers reconstructed from charateristic biomarkers in Nanerersarpik Lake sediments.

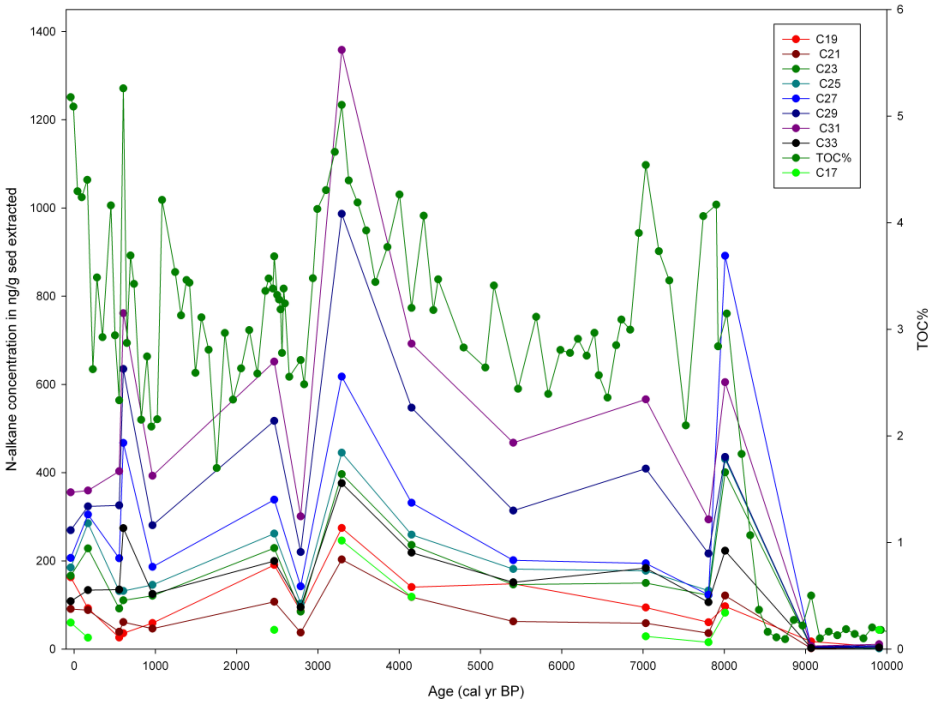

Figure 4.17: Concentrations of straight chain *n*-alkanes from Nanerersarpik Lake. Note the preponderance on longer chain (darker colors) *n*-alkanes suggesting a dominantly terrestrial source of organic matter.

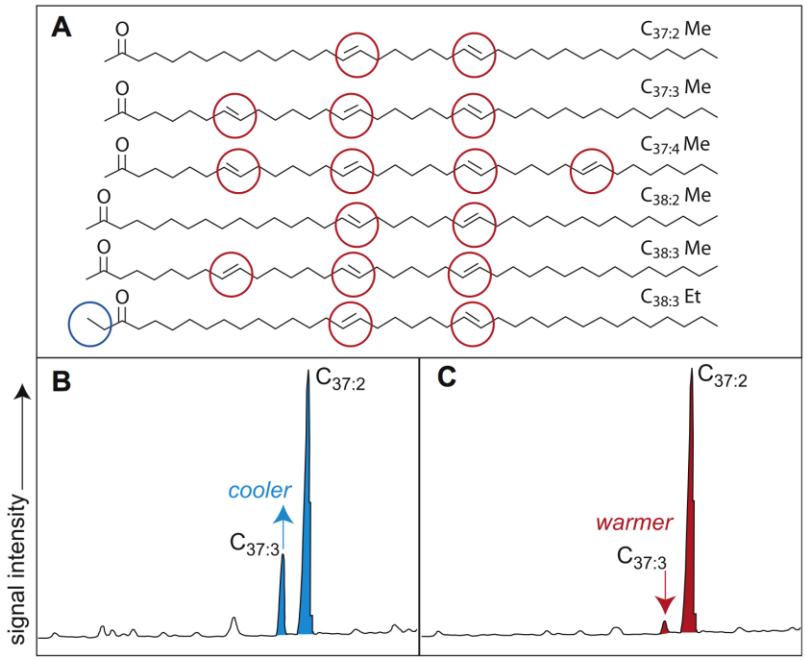

Figure 4.18: A) Structures of methyl (Me) and ethyl (Et) long chain alkenones used for U^{k}_{37} paleo-temperature reconstructions. B) and C) illustrate how concentrations of different alkenones change with temperature, the principle on which alkenone temperature reconstructions are based (modified from Castañeda and Schouten, 2011).

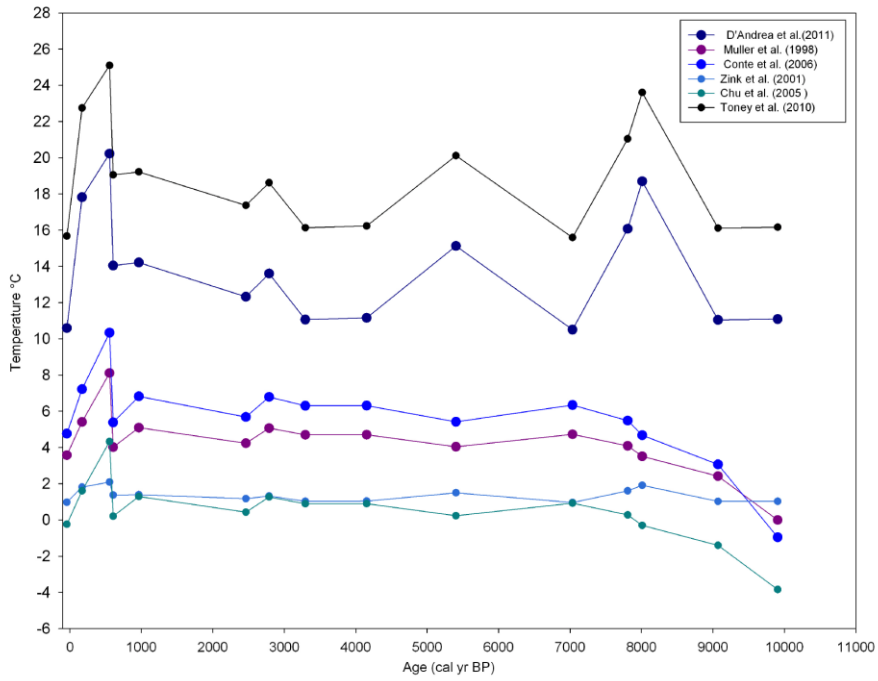

Figure 4.19: Alkenone based paleotemperature reconstructions from Nanerersarpik Lake. As with the MBT/ CBT GDGT temperature estimates, due to the lack of sampling density and high uncertainty associated with this method absolute temperatures are likely inaccurate. See text for details.

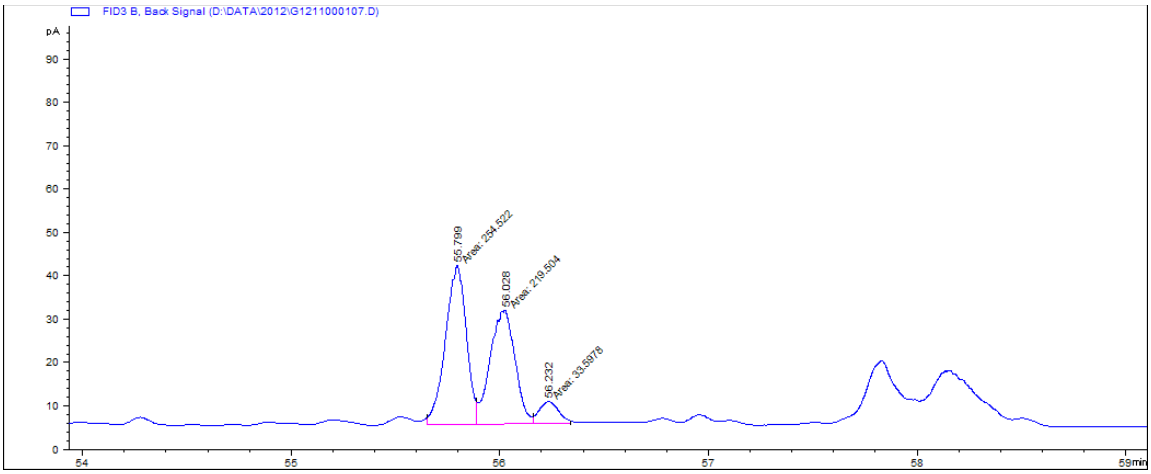

Figure 4.20: Characteristic alkenone peaks from GC-MS chromatogram showing peaks of all three unsaturated ketones in Nanerersarpik Lake sediments.

CHAPTER V

DISCUSSION

Interpretations of paleo-environmental conditions at Nanerersarpik Lake throughout the Holocene are based primarily on concentrations of organic carbon and biogenic silica. These proxies were used due to the relatively high resolution of available samples and their sensitivity to potential environmental/climate changes. C/N ratios and concentrations of total nitrogen also support these primary proxies. Biomarker data and elemental counts from the Itrax were taken into account, although these proxies are limited by low sampling density (biomarkers) and the complex nature of minerogenic input at Nanerersarpik Lake (Itrax data). Due to inconclusive changes in magnetic susceptibility, $\delta^{13}C$, and $\delta^{15}N$ these parameters are generally not discussed below.

5.1) Biomarker paleotemperature reconstructions

5.1.1) Alkenone based U^{k}_{37} paleotemperatures

While alkenone based temperature reconstructions have been widely applied in marine settings, their application in lacustrine settings has only begun more recently. D'Andrea et al. (2011) have shown alkenoes to accurately record temperature in West Greenland, but only after calibrating modern alkenone concentrations and creating a lake-specific transfer function. Application of this transfer function to Nanerersarpik Lake alkenone concentrations produces unrealistic warm temperatures with extremely high temperature variability over the Holocene (temperature range of ~15°C) (Figure 4.19). A similar U^{k}_{37} calibration from lakes in North Dakota (Toney et al., 2010) returns slightly cooler temperatures, but high variability and unrealistically warmth remains.

Interestingly, $U^{k'}_{37}$ reconstructions, which do not include the $C_{37:4}$ unsaturated ketone in their transfer functions (abundant in Nanerersarpik Lake samples (Figure 4.20), return lower temperatures with low variability until the late Holocene (Figure 4.19). While these reconstructions show greater agreement with brGDGT paleotemperatures derived using MBT/CBT (Figure 5.1) (discussed below) and are also most similar to mean summer air temperatures in the region today, they are likely inaccurate as they do not account for the high concentrations of $C_{37:4}$ at Nanerersarpik. These results suggest that lake specific calibrations may be needed before the accurate application of the alkenone based paleotemperature proxy can be applied.

5.1.2) brGDGT based paleotemperatures

Temperature reconstructions from Nanerersarpik based on the MBT/CBT proxy also display little variance until the Late Holocene (Figure 5.1, warm colors). As BIT Index values indicate GDGTs in Nanerersarpik lake sediments are primarily produced by soil bacteria, soil temperatures changes might be expected to be less variable than lake or air temperatures. Even taking this into account, the lack of warming across the deglacial transition for instance, seems to suggest that brGDGTs have a limited response to environmental changes at Nanerersarpik Lake.

In conclusion, the biomarker temperatures reconstructed here, whether from alkenones or GDGTs, should be treated with extreme caution. It is likely that a lake-specific calibration is required to create an accurate transfer function. Applying calibrations from other lakes, even in Western Greenland, appears to yield unrealistic temperatures. The high concentrations of alkenones in Nanererarpik Lake suggest that a paleotemperature reconstruction may be possible, but an in-depth modern calibration and

better understanding of the ecology of alkenone producing algae are necessary before absolute reconstructed temperatures can be reconstructed with any degree of confidence.

5.2) Organic matter source and terrestrial dilution

To correctly interpret the paleo-environmental signal recorded by organic matter in a lake sediment core the source of that organic matter must be understood. Synthesis of multiple lines of evidence from Nanererarpik Lake suggests that the source of organic matter varied through time, with autotochthonous signals periodically overprinted by terrestrial vascular plants.

5.2.1) Bulk geochemical proxies

Downcore C/N ratios generally fall either in between the characteristic values of lacustrine algae or C_3 land plants or fall towards the terrestrial side (Figure 5.2) (~10-30) These values suggest that organic material in Nanerersarpik Lake is coming from mixed sources with a slight preference for terrestrial material. Interestingly, samples with low TOC (red circles on plot) generally have higher C/N ratios as well as $\delta^{13}C$ values. This suggests that the organic matter from these samples was not only terrestrial in origin, but also likely diluted by clastic input, resulting in the low overall organic carbon values.

To further investigate the terrestrial/clastic overprinting of the organic carbon signal TOC was compared with clastic mineral inputs taken from the Itrax core scanner (Figure 5.3). Calcium is highly abundant in the supracrustal rocks underlying Nanerersarpik (Bridgewater, 1976) and is interpreted as an erosional signal from the catchment. It appears that for some parts of the record Ca and TOC follow similar trends, but in many cases peak TOC values are recorded when Ca counts are relatively low (blue outlined boxes on Figure 5.3). Additionally, in many of the outlined peaks where TOC is

low, a corresponding increase in C/N is observed, also suggesting the organic matter in this sample is terrestrially-sourced (Figure 5.4). In other parts of the record, low TOC values are seen when Ca counts are relatively high (red boxes in Figure 5.3) suggesting a complex interaction between terrestrial and aquatic organic matter as well as terrestrial minerogenic material.

5.2.2) Lipid biomarker evidence

While biomarker analysis was only carried out on 15 downcore samples from Nanerersarpik Lake, *n*-alkane and BIT Index information can also contribute to an understanding of the source of organic matter. BIT index values for the post-glacial sediment all fall very close to 1, suggesting a dominantly terrestrial source (Figure 4.13) (the low BIT Index values in the glacial-fluvial facies are likely due to the fact that little soil development had taken place during the deglacial period and the brGDGT producing soil bacteria had not yet fully colonized the catchment). While the BIT Index firmly suggests a terrestrial source, it should be noted that it compares soil –derived brGDGTs against the concentration of GDGT IV, interpreted as being produced by aquatic archea called Thaumarchaeota. It is possible that Thaumarchaeota concentrations are simply low in Nanerersarpik while brGDGT producing bacteria are abundant in the surrounding catchment, leading to the high BIT index values.

The concentrations of n-alkanes in our sediment record also suggest a dominantly terrestrial source of organic matter with higher abundances of long-chain *n*-alkanes throughout the record (Figure 5.5). All chain lengths seem to track TOC well throughout the record, which could be a result of overall increased productivity in the catchment but could also be influenced by the overprint of high concentrations of terrestrial organic

matter being transported to the lake and therefore may not accurately record overall aquatic and terrestrial vegetation development in the catchment and lake.

The main conclusion from these data is that the organic matter in Nanerersarpik is likely representing a mixed signal of both terrestrial and aquatic sources, and is periodically diluted by clastic material. It appears that this overprinting of terrestrial material generally artificially *decreases* the values of organic matter. This is not always the case, however, and at times high terrestrial input apparently brings higher concentrations of terrestrial vegetation into the lake and artificially *increases* TOC concentrations. As discussed below, although a climate signal may be interpreted from the TOC record from Nanerersarpik Lake, the complex nature of the source and signal record by this proxy must be taken into account.

5.3) Biogenic silica, the same terrestrial dilution problem?

Analysis of biogenic silica records from sediment cores are a potentially powerful proxy for reconstructing past variations in lake productivity as they are thought to suffer from fewer interpretative issues than organic carbon concentrations: e.g fewer number of potential sources (Conley, 1988), more likely to respond on short time-scales to climate changes (Williams et al., 1997; Blass et al., 2007; McKay et al., 2008), and less likely to degrade over time. Lacustrine diatom concentrations should be responding primarily to higher summer temperatures, which would decrease seasonal ice coverage and bring about more favorable growing conditions, resulting in higher overall BSi concentrations in sediments (Conley, 1988). Furthermore, by utilizing relatively new FTIRS analytical techniques, BSi can be measured at high resolution quickly and for relatively low cost compared to traditional methods (Vogel et al., 2008; Rosén et al. 2010).

BSi analysis is not without limitations, however. As noted by Swann et al., (2006) large scale changes in lake chemistry can result in diatom dissolution at the sediment water interface, affecting concentrations in the sediment. While the spectral characteristics of biogenic Si bonded to O are well understood, not all BSi studies integrate the same spectral peak areas when creating lake-specific calibration models. While internal consistency should eliminate this issue for specific lake studies, comparisons across lakes could be hampered. More research is needed to refine this method and test/improve cross-laboratory agreement.

Additionally, BSi concentrations at Nanerersarpik Lake are subject to the same issue of terrestrial dilution experienced by organic carbon. This relationship is apparent when biogenic silica is plotted against inputs of clastic minerals from the XRF (Figure 5.6), especially for the earlier part of the record when BSi sampling density is low (Figure 5.7). Importantly however, unlike TOC concentrations, which can be either diluted or increased by clastic material, BSi is only sourced from the lake and therefore is not subject to concentration increases from terrestrial material, only dilution.

Analysis of broad scale trends in TOC and BSi concentrations can help remove some of the uncertainty associated with terrestrial dilution. Also, since BSi can only be decreased by clastic input and not artificially increased, analysis of how BSi maxima change over time may help remove some of this uncertainty. With these considerations in mind the majority of the discussion of Holocene climate intervals presented below will focus on the TOC and BSi records from Nanerersarpik.

5.4) Paleoclimate record from Nanerersarpik Lake

Reconstructed climate intervals during the Holocene are presented in Figure 5.8. Deglaciation of the lake catchment occurred sometime around 8.25 cal kyr BP, as the last remnants of LGM glacial ice retreated into a fjord to the north. The Holocene Thermal Maximum at Nanerersarpik lasted from ~8.25 to between 3 and 4 cal kyr BP, with warm but dry conditions. The transition to Neoglacial conditions is cautiously interpreted as an initial humidification followed by cooling temperatures and decreased primary productivity. The Neoglacial was interrupted by a short-lived Medieval Climate Anomaly (~1300-1000 cal yr BP) when primary productivity increased. The MCA was followed by a return to colder conditions during the Little Ice Age (~1000-250 cal yr BP) when biogenic silica values reached their lowest point since the transition from glacial conditions. The most recent part of the Nanerersarpik Lake record was characterized by the highest values of TOC and BSi of the entire Holocene.

It should be noted that these interpreations are based on proxy records that are undeniably influenced by more than purely climate at Nanerersarpik Lake and are not meant to be definitive boundaries, rather the interpretation made to the best of the available data. Higher sampling density would improve the determination of these intervals, although the complex and multi-faceted nature of the sedimentary record at Nanerersarpik may still preclude exact definitions.

5.4.1) Local Deglaciation

During the LGM, the Nanerersarpik catchment, along with most of the rest of SE Greenland, was covered by the Greenland Ice Sheet. As this ice began to retreat during the Early Holocene it is likely that valley glaciers remained in the valleys and fjords of the area, fed by still-existing glaciers at higher elevations. As glacial ice thinned and

pulled back up Amassalik Fjord, the shoulder where Nanerersarpik sits today would have become unglaciated, resulting in the first deposition of sediment at Nanerersarpik Lake sometime before ~8.25 cal kyr BP. As noted earlier, the lack of dated samples from the basal glaciofluvial sediment of Unit A of precludes accurate dating of the base of this facies.

The dense, variable grain sizes, and high minerogenic character of facies Unit A suggests that this sediment was likely deposited while some remnant of glacial ice were still influencing the catchment. It is likely this glacial ice was sourced from the fjord directly to the north of the lake (Figure 5.9). A small U-shaped notch in the bedrock ridge forming the northern edge of the catchment today likely represents the entry/exit point for this ice from the fjord (Figure 5.10). The small valley below the notch has the greatest concentration of glacial erratics found in the entire catchment (Figure 5.11), suggesting glacial activity was highest in this part of the catchment.

Sometime before 7,850 years ago (radiocarbon date from organic Unit B ~20cm above facies transition) this remnant glacial ice pulled back over the northern ridge and ceased to influence the lake catchment at Nanerersarpik. Based on the constructed age model, the date for this final deglaciation of the catchment is ~8.25 cal kyr BP. The transition is accompanied by dramatic increases in the concentrations of all organic-related proxies: TOC, TN, BSi, and lipid biomarkers (Figures 5.8 & 5.5).

5.4.2) The Holocene Thermal Maximum

While summer insolation values had already reached their early Holocene maxima by ~8 cal kyr BP, remnant glacial ice in Nanerersarpik prevented the effects of the warming to be registered by the lake. Directly after deglaciation however, this high

insolation is manifested as high concentrations of both organic carbon and biogenic silica. TOC notably then decreased for much of the rest of the Middle Holocene, early maxima between 7 and 8 cal kyr BP. BSi remained elevated longer into the middle Holocene, but also showed consistently lower values from approx. 5.5 to 4 cal kyr BP. Some of this decline in primary productivity proxy concentrations during the middle part of the Early Holocene may have been related to arid conditions, noted by numerous studies to have affected Greenland at this time (e.g. Wagner et al., 2000; McGowan et al., 2003; Anderson et al., 2004; Perren et al., 2012; Massa et al., 2012), A similar pattern of organic carbon concentrations was seen in a Holocene lake record from western Greenland (Figure 5.12), suggesting similar patterns of catchment vegetation development (Willemse & Törnqvist, 1999). It could also be a result of the terrestrial dilution during this period. Many of the minima in both TOC and especially BSi fall during periods of elevated deposition of clastic minerals such as Ca and K (Figure 5.7). C/N ratios during much of this interval are high, rarely falling near the value of pure lacustrine algae, and suggesting large amounts of terrestrial influence.

While greater sampling density would help to resolve the issue of terrestrial input overprinting the sedimentary record, versus an actual decline in primary productivity due to arid conditions, the increases in both BSi and TOC beginning at 4.2 cal kyr BP could be related to increased rainfall and higher primary productivity. A similar response to soil formation and nutrient availability was also observed in a Holocene lake record from NE Greenland (Klug et al., 2008). C/N values during the interval from 4.2-3 cal kyr BP were unstable and generally above 10, but not consistently in the >17 range expected of purely vascular plants. Increased precipitation could have washed more nutrients into the lake

(TN and S counts also increase during this interval, Figures 4.8 & 4.10) and caused higher aquatic productivity. The TOC maxima recorded at ~3.3 cal kyr BP has a relatively low corresponding C/N value, suggesting a mixed, if not purely aquatic source. Interestingly, coeval with this maxima are the highest concentrations of the C_{17} n-alkane (produced by lacustrine algae) recorded in the entire record. BSi is low at this point, but it should be noted that dinostanol concentrations, a biomarker for dinoflagellate algae, are higher than the concentrations of isololiolide and loliolide at this time (diatom biomarkers), suggesting that perhaps algae were briefly outcompeting diatoms due to high nutrient availability (Castañeda and Schouten, 2011). The sampling density of biomarkers precludes this from being definitive evidence but supports the hypothesis of increased nutrient transport to the lake.

Subsequent declines in all primary productivity proxies after this maxima ~3.3-3.5 cal kyr BP are interpreted as the transition to Neoglacial conditions in at Nanerersarpik Lake.

5.4.3) The Neoglacial period

The onset of Neoglaciation at Nanerersarpik is difficult to precisely date as the manifestation of this period was complex in Greenland. If precipitation changes did in fact cause the changes in concentration of primary productivity proxies as presented above, the onset of increased precipitation would place the beginning of the Neoglacial at ~4.2 cal kyr BP. Marked decreased in proxies (attributed to the deterioration of climate conditions in the catchment) occurred later, between ~3.5 and 3 cal kyr BP. TOC concentrations remained low throughout the proposed Neoglacial until they rebounded during the Medieval time, ~1300 cal yr BP. Biogenic silica values, sampled at high

density for parts of this interval, display high variability but generally also show a decreasing trend until 1300 cal yr BP (Figure 5.8).

The timing of the Neoglacial transition is generally synchronous with published proxy records from elsewhere on Greenland and the surrounding North Atlantic. In Southern Greenland, Massa et al. (2012) noted a substantial cooling trend beginning around 3 cal kyr BP. Kaplan et al. (2002) and Andresen et al. (2004) also noted decreases in BSi percentages after 3 cal kyr BP. A study by Wagner et al. (2000) in East Greenland also found the culmination of Neoglacial conditions from ~3ky -1 cal kyr BP. At nearby Lower Sermilik Lake, Davin (2013, unpublished Masters thesis) and Humlum and Christiansen (2008) found that the Mittivaket glacier reappeared around this time. Jennings et al. (2011) found evidence for increased advection of polar East Greenland current water at ~3.5 cal kyr BP, with a subsequent decrease in warm Atlantic Irminger current water reaching SE Greenland, which would compound the cooling effect of decreased summer insolation at this time.

5.4.4) The Medieval Climate Anomaly

The Medieval Climate Anomaly (MCA) at Nanerersarpik is manifested as increases in both TOC and BSi percentages from approx. 1300-1000 cal yr BP (Figure 5.13). BSi concentrations reached their second highest values of the entire Holocene during this interval and interrupted the decreasing trend seen during the Neoglacial. While the TOC maximum observed around 1060 cal yr BP is not the highest value seen during the late Holocene, the corresponding C/N ratio from this time is much lower (i.e. more likely to represent both algal and terrestrial sources) than the maxima at ~625 cal yr BP for instance, which was likely influenced by high amounts of terrestrial organic

carbon washing into the lake. Kaplan et al. (2002) also found similar timing of a MCA signal in Southern Greenland (higher BSi, LOI%).

5.4.5) The Little Ice Age

The Little Ice Age signal at Nanerersarpik is convoluted as TOC values are high in this interval, but are overprinted by terrestrial sources as evidenced by high C/N ratios and high clastic mineral input (Figure 5.14). BSi values also display high variability but do exhibit a generally decreasing trend from ~1000 to 250 cal yr BP, when they reached the lowest values recorded in the entire post glacial record. This overall decreasing trend is consistent with decreasing summer insolation at high northern latitudes and the expression of the Little Ice Age across the Arctic (Kaufman et al., 2004).

5.4.6) Modern warming

The termination of the Little Ice Age was recorded by rapidly increasing values of both TOC and BSi ~200 cal yr BP. Low corresponding C/N values suggest this TOC increase was the result of increased primary productivity and not terrestrial overprinting. Both TOC and BSi reach maximum values during this most recent interval, possibly suggesting modern conditions have no analogue throughout the Holocene, although increased sampling density throughout the Holocene Thermal Maximum is needed to confirm this assertion.

5.5) Potential response of BSi to temperature on short timescales

Biogenic silica concentrations have been used a proxy for climate by multiple studies on highly varying time scales. Paleoclimate reconstructions from Lake Baikal (Williams et al., 1997) and Lake Elgygytn (Melles et al., 2013) have shown BSi to respond on glacial/interglacial timescales. In the shorter term, Kaplan et al. (2002) and

Andresen et al. (2004) have shown BSi concentrations responded to Holocene climate changes. McKay et al. (2008) quantitatively reconstructed summer air temperature in Alaska over the past 80 years, showing that BSi concentrations can respond on extremely short (~annual) timescales. Interestingly, BSi concentrations over the past ~1500 years from Nanerersarpik show striking similarity to ice core-based temperature reconstructions from GISP2 (Kobashi et al., 2011) and Agassiz/Renland (Vinther et al., 2009) (Figures 5.15-5.17). While it was argued above that decreases in BSi concentration during the mid-Holocene were caused by terrestrial overprinting of the biogenic silica signal, the relationship between BSi concentrations and clastic mineral input appears to break down in the late Holocene (Figure 5.18), suggesting that the variability seen in the BSi record for the past 1500 cal yr BP may be primarily a response to temperature changes. Some vestige of this relationship may also be evident further back in time, but more sampling is needed to confirm or deny this (Figure 5.19) Interestingly the Nanerersarpik biogenic silica record bears some similarities with reconstructed temperatures from Braya Sø in Western Greenland (von Gunten et al., 2011) (Figure 5.20). Braya Sø temperatures have been linked to fluctuations in the Atlantic Multidecadal Oscillation, which also influences SE Greenland temperatures. This observation is meant to highlight the potential of high-resolution records across different regions. The record from Nanerersarpik as it stands is currently not sufficiently dated or sampled at high enough resolution to make such comparisons definitive.

More research is needed to confirm linkages such as the ones described above. While planned high resolution BSi sampling downcore may shed light on the validity of these relationship, the highly unstable nature of the Nanerersarpik catchment may

preclude its usefulness. The purpose of this section is merely to highlight the potential for high-resolution paleoclimate studies utilizing biogenic silica primarily analyzed using the FTIRS.

5.6) Future work

Planned future work at Nanerersarpik is focused on increasing the period of high resolution sampling biogenic silica sampling further back in time. More biomarker samples have also been extracted going back to ~4 cal kyr BP to better approximate temperature and organic carbon sources during the Late Holocene. Improvement of the age model is also desirable, with tephrochronology as an alternative to radiocarbon dating.

CHAPTER VI

CONCLUSIONS

The analyzed sediment core from Nanerersarpik Lake records a complex paleo-environmental signal influenced by a numerous factors, some of which appear to be climate related and other which are likely caused by the unstable nature of the catchment. This complexity potentially precludes the reconstruction of a simple paleoclimate reconstruction from this site. However, by understanding when terrestrial overprinting occurs and taking it into account, the timing of known paleoclimatic intervals can be estimated at Nanerersarpik Lake. Based primarily on organic carbon and biogenic silica accumulations, but supported by numerous other proxies, deglaciation of the catchment occurred ~8.25 cal kyr BP. The Holocene Thermal Maximum was registered at Nanerersarpik from 8.25 cal kyr BP to sometime between 3 and 4.2 cal kyr BP, when a multi-faceted transition to Neoglacial conditions occurred. High concentrations of BSi during were observed during the Medieval Climate Anomaly (1300-1000 cal yr BP), which was followed by a return to harsher conditions during the Little Ice Age. Dramatic rises in primary productivity occurred during the most recent ~250 years of the record.

Biogenic silica analysis using the FTIRS provided a relatively robust and inexpensive technique to measure concentrations downcore at a high resolution and comparison with ice core temperature reconstructions during the Late Holocene suggest BSi may be responding on short timescales to temperature. It is recommended that future lake studies utilize this analytical method to supplement paleo-environmental reconstructions. Alkenones and brGDGTs were present and easily identifiable in

Nanerersarpik Lake sediments. Without a lake-specific calibration however, reconstructed paleo-temperatures are likely inaccurate.

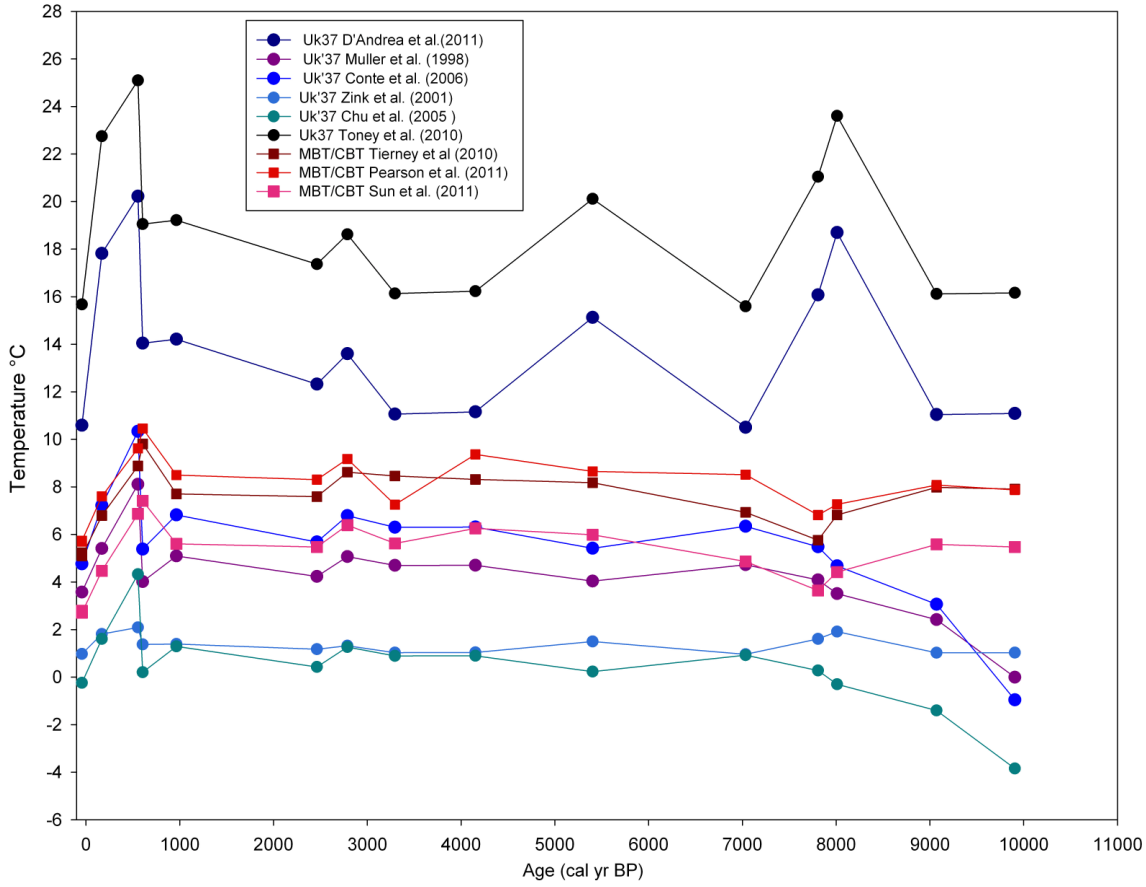

Figure 5.1: Alkenone (cooler colors) and brGDGT (warmer colors) based paleotemperature reconstructions from Nanerersarpik Lake. The wide range of temperatures likely results from the lack of a lake-specific calibration.

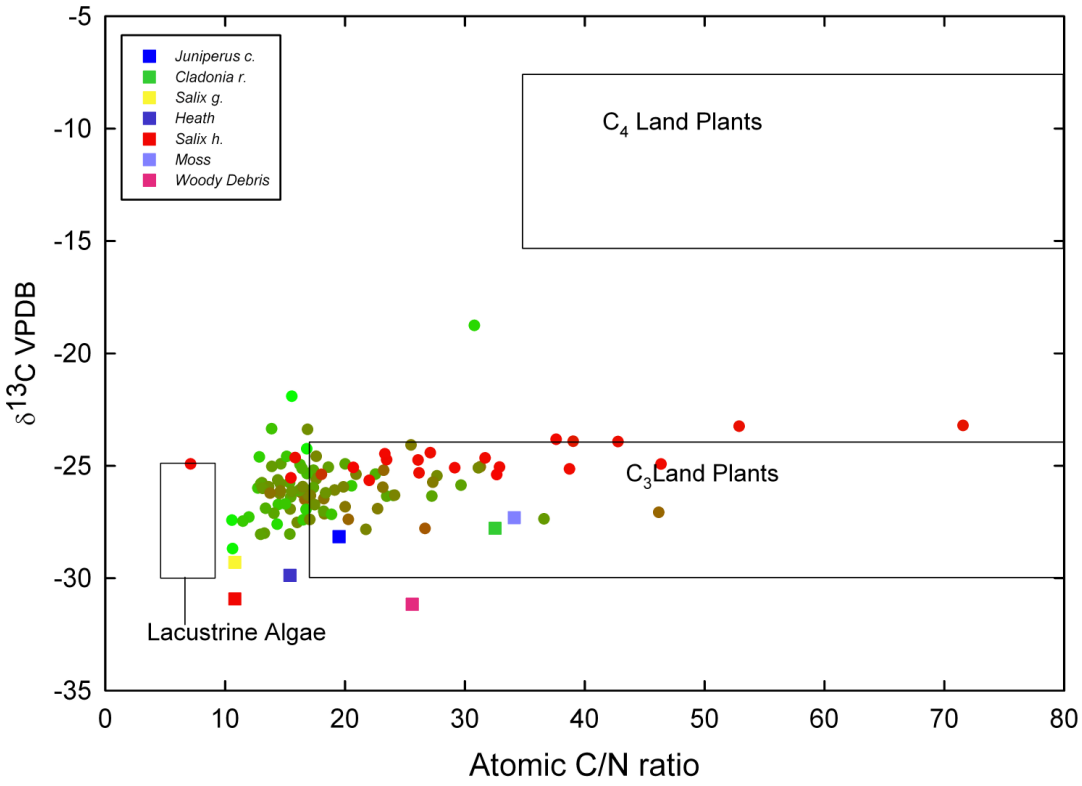

Figure 5.2: C/N versus $\delta^{13}C$ for Nanerersarpik Lake samples and modern vegetation collected from the region by Davin and de Wet in the summer of 2012. Circles are colored based on TOC concentrations, red circles = low TOC, green = high TOC.

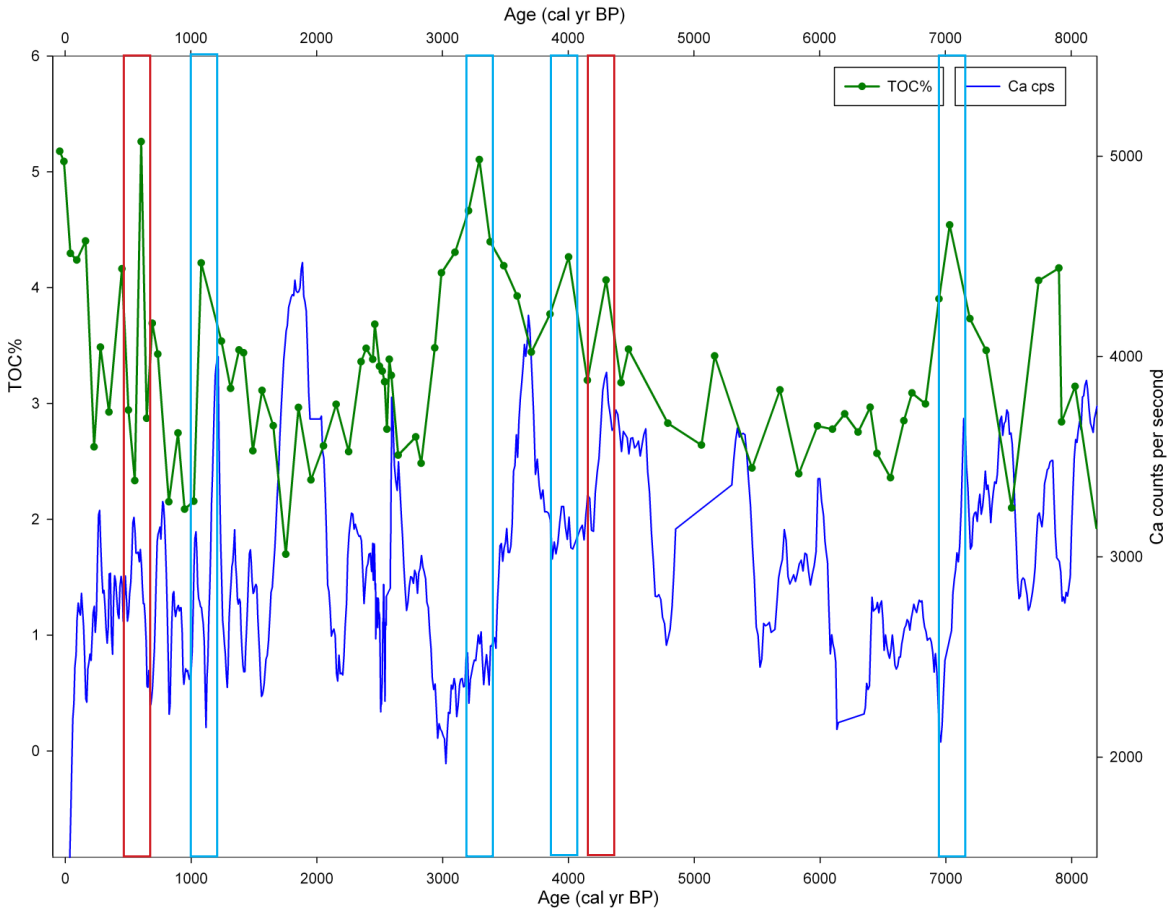

Figure 5.3: TOC values plotted with Ca counts per second over the past ~8.1 cal kyr B.P. from Nanerersarpik Lake. Blue boxes outline periods when TOC concentrations are high and Ca counts are relatively low. Red boxes outline periods when high TOC is accompanied by high Ca counts.

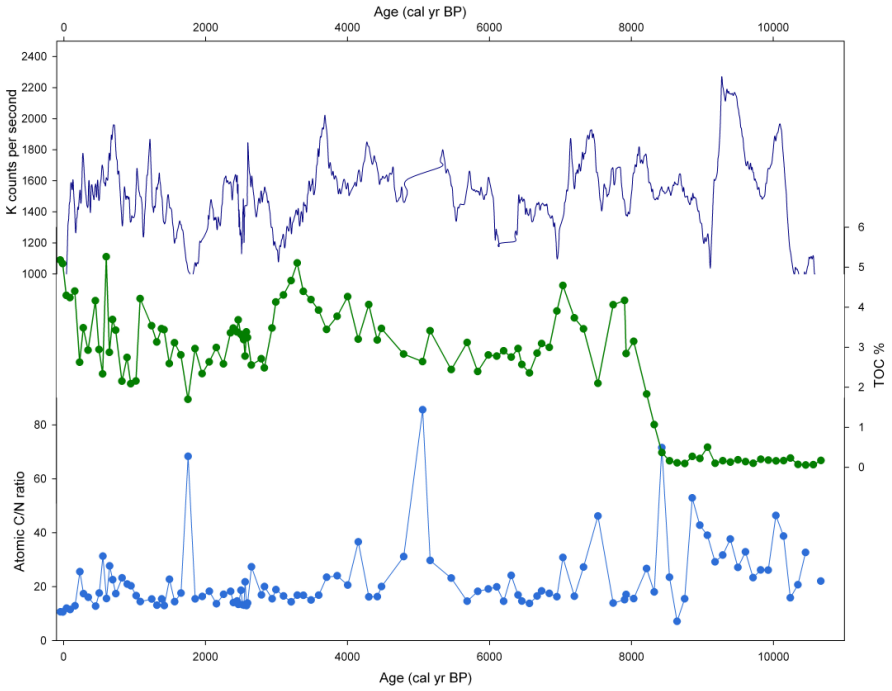

Figure 5.4: K counts per second (upper dark blue line), TOC concentrations (green line) and atomic C/N ratios (lower blue line) for Nanerersarpik Lake. Note high C/N ratios correspond with low TOC concentrations.

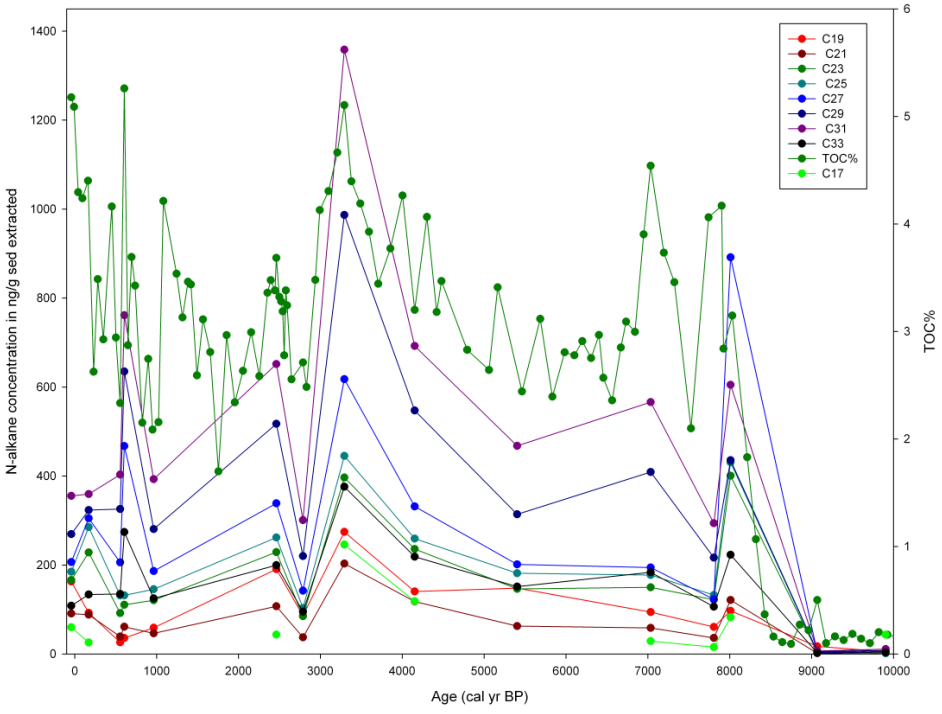

Figure 5.5: *N*-alkane concentrations from Nanerersarpik. Note the dominance of long-chain *n*-alkanes throughout the record.

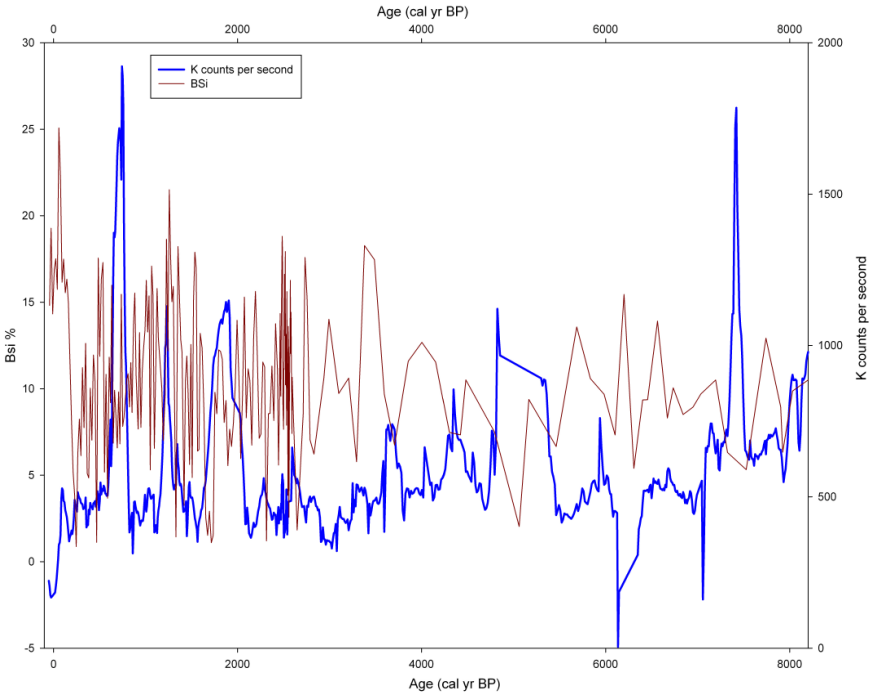

Figure 5.6: Biogenic silica concentrations and K counts per second. Note the low values of BSi when K counts are relatively high, suggesting a terrestrial dilution of biogenic silica concentrations.

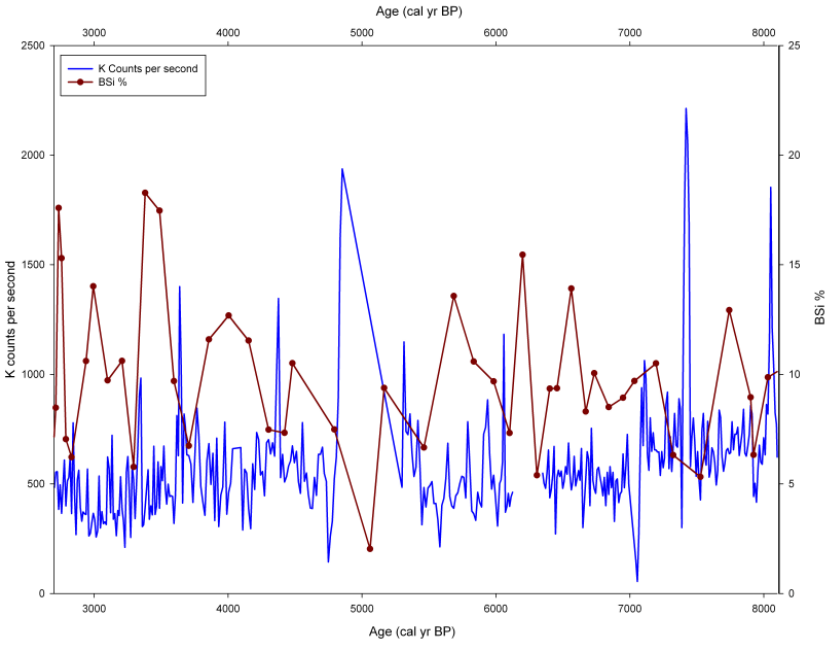

Figure 5.7: Biogenic silica concentrations and K counts per second from ~2.6 - 8.1 cal kyr B.P. Again, note high correspondance between low BSi values and high K counts per second.

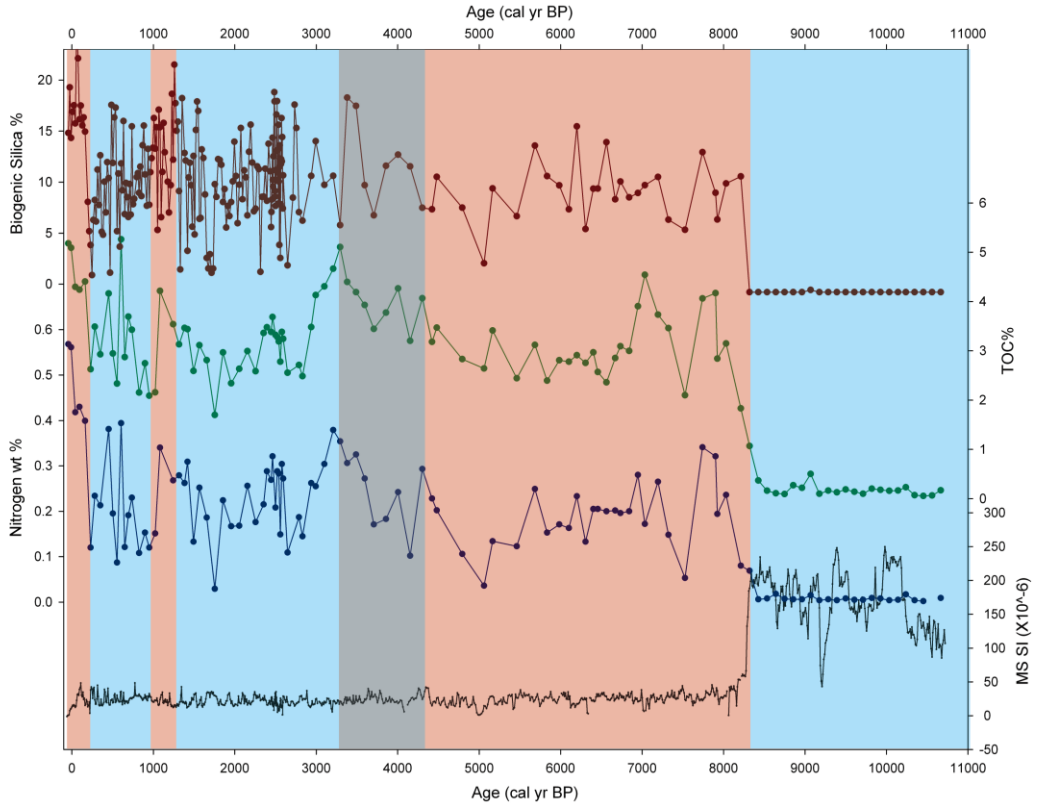

Figure 5.8: Composite record of paleoclimate proxies from Nanerersarpik Lake. Shaded rectangles correspond to indentified Holocene climate intervals: Deglaciation, the Holocene Thermal Maximum, Neoglaciation, the Medieval Climate Anomaly, the Little Ice Age, and modern warming.

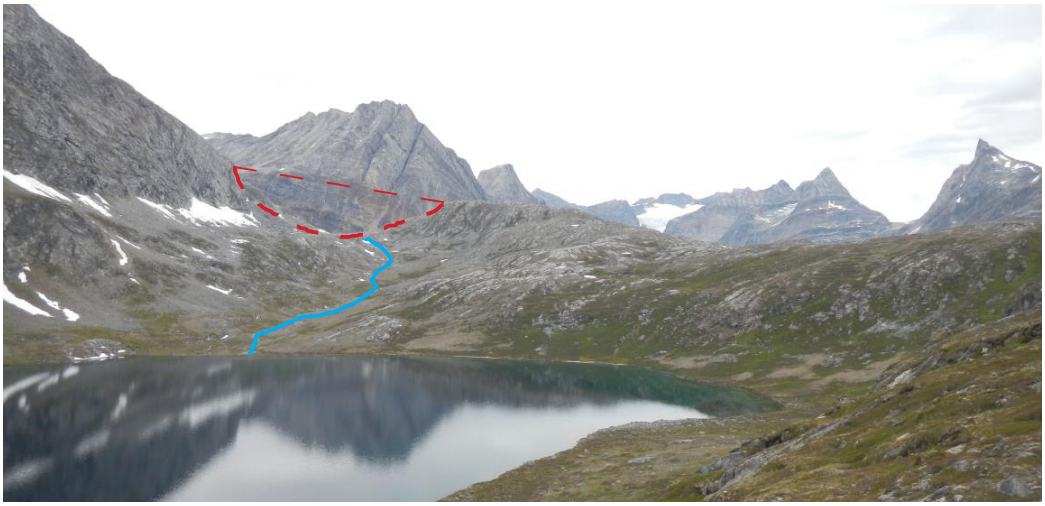

Figure 5.9: View to the northwest from the eastern edge of Nanerersarpik Lake catchment. Notch in bedrock ridge is denoted in red. Glacial ice from fjord just beyond the ridge likely spilled into the catchment during the deglacial period. Once this ice retreated, normal lacustrine sedimentation began in the lake.

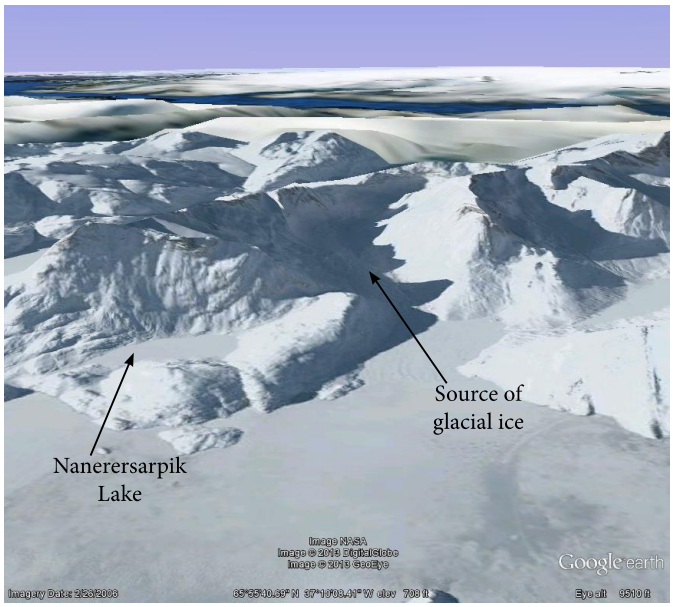

Figure 5.10: View looking to the west towards Nanerersarpik Lake showing fjord to the North where the last remnants of glacial ice to influence the cactchment were sourced.

Figure 5.11: Image of one of many glacial erratics present in catchment near notch in northwestern bedrock ridge.

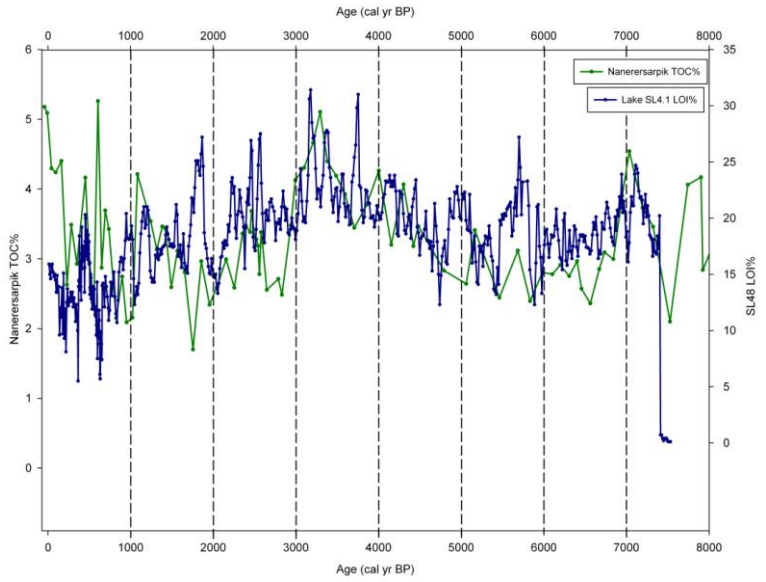

Figure 5.12: Nanerersarpik TOC and Loss on ignition values from Lake SL4.1 in Western Greenland showing similar trends in the accumulation of organic matter over the Holocene (Willemse & Törnqvist, 1999).

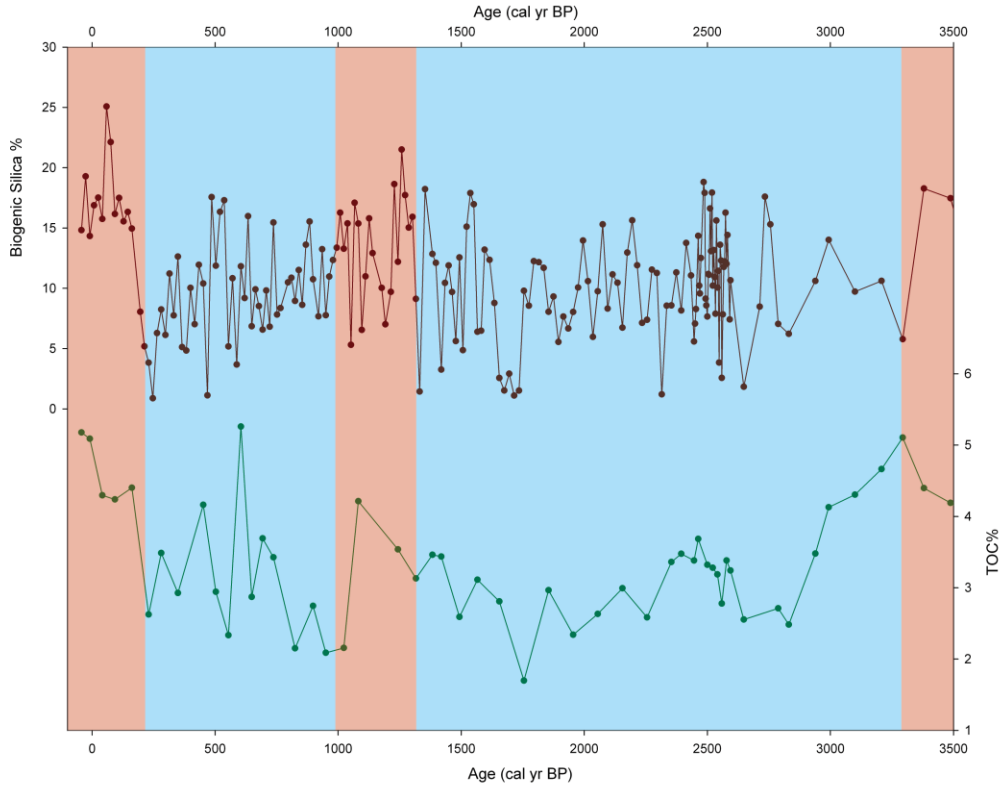

Figure 5.13: TOC and BSi values over the Late Holocene from Nanerersarpik, with interpreted climate intervals outlined (end of HTM, Neoglacial, MCA, LIA, modern warming).

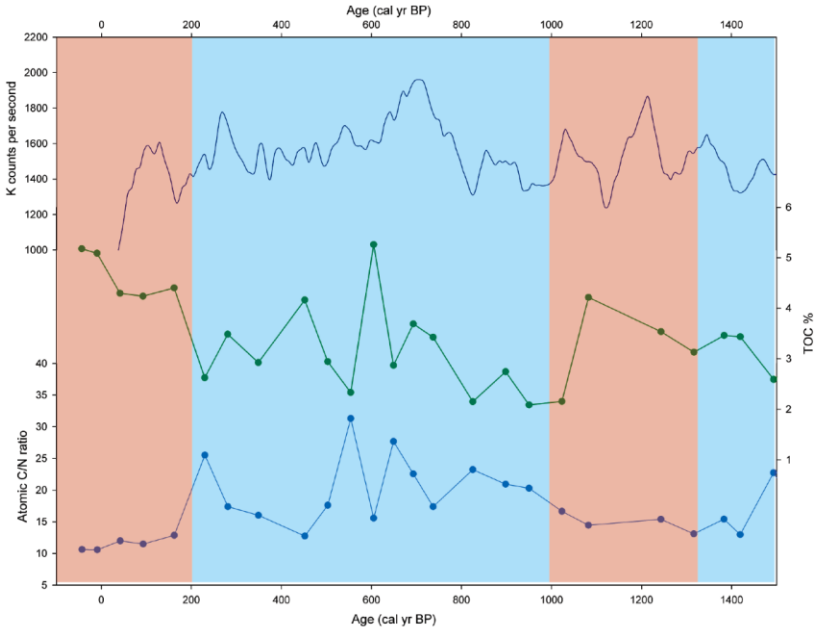

Figure 5.14: TOC, C/N, and K counts during the Little Ice Age. Note relatively high C/N ratios throughout the LIA, suggesting a mixed source of terrestrial and aquatic organic carbon.

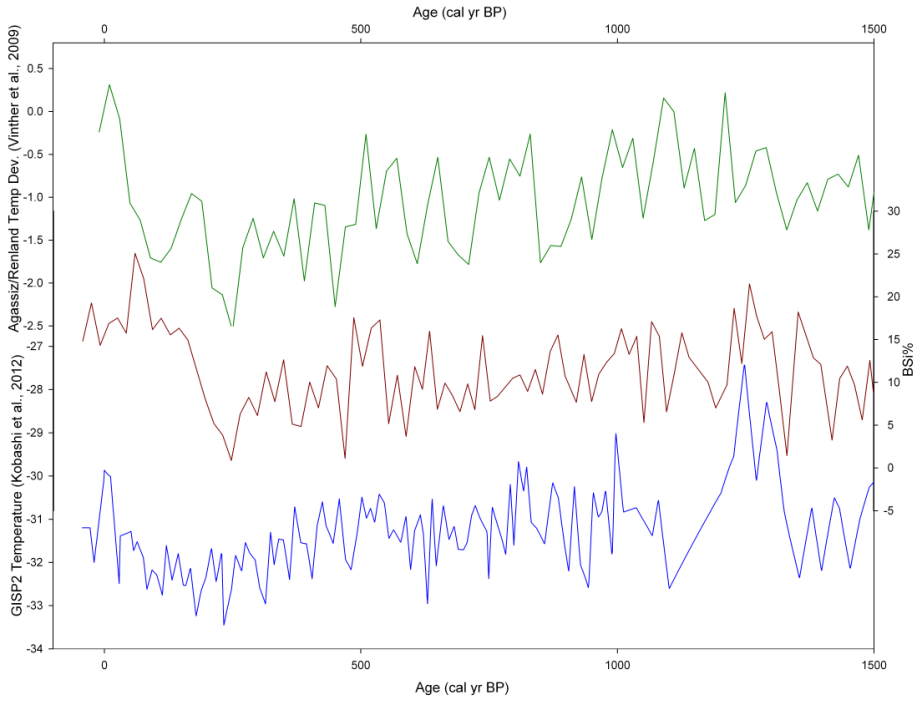

Figure 5.15: Nanerersarpik BSi values plotted with ice core temperature reconstructions from GISP2 (Kobashi et al., 2011) and Renland/Aggasiz (Vinther et al., 2009). It appears that BSi concentrations could be responding on short timescales to the same temperature changes recorded by the ice cores.

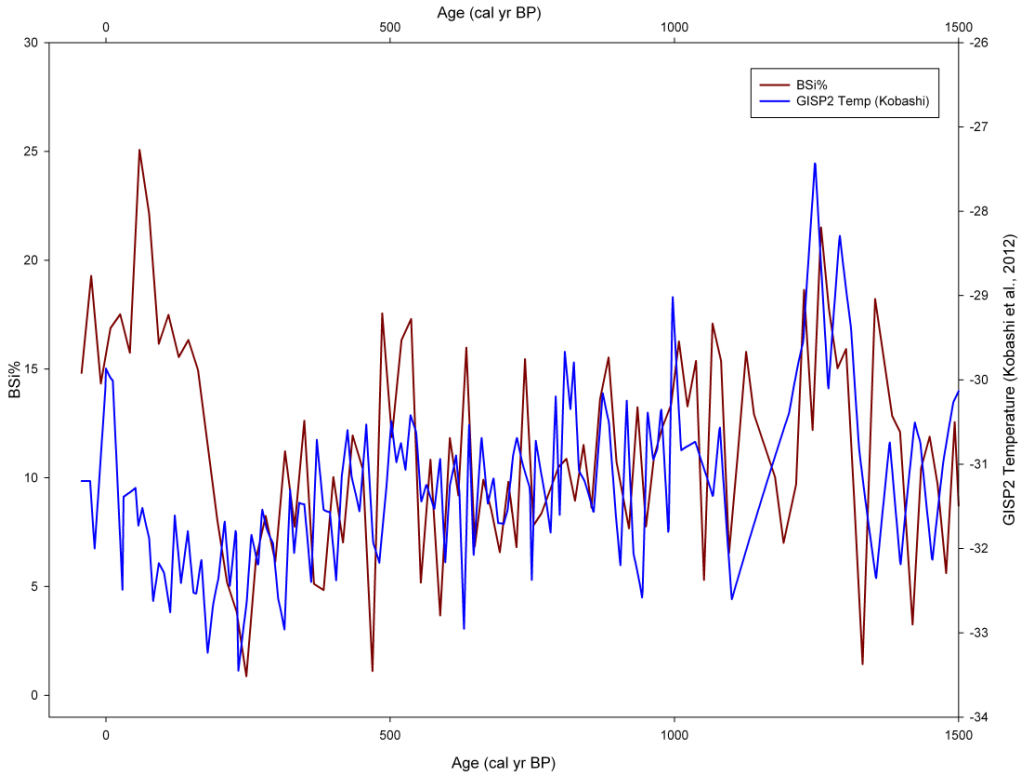

Figure 5.16: Nanerersarpik BSi concentrations plotted with GISP2 Late Holocene temperature reconstructions (Kobashi et al., 2011).

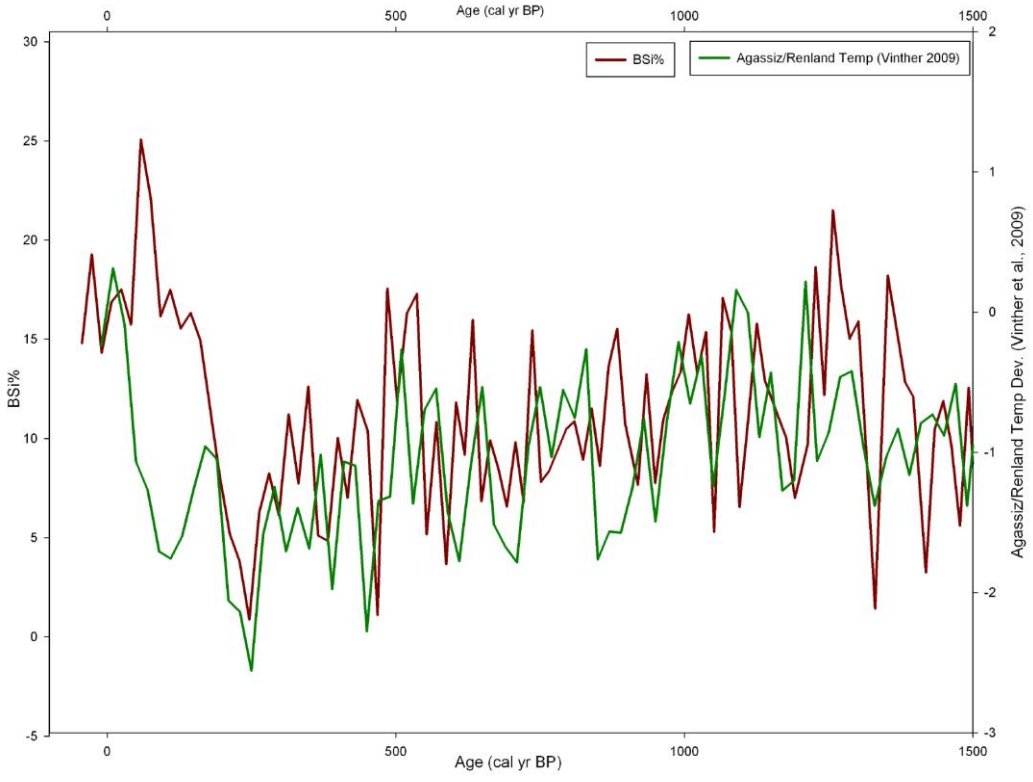

Figure 5.17: Analagous plot to Figure 5.16 but with BSi plotted against Agassiz/Renland Late Holocene temperatures (Vinther et al., 2009).

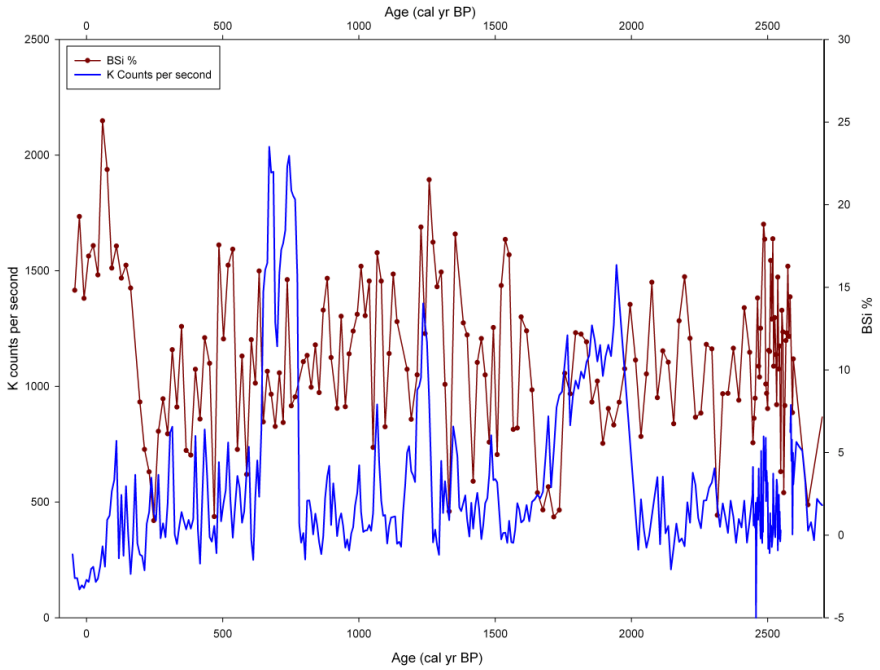

Figure 5.18: Biogenic silica plotted against K counts per second for the Late Holocene. Contrary to the relationship observed during the Early Holocene, the amount of potassium seems to have a minimal effect on BSi concentrations during this interval.

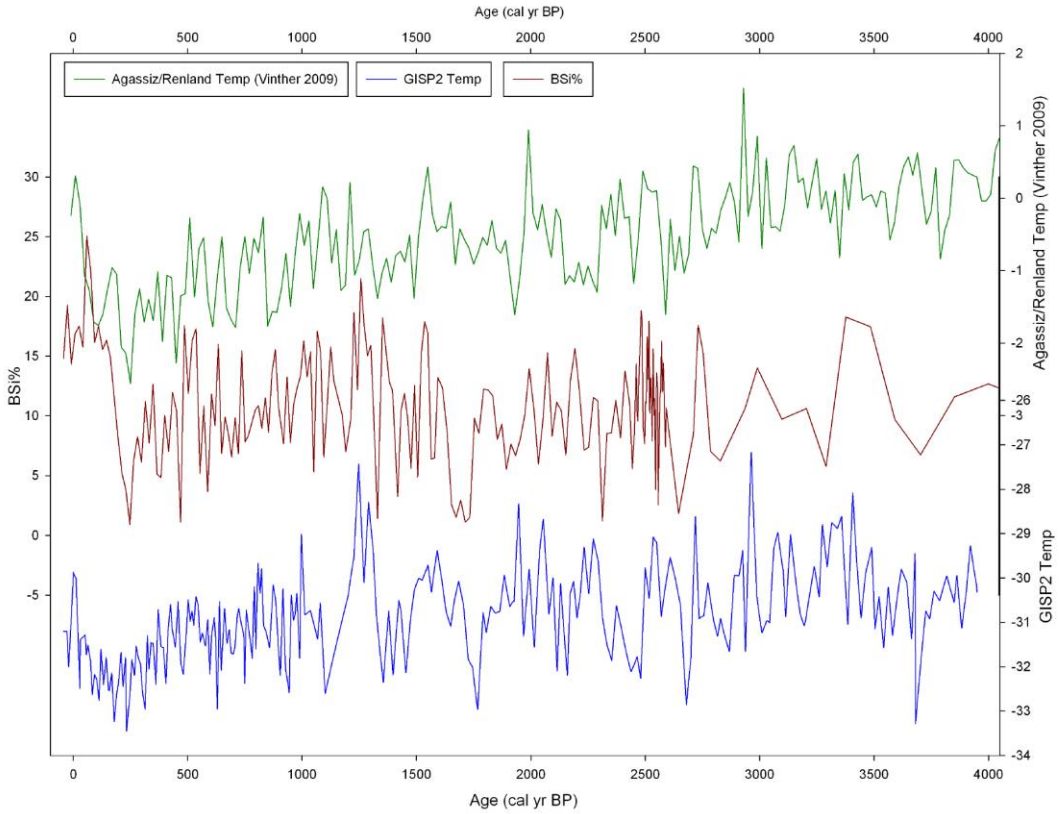

Figure 5.19: BSi concentrations plotted with the two ice core temperature reconstructions for the past ~4000 years. Higher sampling density is needed to determine if there is a robust relationship between the records.

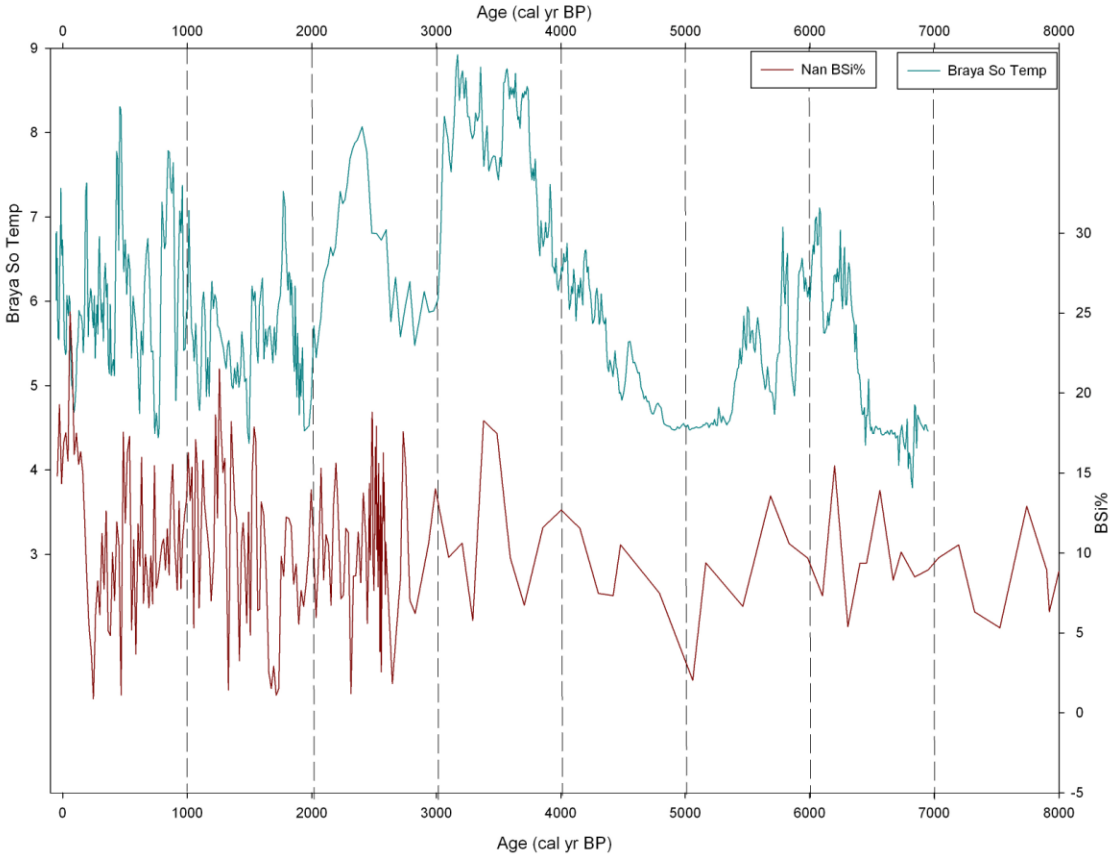

Figure 5.20: Temperature reconstruction from Lake Braya Sø in Western Greenland (von Gunten et al., 2011), showing possible relationship with BSi concentrations in Nanerersarpik.

BIBLIOGRAPHY

Alley, R., Mayewski, P., Sowers, T., Stuiver, M., Taylor, K., Clark, P., 1997. Holocene climatic instability: A prominent, widespread event 8200 yr ago. Geology 25, 483-486.

Anderson, N.J., Leng, M., 2004. Increased aridity during the early Holocene in West Greenland inferred from stable isotopes in laminated-lake sediments. Quaternary Science Reviews 23, 841-849.

Anderson, N.J., Stedmon, C., 2007. The effect of evapoconcentration on dissolved organic carbon concentration and quality in lakes of SW Greenland. Freshwater Biology 52, 280-289.

Anderson, N., Liverside, A., McGowan, S., Jones, M., 2012. Lake and catchment response to Holocene environmental change: spatial variability along a climate gradient in southwest Greenland. J Paleolimnology 48, 209-222.

Andresen, C., Bjorck, S., Bennike, O., Bond, G., 2004. Holocene climate changes in Southern Greenland: evidence from lake sediments. Journal of Quaternary Science 19, 783-795.

Axford, Y., Losee, S., Briner, J., Francis, D., Langdon, P., Walker, I., 2013. Holocene temperature history at the western Greenland Ice Sheet margin reconstructed from lake sediments. Quaternary Science Reviews 59, 87-100.

Bitz, C., Ridley, J., Holland, M., Cattle, H., 2010. Global climate models and 20thand 21st century Arctic climate change. Arctic Climate Change –the ACSYS Decade and Beyond (Ed. P. Lemke).

Blass, A., Bigler, C., Grosjean, M., Sturm, M., 2007. Decadal-scale autumn temperature reconstruction back to AD 1580 inferred from the varved sediments of Lake Silvaplana (southeastern Swiss Alps). Quaternary Research 68, 184-195.

Blaauw, M., 2010. Methods and code for 'classical' age-modelling of radiocarbon sequences. Quaterarny Geochronology 5, 512-518.

Brassell, S.C., Eglinton, G., Marlowe, I.T., Pflaumann, U., Sarnthein, M., 1986. Molecular Stratigraphy – a new tool for climatic assessment. Nature 320, 129-133.

Bridgwater, D., 1976. Nagssustoqidian mobile belt in East Greenland. Geology of Greenland 7, 97-103.

Briner, J., Stewart, H.A.M., Young, N.E., Phillips, W., Losee, S., 2010. Using proglacial-threshold lakes to constrain fluctuations of the Jakobshavn Isbrae ice margin, western Greenland, during the Holocene. Quaternary Science Reviews 29, 3861-3874.

Broeker, W., Denton, G., 1989. The role of ocean-atmosphere reorganizations in glacial cycles. Geochimica et Cosmochimica Acta 53, 2465-2501.

Callaghan, T., Bergholm, F., Christensen, T., Jonasson, C., Kokfelt., U., Johansson, M., 2010. A new climate era in the sub-Arctic: Accelerating climate changes and multiple impacts. Geophysical Research Letters 37, L14705.

Cappelen J, Laursen EV, Jörgensen, PV, Kern-Hansen C, 2011. DMI monthly climate data collection 1768–2010, Denmark, The Faroe Islands and Greenland. *DMI Technical Report 11-05*. Copenhagen, Ministry of Climate and Energy, p. 54.

Castañeda, I., Schouten, S., 2011. A review of molecular organic proxies for examining modern and ancient lacustrine environments. Quaternary Science Reviews 30, 2851-2891.

Christiansen, H., Murray, A., Mejdahl, V., Humlum, O., 1999. Luminescence dating of Holocene geomorphic activity on Ammassalik Island, SE Greenland. Quaternary Geochronology 18, 191-205.

Chu, G.Q., Sun, Q., Li, S.Q., Zheng, M.P., Jia, X.X., Lu, C.F., Liu, J.Q., Liu, T.S., 2005. Long-chain alkenone distributions and temperature dependence in lacustrine surface sediments from China. Geochimica et Cosmochimica Acta 69, 4985-5003.

Clark, P., Pisias, N., Stocker, T., Weaver, A., 2002. The role of thermohaline circulation in abrupt climate change. Nature 415, 863-869.

Colman, S., Peck, J., Hatton, J., Karabanov, E., King, J., 1999. Biogenic silica records from the BDP93 drill site and adjacent areas of the Selenga Delta, Lake Baikal, Siberia. J Paleolimnol 21, 9-17.

Conley, D., 1988. Biogenic Silica as an Estimate of Siliceous Microfossil Abundance in Great Lakes Sediments. Biogeochemistry 6, 161-179.

Conte, M.H., Sicre, M., Rühlemann, C., Weber, J., Schulte, S., Schulz-Bull, D., Blanz, T., 2006. Global temperature calibration of the alkenones unsaturation index (U^{k}_{37}') in surface waters and comparison with surface sediments. Geochemistry, Geophysics, Geosystems 7.

Cremer, H., Melles, M., Wagner, B., 2001. Holocene climate changes reflected in a diatom succession from Basaltø, East Greenland. Can. J. Bot. 79, 649-656.

D'Andrea, W., Huang, Y., Fritz, S., Anderson, N.J., 2011. Abrupt Holocene climate change as an important factor for human migration in West Greenland. PNAS 108, 9765-9769.

Dowdeswell, J., Uenzelmann-Neben, G., Whittington, R., Marienfeld, P., 1994. The Late Quaternary sediment record in Scoresby Sund, East Greenland. Boreas 23, 294-310.

Funder, S., Hansen, L., 1996. The Greenland ice sheet – a model for its culmination and decay during and after the last glacial maximum. Bulletin of the Geological Society of Denmark 42, 137-152.

Funder, S., Hjort, C., Landvik, J., Man, S., Ree, N., Stein, R., 1998. History of a stable ice margin- East Greenland during the Middle and Upper Pleistocene. Quaternary Science Reviews 17, 77-125.

Geirsdottir, A., Hardardottir, J., Andrews, J., 2000. Late-Holocene terrestrial glacial history of Miki and I.C. Jacobsen Fjords, East Greenland. The Holocene 10, 123-134.

Gregory, J., Huybrechts, P., Raper, S., 2004. Threatened loss of the Greenland ice-sheet. Nature 428, 616.

Hakansoon, L., Briner, J., Alexandersson, H., Aldahand, A., Possnerte, G., 2007. 10Be ages from central east Greenland constrain the extent of the Greenland ice sheet during the Last Glacial Maximum. Quaternary Science Reviews 26, 2316-2321.

Hanna, E., Cappelen, J., Fettweis, X., Huybrechts, P., Luckman, A., Ribergaard, M., 2009. Hydrologic response of the Greenland ice sheet: the role of oceanographic warming. Hyrol. Process 23, 7-30.

Hasholt, B., Mernild, S., 2008. Hydrology, sediment transport and water resources of Ammassalik Island, SE Greenland. Danish Journal of Geography 108, 73-95.

Hopmans, E.C., Schouten, S., Pancost, R.D., van der Meer, M.T.J., Sinninghe Damsté, J.S., 2000. Analysis of intact tetraether lipids in archeal cell material and sediments by high performance liquid chromatography/atmospheric chemical ionization mass spectrometry. Rapid Communications in Mass Spectrometry 14, 585-589.

Humlum, O., Christiansen, H., 2008. Geomorphology of the Ammassalik Island, SE Greenland. Danish Journal of Geography 108, 5-20.

Hurrell, J., Deser, C., 2009. North Atlantic climate variabililty: the role of the North Atlantic Oscillation. Journal of Marine Systems 78, 28-41.

Johnsen, S., Dahl-Jensen, D., Gundestrup, N., Steffensen, J., Clausen, H., Miller, H., Masson-Delmotte, V., Sveinbjörnsdottir, A., White, J., 2001. Oxygen isotope and paleotemperature records from six Greenland ice-core stations: Camp Century, Dye-3, GRIP, GISP2, Renland, and NorthGRIP. Journal of Quaternary Science 16, 299-307.

Jennings, A., Andrews, J., Wilson, L., 2011. Holocene environmental evolution of the Se Greenland Shelf North and South of the Denmark Strait: Irminger and East Greenland current interactions. Quaternary Science Reviews 30, 980-998.

Justwan., A., Koc, N., Jennings, A., 2008. Evolution of the Irminger and East Icelandic Current systems through the Holocene, revealed by diatom-based sea surface temperature reconstructions. Quaternary Science Reviews 27, 1571-1582.

Kaplan, M., Wolfe, A., Miller, G., 2002. Holocene Environmental Variability in Southern Greenland Inferred from Lake Sediments. Quaternary Research 58, 149-159.

Kaplan, M., Wolfe, A., 2006. Spatial and temporal variability of Holocene temperature in the North Atlantic Region. Quaternary Research 65, 223-231.

Kattsov, V., Kallen, E., Cattle, H., Christensen, J., Drange, H., Hanseen-Baurer, I., Johannesen, T., Karol, I., Raisanen, J., Svensson, G., Vavulin, S., 2007. Future Climate Change: Modeling and Scenarios for the Arctic. Arctic Climate Impacts Assesment (ACIA).

Kaufman, D., Schneider, D., McKay, N., Ammann, C., Bradley, R., Briffa, K., Miller, G., Otto-Bliesner, B., Overpeck, J., Vinther, B., Arctic Lakes 2k Project Members, 2009. Recent Warming Reverses Long-Term Arctic Cooling. Science 325, 1236-1239.

Kaufman, D., Ager, T., Anderson, N., Anderson, P., Andrews, J., Bartlein, P., Brubaker, L., Coats, L., Cwynar, L., Duvall, M., Dyke, A., Edwards, M., Eisner, W., Gajewski, K., Geirsdottir, A., Hu, F., Jennings, A., Kaplan, M., Kerwin, M., Loshkin, A., MacDonald, G., Miller, G., Mock, C., Oswald, W., Otto-Bliesner, B., Porinchu, D., Ruhland, K., Smol, J., Steig, E., Wolfe, B., 2004. Holocene Thermal Maximum in the western Arctic (0-180°W). Quaternary Science Reviews 23, 529-560.

Kelly, M., Lowell, T., Hall, B., Schaefer, J., Finkel, R., Goehring, B., Alley, R., Denton, G., 2008. A 10Be chronology of lateglacial and Holocene mountain glaciation in the Scoresby Sund region, east Greenland: implications for seasonality during lateglacial time. Quaternary Science Reviews 1-10.

Klug, M., Schmidt, S., Bennike, O., Heiri, O. Melles, M., Wagner, B., 2008. Lake sediments from Store Koldewey, Northeast Greenland, as archive of Lake Pleistocene and Holocene climatic and environmental changes. Boreas, 59-71.

Klug, M., Bennike, O., Wagner, B., 2009. Repeated short-term bioproductivity changes in a coastal lake on Store Koldewey, northeast Greenland: an indicator of varying sea ice coverage? The Holocene, 19, 653-663.

Kobashi, T., Kawamura, K., Severinghaus, J., Barnola, J., Nakaegawa, T., Vinther, B., Johnsen, S., Box, J., 2011. High variability of Greenland surface temperature over the past 4000 years estimated from trapped air in an ice core. Geophysical Research Letters 38, L21301.

Kuijpers, A., Troelstra, S., Prins, A., Linthout, K., Akhmetzhaov, A., Bouryak, S., Bachmann, M., Lassen, S., Rassmussen, S., Jensen, J., 2003. Late Quaternary sedimentary processes and ocean circulation changes at the Southeast Greenland margin. Marine Geology 195, 109-129.

Kutzbach, J., Guetter, P., 1986. The influence of changing orbital parameters and surface boundary conditions on climate simulations for the past 18,000 years. Journal of the Atmospheric Sciences 43, 1726-1759.

Landvik, J., 1994. The last glaciation of Germania Land and adjacent areas, northeast Greenland. Journal of Quaternary Science 9, 81-92.

Last, W., Smol, J., 2001. Tracking Environmental Change Using Lake Sediments, Volume 2: Physical and Geochemical Methods. Kluwer Academic Publishers, Dordrecht, The Netherlands.

Mann, M., Zhang, Z., Rutherford, S., Bradley, R., Hughes, M., Shindell, D., Ammann, C., Faluvegi, G., Ni, F., 2009. Global Signatures and Dynamical Origins of the Little Ice Age and Medieval Climate Anomaly. Science 326, 1256-1260.

Marcott, S., Shakun, J., Clark, P., Mix, A., 2013. A reconstruction of Regional and Global Temperature for the past 11,300 years. Science 339, 1198-1201.

Massa, C., Perren, B., Gauthier, E., Bichet, V., Petit, C., Richard, H., 2012. A multiproxy evaluation of Holocene environmental change from Lake Igaliku, South Greenland. J Paleolimnology 48, 241-258.

Masson-Delmotte, V., Swingedouw, D., Landais, A., Seidenkrantz, M., Gauthier, E., Bichet, V., Massa, C., Perren, B., Jomelli, V., Adalgeirsdottir, G., Christensen, J., Arneborg, J., Bhatt, U., Walker, D., Elbering, B., Gillet-Chaulet, F., Ritz, C., Gallee, H., van den Broeke, M., Fettweis, X., de Vernal, A., Vinther, B., 2012. Greenland climate change: from the past to the future. WIREs Clim Change 10.1002/wcc.186.

Mayeweski, P., Rohling, E., Stager, C., Karlen, W., Massch, K., Meeker, D., Meyerson, E., Gasse, F., van Kreveld, S., Holmgren, K., Lee-Thorp, J., Rosqvist, G., Rack, F., Staubwasser, M., Schneider, R., Steig, E., 2004. Holocene Climate Variability. Quaternary Research 62, 243-255.

McGowan, S., Ryves, D., Anderson, N.J., 2003. Holocene records of effective precipitation in West Greenland. The Holocene 13, 239-249.

McKay, N., Kaufman, D., Michelutti, N., 2008. Biogenic silica concentration as a high-resolution, quantitative temperature proxy at Hallet Lake, south-central Alaska. Geophysical Research Letters 35.

Melles, M., Brigham-Grette, Minyuk, P., Nowaczyk, N., Wennrich, V., DeConto, R., Anderson, P., Andreev, A., Coletti, A., Cook, T., Haltia-Hovi, E., Kukkonen, M., Lozhkin, A., Rosén, Tarasov, P., Vogel, H., Wagner, B., 2012. 2.8 Million Years of Arctic Climate Change from Lake El'gygytgyn, NE Russia. Science 20, 315-320.

Meyers, P. 2003. Applications of organic geochemistry to paleolimnological reconstructions: a summary of examples from the Laurentian Great Lakes. Organic Geochemistry 34, 261-289.

Meyers, P., Ishiwatari, R., 1993. Lacustrine organic geochemistry – an overview of indicators of organic matter sources and diagenesis in lake sediments. Org. Geochemistry 20, 867-900.

Meyers, P., Lallier-Vergés, E., 1999. Lacustrine sedimentary organic matter records of Late Quaternary paleoclimates. Journal of Paleolimnology 21, 345-372.

Meyers, P., Teranes, J., 2002. Sediment Organic Matter in Tracking Environmental Change Using Lake Sediments Developments in Paleoenvironmental Research Volume 2, 239-269. Kluwer Academic Publishers.

Moenke, H.H.W., 1974. Silica, the three-dimensional silicates, borosilicates, and beryllium silicates. The infrared spectra of minerals 4, 365-382.

Mortlock, R., Froelich, P., 1989, A simple method for the rapid determination of biogenic opal in pelagic marine sediments. Deep Sea Research Part A. Oceanographic Research Papers 36, 1415-1426.

Müller, P.J., Kirst, G., Ruhland, G., von Storch, I., Rosell-Mele, A., 1998. Calibration of the alkenone paleotemperature index U^{k}_{37}' based on core-tops form the eastern South Atlantic and the global ocean (60 degrees N- 60 degrees S). Geochimica et Cosmochimica Acta 62, 1757-1772.

Olsen, J., Anderson, N.J., Knudsen, M., 2012. Variability of the North Atlantic Oscillation over the past 5,200 years. Nature Geoscience 5, 808-812.

Overland, J., Wang, M., Salo, S., 2008. The recent Arctic warm period. Tellus 60A, 589-597.

Overpeck, J., Hughen, K., Hardy, D., Bradley, R., Case, R., Douglas, M., Finney, B., Gajewski, K., Jacoby, G., Jennings, A., Lamoureux, S., Lasca, A., MacDonald, G., Moore, J., Retelle, M., Smith, S., Wolfe, A., Zielinski, G., 1997. Arctic Environmental Change of the Last Four Centuries. Science 278, 1251-1256.

Perren, B., Anderson, J., Douglas, M., Fritz, S., 2012. The influence of temperature, moisture, and eolian activity on Holocene lake development in West Greenland. J Paleolimnology 48, 223-239.

Reimer, P.J., Baillie, M.G.L., Bard, E., Bayliss, A., Beck, J.W., Blackwell, P.G., Bronk Ramsey, C., Buck, C.E, Burr, G.S., Edwards, R. L., Friedrich, M., Grootes, P.M., Guilderson, T.P., Hajdas, I., Heaton, T.J., Hogg, A.G., Hughen, K.A., Kaiser, K.F., Kromer, B., McCormac, F.G., Manning, S.W., Reimer, R.W., Richards, D.A., Southon, J.R., Talamo, S., Turney, C.S.M., van der Plicht, J., Weyhenmeyer, C.E., 2009. IntCal09 and Marine09 radiocarbon age calibration curves, 0-50,000 years cal BP. Radiocarbon 51, 1111-1150.

Roberts, D., Long, A., Schnabel, C., Freeman, S., Simpson, M., 2008. The deglacial history of southeast sector of the Greenland Ice Sheet during the Last Glacial Maximum. Journ. Quart. Sci. Rew.

Rosén, P., Vogel, H., Cunningham, L., Reuss, N., Conley, D., Persson, P., 2010. Fourier transform infrared spectroscopy, a new method for rapid determination of total organic and inorganic carbon and biogenic silica concentration in lake sediments. J Paleolimnol 43, 247-259.

Schouten, S., Huguet, C., Hopmans, E.C., Kienhuis, M.V.M., Langer, G., Benthien, A., Bijma, J., 2007. Analytical methodology for TEX_{86} paleothermometry by high-performance liquid chromatography/atmospheric pressure chemical ionization-mass spectrometry. Analytical Chemistry 79, 2940-2944.

Serreze, M., Barrett, A., Stroeve, J., Kindig, D., Holland, M., 2009. The emergence of surface-based Arctic amplification. The Cryosphere 3, 11-19.

Smol, J., Cumming, B., 2000, Tracking Long-Term Changes in Climate using Algal Indicators in Lake Sediments. J. Phycol 36, 986-1011.

Spofforth, D., Palike, H., Green, D., 2008. Paleogene record of elemental concentrations in sediments from the Arctic Ocean obtained by XRF analysis. Paleoceanography 1, PA1S09.

Steffen, K., Box, J., 2001. Surface climatology of the Greenland ice sheet: Greenland Climate Network 1995-1999. Journal of Geophysical Research 100.

Stein, R., Nam, S., Grobe, H., Hubberten, H., 1996. Late Quaternary glacial history aand short-term ice-rafted debris fluctuations along the East Greenland continental margin. In: Andrews, J., Austin, W.,

Bergsten, H., Jennings, A., (eds.), Late Quaternary Paleoceanography off the North Atlantic Margins. Geological Society, London, Special Publication 111: 135-151.

Sutherland, D., Pickart, R., 2008. The East Greenland Current: Structure, variability, and forcing. Progress in Oceanography 78, 58-77.

Swann, G., Mackay, A., 2006. Potential limitations of biogenic silica as an indicator of abrupt climate change in Lake Baikal, Russia. J Paleolimnol 36, 81-89.

Thomas, E., Wolff, E., Mulvaney, R., Steffensen, J., Johnsen, J., Arrowsmith, C., White, J., Vaughn, B., Popp, T., 2007. The 8.2 ka event from Greenland ice cores. Quaternary Science Reviews 26, 70-81.

Toney, J., Huang, Y., Fritz, S., Baker, P., Grimm, E., 2010. Climatic and Environmental Controls on the Occurrence and Distribution of Long Chain Alkenones in Lakes of the Interior United States. Papers in the Earth and Atmospheric Sciences, Paper 124.

Trouet, V., Esper, J., Graham, N., Baker, A., Scourse, J., Frank, D., 2009. Persistent Positive North Atlantic Oscillation Mode Dominated the Medieval Climate Anomaly. Science 324, 78-80.

Vinther, B., Buchardt, S., Clausen, H., Dahl-Jensen, D., Johnsen, S., Fisher, D., Koerner, R., Raynaud, D., Lipenkov, V., Andersen, K., Blunier, T., Rasmussen, O., Steffensen, J., Svensson, A., 2009. Holocene thinning of the Greenland ice sheet. Nature 461, 385-388.

Vinther, B., Clausen, H., Fisher, D., Koerner, R., Johnsen, S., Andersen, K., Dahl-Jensen, D., Rasmussen, S., Steffensen, J., Svensson, A., 2008, Synchronizing ice cores from the Renland and Agassiz ice caps to the Greenland Ice Core Chronology. Journal of Geophysical Research, 113, D08115.

Vogel, H., Rosen, P., Wagner, B., Melles, M., Persson, P., 2008. Fourier transform infrared spectroscopy, a new cost-effective tool for quantitative analysis of biogeochemical properties in long sediment records. Journal of Paleolimnology 40, 689-702.

Volkman, J.K., 2003. Sterols in microorganisms. Applied Microbiology and Biotechnology 60, 495-506.

von Gunten, L., D'Andrea, W., Bradley, R., Huang, Y., 2012. Proxy-to-proxy calibration: Increasing temporal resolution of quantitative climate reconstructions. Scientific Reports 2, 10.1038/srep00609.

Wagner, B., Melles, M., Hahne, J., Niessen, F., Hubberten, H., 2000. Holocene climate history of Geographical Society Ø, East Greenland- evidence from lake sediments. Paleoceanography, Paleoclimatology, Paleoecology 160, 45-68.

Wagner, B., Melles, M., 2002. Holocene environmental history of western Ymer Ø, East Greenland, inferred from lake sediments. Quaternary International 89, 156-176.

Wanner, H., Beer, J., Butikofer, J., Crowley, T., Cusbach, U., Fluckiger, J., Goosse, H., Grosjean, M., Joos, F., Kaplan, J., Kuttel, M., Muller, S., Prentice, C., Solomina, O., Stocker, T., Tarasov, P., Wagner, M., Widmann, M., 2008. Mid-to Late Holocene climate change: an overview. Quaternary Science Reviews, 1-38.

Willemse, N., Tornqvist, T., 1999. Holocene century-scale temperature variability from West Greenland lake records. Geology, 27. 580-584.

Williams, D., Peck, J., Karabanov, E., Prokopenko, A., Kravchinsky, V., King, J., Kuzmin, M., 1997. Lake Baikal Record of Continental Climate Response to Orbital Insolation During the Past 5 Million Years. Science 278, 1114-1117.

Zink, K., Leythaeuser, D., Melkonian, M., Schwark, L., 2001. Temperature dependency of long-chain alkenone distributions in Recent to fossil limnic sediments and in lake waters. Geochimica et Cosmochimica Acta 65, 253-265.

Zwang, M., Munchow, A., 2006. Warming and freshening of Baffin Bay. J. Geophys Res Oceans 111:C7.